Adaptive and Optimal Motion Control of Multi-UAV Systems

by

Nasrettin Köksal

A thesis
presented to the University of Waterloo
in fulfillment of the
thesis requirement for the degree of
Doctor of Philosophy
in
Mechanical and Mechatronics Engineering

Waterloo, Ontario, Canada, 2019

Examining Committee Membership

The following served on the Examining Committee for this thesis. The decision of the Examining Committee is by majority vote.

External Examiner	Professor Farrokh Janabi-Sharifi
Supervisor	Associate Professor Baris Fidan
Internal Members	Professor William Melek
	Associate Professor Soo Jeon
Internal-external Member	Associate Professor Nasser Lashgarian Azad

Author's Declaration

I hereby declare that I am the sole author of this thesis. This is a true copy of the thesis, including any required final revisions, as accepted by my examiners.

I understand that my thesis may be made electronically available to the public.

Abstract

This thesis studies trajectory tracking and coordination control problems for single and multi unmanned aerial vehicle (UAV) systems. These control problems are addressed for both quadrotor and fixed-wing UAV cases. Despite the fact that the literature has some approaches for both problems, most of the previous studies have implementation challenges on real-time systems. In this thesis, we use a hierarchical modular approach where the high-level coordination and formation control tasks are separated from low-level individual UAV motion control tasks. This separation helps efficient and systematic optimal control synthesis robust to effects of nonlinearities, uncertainties and external disturbances at both levels, independently. The modular two-level control structure is convenient in extending single-UAV motion control design to coordination control of multi-UAV systems. Therefore, we examine single quadrotor UAV trajectory tracking problems to develop advanced controllers compensating effects of nonlinearities and uncertainties, and improving robustness and optimality for tracking performance. At first, a novel adaptive linear quadratic tracking (ALQT) scheme is developed for stabilization and optimal attitude control of the quadrotor UAV system. In the implementation, the proposed scheme is integrated with Kalman based reliable attitude estimators, which compensate measurement noises. Next, in order to guarantee prescribed transient and steady-state tracking performances, we have designed a novel backstepping based adaptive controller that is robust to effects of underactuated dynamics, nonlinearities and model uncertainties, e.g., inertial and rotational drag uncertainties. The tracking performance is guaranteed to utilize a prescribed performance bound (PPB) based error transformation. In the coordination control of multi-UAV systems, following the two-level control structure, at high-level, we design a distributed hierarchical (leader-follower) 3D formation control scheme. Then, the low-level control design is based on the optimal and adaptive control designs performed for each quadrotor UAV separately. As particular approaches, we design an adaptive mixing controller (AMC) to improve robustness to varying parametric uncertainties and an adaptive linear quadratic controller (ALQC). Lastly, for planar motion, especially for constant altitude flight of fixed-wing UAVs, in 2D, a distributed hierarchical (leader-follower) formation control scheme at the high-level and a linear quadratic tracking (LQT) scheme at the low-level are developed for tracking and formation control problems of the fixed-wing UAV systems to examine the non-holonomic motion case. The proposed control methods are tested via simulations and experiments on a multi-quadrotor UAV system testbed.

Acknowledgments

First, I would like to thank Prof. Baris Fidan. I am indebted to him for all his contribution of time, ideas and material, which made the completion of this thesis possible.

I would also like to thank Prof. Farrokh Janabi-Sharifi, Prof. William Melek, Prof. Soo Jeon and Prof. Nasser Lashgarian Azad for being in my committee and for their helpful comments.

Here, I would like to thank Prof. Teng-Hu Cheng from National Chiao Tung University for his hospitality and support during my summer research visit in Taiwan.

I would like to extend my sincere thanks to Hao An and Mehdi Jalalmaab for countless works we have collaborated.

Finally, my special thanks go to my lovely family for all their support.

Dedication

To my beloved ones ♡

Table of Contents

List of Figures

List of Tables

List of Abbreviations

UAV	Unmanned Aerial Vehicle
UGV	Unmanned Ground Vehicle
SLAM	Simultaneous Localization and Mapping
NGC	Navigation, Guidance and Control
NS	Navigation System
GS	Guidance System
CS	Control System
IMU	Inertial Measurement Unit
GPS	Global Positioning System
RADAR	Ranging or Radio Direction and Ranging
LIDAR	Light Detection and Ranging
SONAR	Sound Navigation and Ranging
P	Proportional
PD	Proportional-Derivative
PID	Proportional-Integral-Derivative
LQ	Linear Quadratic
LQR	Linear Quadratic Regulator
LQT	Linear Quadratic Tracking
ALQT	Adaptive Linear Quadratic Tracking
ALQC	Adaptive Linear Quadratic Control

AMC	Adaptive Mixing Control
ARE	Algebraic Riccati Equation
DRE	Differential Riccati Equation
BC	Backstepping Control
ABC	Adaptive Backstepping Control
PI	Parameter Identification
LS	Least Squares
PWM	Pulse Width Modulation
CG	Center of Gravity
DOF	Degree of Freedom

List of Symbols

$\{O_b, x_b, y_b, z_b\}$	Body frame
$\{O_g, x, y, z\}$	Global frame
$R_m \in SO(3)$	Rotational matrix from O_b to O_g
$p = [p_x, p_y, p_z]^T$	Position of O_g
$\varphi \triangleq [\phi, \vartheta, \psi]^T$	Euler Angles of O_b
$w_\varphi = [\dot{\phi}, \dot{\vartheta}, \dot{\psi}]^T$	Angular velocity of quadrotor UAV
$J_\varphi = \text{diag}(J_\phi, J_\vartheta, J_\psi)$	Rotational Inertia Matrix of quadrotor UAV
$d_\varphi = [d_\phi, d_\vartheta, d_\psi]^T$	Rotational Drag Parameters of quadrotor UAV
$F_b = [F_{xb}, F_{yb}, F_{zb}]^T$	Applied forces generated by actuator motors of quadrotor UAV
$T_r = [T_1, T_2, T_3, T_4]^T$	Total thrust forces generated by actuator motors of quadrotor UAV
$T_z,\ T_\varphi$	Altitude and attitude thrust forces of quadrotor UAV
$u_z,\ u_\varphi$	Altitude and attitude control inputs of quadrotor UAV
$v_r = [v_1, v_2, v_3, v_4]^T$	PWM control inputs of quadrotor UAV
G	PWM generator matrix of quadrotor UAV
t	Time
i	Number of UAVs
r	Number of actuator motors of quadrotor UAV
m	Total Mass of quadrotor UAV
K	Positive Armature Gain of quadrotor UAV
K_ψ	Thrust-to-Moment Gain of quadrotor UAV

b	The actuator motor bandwidth of quadrotor UAV
l	Distance between CG and actuator motors of quadrotor UAV
g	Gravitational Acceleration
v_c	Lateral speed command input of fixed-wing UAV
w_c	Heading command input of fixed-wing UAV
p_{zc}	Altitude command input of fixed-wing UAV
e	Tracking error
J	Cost function
$Q,\ R$	Weighting Matrices
P	Symmetric, positive definite matrix
$g(t)$	Vector signal
$\bar{g}(t)$	Approximate vector signal
$\mathbf{P}$	Positive covariance
θ^*	Uncertain parameter
$\hat{\theta}$	Estimated parameter
Φ	Regressor signal
m_n	Normalizing signal
β	Forgetting factor
ϵ	Estimation error
T_s	Sampling time
$Pr(.)$	Projection operator
ρ_j	Smooth decreasing performance function
S_j	Smooth increasing function
ε_j	Transformed error
$\bar{\delta}_j,\ \underline{\delta}_j$	Prescribed scalars
$\rho_{j0},\ \rho_{j\infty}, k_j$	PPB design parameters
p_r	Reference way-points

V_i	ith UAV
V_j	jth neighbor UAV
$R_{(ij)}$	Relative position between responsible UAV Pairs
$R^*_{(ij)}$	Desired relative position between responsible UAV Pairs
$d_{(ij)}$	Distance between responsible UAV Pairs
$d^*_{(ij)}$	Desired distance between responsible UAV Pairs
n	Number of candidate controllers
Ω^h_i	Candidate control subset
η^h_i	Bump function
$a^h_i,\ b^h_i$	Bump function parameters

Chapter 1

Introduction

1.1 General Overview and Motivation

Recent robotic interests have focused on improvements of human-like decision-making systems such as humanoid robots, animal-like robots, unmanned vehicle systems because of their self-control mechanisms and autonomous decision abilities without any external command. These kinds of studies aim at reaching fully-autonomous systems to use in different environments and in many tasks instead of human in the near future. By this motivation, control researchers over the last decades are interested in autonomous unmanned aerial vehicles (UAVs) which are used for various defense and civilian applications. Furthermore, UAVs have been critical flight systems to perform in dangerous and unsuitable environments compared to conventional aerial vehicles since they have dynamical and design advantages such as their smaller sizes, dynamical simplicities, maneuverabilities, high performances and being unpersonalized.

In the existing UAV literature, researchers have utilized various types of UAVs in research and development of autonomous flight tasks. According to the importance of demand and supply in-flight duties, UAVs can be classified into three main types, namely, fixed-wing [20, 23], rotary, including single-rotor helicopters [1, 80], multi-rotor aerial copters [135], quadrotors [8, 30, 35], and hybrid aircrafts, including tilt-rotor UAVs [164].

Small fixed-wing UAVs recently have gained attention for particular flight tasks and especially been preferred in air defense missions instead of large and expensive aerial vehicles, e.g. Predator, Global Hawk, and Aerosonde. In particular, fixed-wing UAVs are very effective for surveillance tasks in high altitudes and they can be easily developed in different

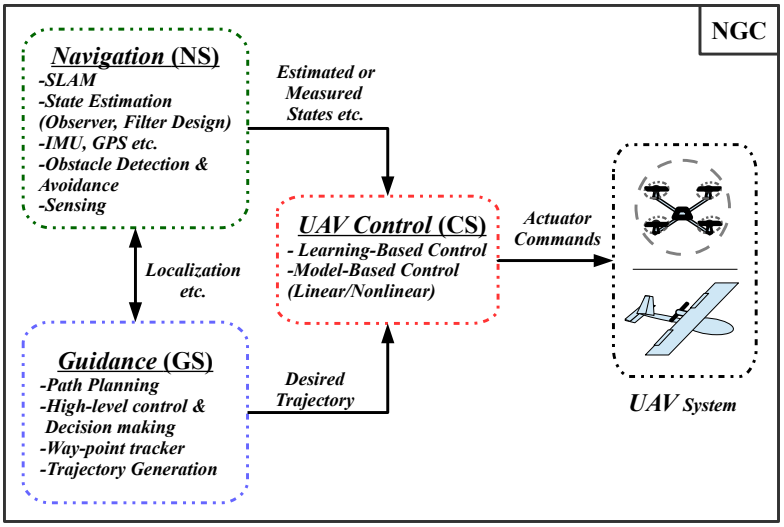

Figure 1.1: Autonomous system architecture for a UAV.

sizes depending on flight mission requirements. As mentioned in [21], design and control methods of small fixed-wing UAVs differ from larger fixed-wing UAVs and conventional aircrafts. In earlier studies [21, 23], autonomous fixed-wing UAVs have been developed successfully with a small and strong lightweight platform, low-power consumption and facilitated system architectures including navigation, guidance and control units.

For rotary type UAVs, there are several varieties of them such as single-rotor, tri-rotor, quad-rotor, hexa-rotor, octo-rotor copters. Rotary type UAVs are able to take off and land vertically inside dangerous and hard-to-reach areas in 3D thanks to their actuator design and holonomic motion capabilities. One of the rotary type UAVs is quadrotor UAV that recently has been popular for researchers and customers. Quadrotor UAVs have favorable accurate dynamic models and stability characteristics as well as hovering at close proximity of specified locations compared to other rotary and fixed-wing UAVs. As another reason to gain more fame, they have lower cost and simple structure in design. Therefore, for research studies and commercial usage, control researchers have been interested in developing new controllers for quadrotor UAVs to provide well-formed performances for various complicated indoor and outdoor tasks such as patrol duties, agricultural activities, delivery services, surveillance and rescue. Some earlier research prototypes have been studied in [8, 30, 35, 108, 145]. In the last decade, for difficult mission applications of quadrotor UAVs, technical requirements have been increased, and accordingly it has been needed to develop new control methods and improve their performances.

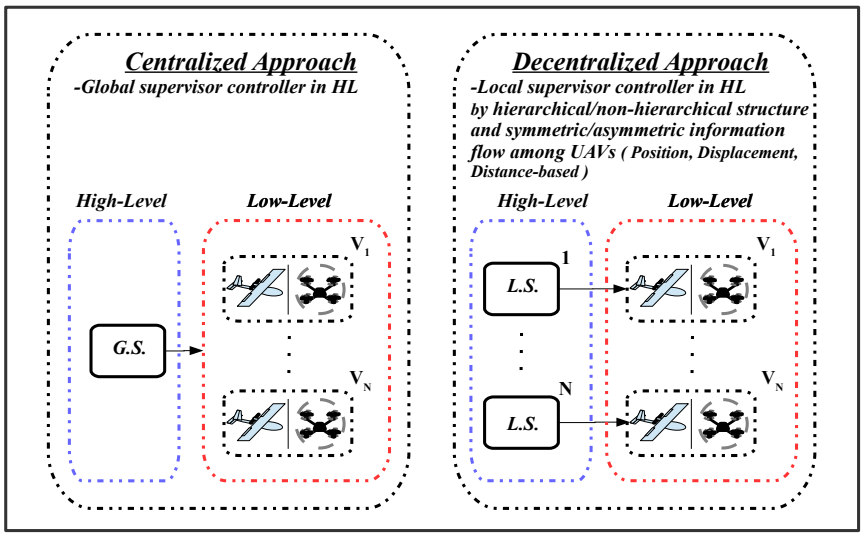

Figure 1.2: Formation control approaches for a multi-UAV system.

In autonomous flight control missions of single-UAV systems, overall system architectures and their components are discussed using different approaches in [23, 84]. These components are gathered into three main groups: navigation, guidance, and control (NGC) systems as presented in Figure 1.1. In the literature, NGC systems are not only developed to accomplish their objectives separately, but also interrelated throughout autonomous flight missions. The purpose of NGC systems is briefly explained as follows. Navigation system (NS) provides motion (state) and environmental information to other parts of NGC systems to support the overall system architecture. The motion (state) information can be orientation, position, angular and linear velocities which are measured or estimated by using hardware equipments on single-UAVs such as inertial measurement unit (IMU) and global positioning system (GPS) as well as using software computing algorithms: Kalman filter and observers. To detect environmental information during autonomous flights, NS contains visual monitoring and sensing methods using camera, sound navigation and ranging (SONAR), light detection and ranging (LIDAR), ranging or radio direction and ranging (RADAR), infrared sensor, etc. to support guidance system (GS). In GS algorithms, desired trajectories are produced by way-point tracker to supply control system (CS) using motion and environmental information from NS. Before the desired trajectory generation, GS also includes path planning strategies to locate way-points, optimally. Overall, GS algorithms are to guide single-UAVs, e.g., both fixed-wing and quadrotor UAVs, by generating the desired position. CS is responsible for controlling and stabilizing single-UAVs

using information from NS and GS, and then it completes autonomous flight tasks.

Another research field that has recently gained significant attention is cooperative control of multi-UAV systems. Cooperative multi-UAV systems are potentially more effective than the use of single-UAV systems in various complicated tasks including defense patrol duties, agricultural monitoring, surveillance, and rescue. One particular aspect of such cooperative multi-UAV tasks, is coordinated motion control, which involves path planning, flocking, consensus, obstacle and inter-agent avoidance, formation acquisition and maintenance [20, 22, 57, 89, 93, 112, 134]. In coordinated motion of multi-UAV systems, formation is used for a UAV team to perform certain cooperative mission requirements, optimally [163]. As presented in Figure 1.2, formation control schemes of multi-UAV systems can be classified into two main approaches as centralized and decentralized [120]. The centralized approach needs a global supervisor to coordinate all members of a UAV team, and its theoretical analysis gets complicated when the number of UAVs enlarges. Therefore, the literature works mostly focus on the decentralized approach to design easy and practical control solutions.

In this thesis, we focus on two UAV types: rotary and fixed-wing, in particular, quadrotor and small fixed-wing UAVs. By motivation of contributing to tracking control problems of single-UAVs, we develop novel and advanced (adaptive and optimal) control methods using model-based (linear and nonlinear) approaches in the CS. Also, we partially deal with the design problems of the NS and the GS during real-time flight tests. As another motivation, with the easiness of proposed flight control architectures and distributed approach in high (formation) level, we extend single UAV control designs to formation control of Multi-UAVs. Proposed techniques as presented in the main contribution chapters are practical and easily implementable as verified by experiments and real-data based high-fidelity simulations.

1.2 Contributions of the Thesis

This thesis contributes to the literature on tracking and formation control of single and multi-UAV systems, with focus on adaptive, optimal and nonlinear aspects. The main contributions of the thesis chapters are stated as follows:

- Chapter 3: A novel adaptive linear quadratic tracking (ALQT) control scheme is designed for optimal attitude tracking of a quadrotor UAV based on IMU sensor data fusion [91].

(i) The proposed control design is experimentally validated in the presence of real-world uncertainties in quadrotor UAV parameters and sensors measurement.

(ii) To improve tracking in the presence of IMU sensor noises, reliable attitude estimation schemes based on Kalman and complementary filters are designed and compared with each other via experimental tests on the quadrotor UAV.

- Chapter 4: A backstepping based robust adaptive control with guaranteed tracking error performance is proposed for trajectory tracking of a quadrotor UAV [90].

  (i) The under-actuated nonlinear dynamics is separated into three sub-models: lateral, altitude and attitude dynamics, and considered in the two-layer: position and attitude. The separation allows to easily design particular controllers for each model based on their different control demands.

  (ii) Transient and steady-state tracking performances of the quadrotor UAV are guaranteed within prescribed bounds in the presence of inertia and drag uncertainties. The effectiveness of the proposed control design is experimentally validated.

- Chapter 5: A distributed adaptive mixing control design is presented for formation maintenance of a multi quadrotor UAV system during commanded path tracking maneuvers.

  (i) A two-level control structure is introduced for constructing high (formation) and low (individual) level controllers, separately. The low-level controllers are designed to compensate effect of real dynamics issues for enhancing tracking performance and robustness while the rigid graph theory based tools are utilized for formation maintenance at the high level.

  (ii) At the low-level by using a smooth switching method based on online estimation, the adaptive mixing control (AMC) scheme is proposed to increase individual tracking performance and robustness as well as formation maintenance.

- Chapter 6: Optimal trajectory tracking control of fixed-wing UAVs and formation control of a multiple fixed-wing UAV system are designed for 2D surveillance tasks.

  (i) The proposed single-UAV LQT control and multi-UAV two-level control designs are extended and applied to fixed-wing UAV systems for fixed altitude 2D trajectory tracking and formation control problems.

1.3 Organization of the Thesis

The thesis consists of one background and literature review chapter and four contribution chapters. Results, discussions, and summaries of numerical simulations and experiments are provided in each contribution chapter to make it self-contained.

Chapter 2 presents modeling of UAV motion dynamics for quadrotor and small fixed-wing UAV systems. Then, the literature is reviewed for single-UAV motion control and multi-UAV formation control of quadrotor and small fixed-wing UAV systems. Lastly, control architectures are presented and discussed.

Chapter 3 presents an infinite-horizon ALQT control scheme for optimal attitude tracking of a quadrotor UAV. The proposed control scheme is experimentally validated in the presence of real-world uncertainties in quadrotor system parameters and sensor measurement. The designed control scheme guarantees asymptotic stability of the closed-loop system with the help of complete controllability of the attitude dynamics in applying optimal control signals. To achieve robustness against parametric uncertainties, the optimal tracking solution is combined with an on-line least squares based parameter identification scheme to estimate the instantaneous inertia of the quadrotor. Sensor measurement noises are also taken into account for the on-board IMU sensors. To improve controller performance in the presence of sensor measurement noises, two sensor fusion techniques are employed, one based on Kalman filtering and the other based on complementary filtering. The ALQT control performance is compared for the use of these two sensor fusion techniques.

In Chapter 4, a backstepping based robust adaptive control design with guaranteed transient and steady-state tracking performances is proposed for a quadrotor UAV. Backstepping techniques, combined with a prescribed performance function based error transformation, are employed to achieve the bounded transient and steady-state tracking errors of the strict-feedback position system which comprises of the lateral position and the altitude dynamics. To compensate the effects of model uncertainties such as inertia and drag uncertainties on attitude regulation, an indirect adaptive control scheme is designed, where the least squares based parameter identification algorithm is combined with a backstepping based nonlinear control law. Simulation and experimental test results are provided to verify the effectiveness of the proposed control design.

Chapter 5 presents a distributed adaptive mixing control design for the formation maintenance of a multi quadrotor UAV system during commanded path tracking maneuvers. The formation control design is constructed at the two-level: At the high (formation) level, the rigid and persistent motion is satisfied in 3D to maintain the predefined for-

mation shape. At the low (individual) level, an indirect adaptive mixing control (AMC) law is designed based on Least Squares (LS) parameter identification (PI) to ensure better tracking performances and robustness to parametric uncertainties and disturbances in quadrotor UAV equations of motion. The proposed scheme adaptively blends a set of pre-designed linear quadratic control gains based on the bump function, and it provides smooth transition between pre-designed control sets. The proposed scheme is also compared with an adaptive linear quadratic control (ALQC) design. Stability analyses of both controllers are provided. Formation performances are tested and compared by real-time based simulations.

In Chapter 6, a linear quadratic tracking (LQT) control design is studied for the lateral motion tracking of fixed-wing UAVs. Then, the low-level LQT control design is extended to the formation control of a multiple fixed-wing UAV system by using the two-level, hierarchical, distributed formation structure. For both cases, the proposed control designs are validated for 2D surveillance tasks by numerical simulations.

Chapter 7 offers conclusions and discussions on the proposed methods.

Chapter 2

Background and Control Architecture

This chapter first introduces equations of motion for quadrotor and small fixed-wing UAV systems. Then, regarding current control strategies and problems, the literature is reviewed on tracking and formation control of single and multi-UAV systems for both UAV types. Lastly, control architectures of single and multi-UAV systems are discussed and presented.

2.1 Modeling of UAV Motion Dynamics

UAV systems can be classified according to many different aspects based on their dynamics, design structure, motion facility or working environment, etc. In this thesis, depending on the taking-off and landing abilities of UAV systems, we consider that there are two types, namely, quadrotor and small fixed-wing UAV systems. In the literature, both systems have various equations of motion models as presented in [8, 20, 23, 30, 35, 41, 64, 88, 108, 133]. These motion models can consist of highly nonlinear dynamics with coupled states and aerodynamics parameters, simplified nonlinear models with ignored effects, linearized forms neglecting many important aspects, kinematic models avoiding complex control design, dynamical uncertainties, and environmental or model disturbances.

We first define the equations of motion models in the form of a generic nonlinear representation for both UAV types to efficiently utilize in further control analyses. On $\mathbb{R}^3$, the equations of motion models are written in the nonlinear model as

$$\dot{X} = F(X, u), \tag{2.1}$$

where $X \in \mathbb{R}^n$ and $u \in \mathbb{R}^m$ are state and control input vectors of UAV systems, respectively.

2.1.1 Quadrotor UAV Motion Dynamics

The coordinates of the quadrotor UAV system's body frame $\{O_b, x_b, y_b, z_b\}$ centered at the center of gravity (CG), the global frame $\{O_g, x, y, z\}$, thrusts, moments and gravity are represented in Figure 2.1. Using Euler angles $\varphi \triangleq [\phi, \vartheta, \psi]^T$ and the rotational matrix $R_m \in SO(3)$ from O_b to O_g, and following the Newton-Euler formalism, nonlinear dynamics of the quadrotor UAV are described in terms of applied forces and moments, as

$$F = R_m F_b = m\ddot{p} \in \mathbb{R}^3 \quad \text{and} \quad M = J_\varphi \dot{w}_\varphi + w_\varphi \times J_\varphi w_\varphi \in \mathbb{R}^3, \tag{2.2}$$

where $F_b = [F_{xb}, F_{yb}, F_{zb}]^T = [0, 0, \sum_{r=1}^{4} T_r]^T$ is the applied force vector generated by actuators' thrust forces T_r, $r = 1, 2, 3, 4$, in the body frame; m is the total mass of the system; $J_\varphi = \text{diag}(J_\phi, J_\vartheta, J_\psi)$ is the rotational inertia matrix in the body frame; $w_\varphi = [\dot{\phi}, \dot{\vartheta}, \dot{\psi}]^T$ is the angular velocity of O_b. Equations (2.2) lead to the following equations of motion [89]:

$$\begin{aligned}
\ddot{p}_x &= \frac{(T_1 + T_2 + T_3 + T_4)(\sin\psi \sin\phi + \cos\phi \sin\vartheta \cos\psi)}{m}, \\
\ddot{p}_y &= \frac{(T_1 + T_2 + T_3 + T_4)(-\sin\phi \cos\psi + \cos\phi \sin\vartheta \sin\psi)}{m}, \\
\ddot{p}_z &= \frac{(T_1 + T_2 + T_3 + T_4)(\cos\phi \cos\vartheta)}{m} - g, \\
\ddot{\phi} &= \frac{l(T_1 - T_2)}{J_\phi} + \frac{(J_\vartheta - J_\psi)\dot{\psi}\dot{\vartheta}}{J_\phi} - d_\phi \dot{\phi}, \\
\ddot{\vartheta} &= \frac{l(T_3 - T_4)}{J_\vartheta} + \frac{(J_\psi - J_\phi)\dot{\psi}\dot{\phi}}{J_\vartheta} - d_\vartheta \dot{\vartheta}, \\
\ddot{\psi} &= \frac{K_\psi(T_1 + T_2 - T_3 - T_4)}{J_\psi} + \frac{(J_\phi - J_\vartheta)\dot{\vartheta}\dot{\phi}}{J_\psi} - d_\psi \dot{\psi},
\end{aligned} \tag{2.3}$$

where $p = [p_x, p_y, p_z]^T$ is the position of O_b; $d_\varphi = [d_\phi, d_\vartheta, d_\psi]^T$ are rotational drag parameters; T_r, $r = 1, ., 4$ are thrust forces generated on each actuator; l is the distance between the center of gravity (O_b) and each propeller; K_ψ is thrust-to-moment gain; g is gravitational acceleration.

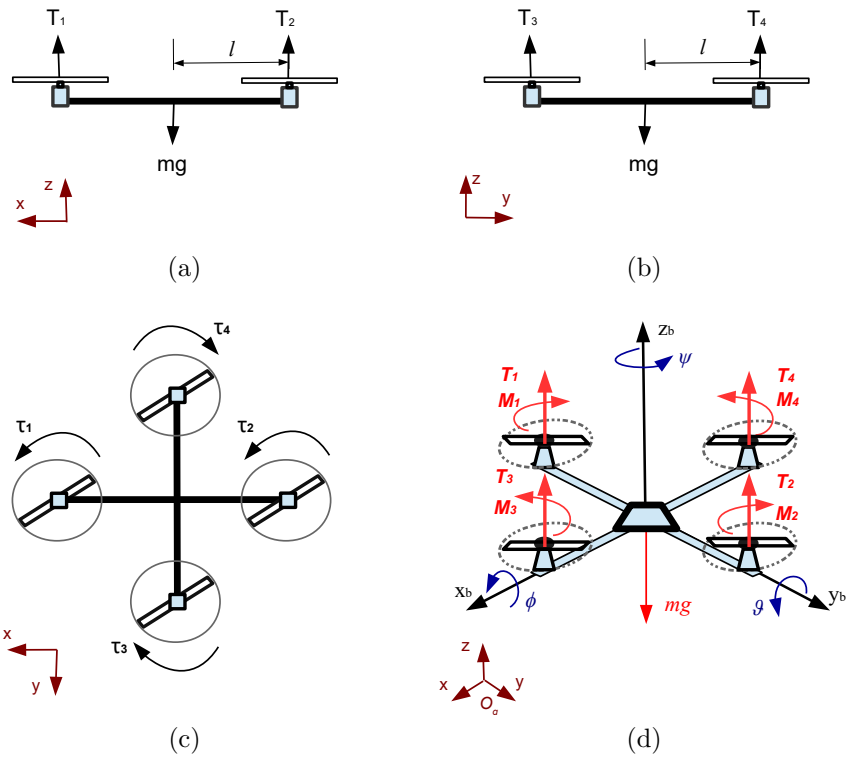

Figure 2.1: The quadrotor UAV's attitude motion: (a) pitch; (b) roll; (c) yaw, and (d) coordinate representation with thrusts, moments and gravity force.

Besides, as an attempt to generate thrust forces using actuators, we use the first-order thrust-input model [172] in the Laplace domain as follows:

$$T_r(s) = K\frac{b}{s+b}v_r(s) \tag{2.4}$$

where b is the actuator bandwidth; K is a positive armature gain.

In the control design, we separate the attitude and altitude dynamics. Using the control inputs of separated dynamics, a pulse width modulation (PWM) input generator is

obtained as

$$v_r = Gu = \begin{bmatrix} 0 & 1 & 1 & 1 \\ 0 & -1 & 1 & 1 \\ 1 & 0 & -1 & 1 \\ -1 & 0 & -1 & 1 \end{bmatrix} \begin{bmatrix} u_\varphi \\ u_z \end{bmatrix}, \tag{2.5}$$

where $v_r = [v_1, v_2, v_3, v_4]^T \in \mathbb{R}^4$ is the PWM input for each actuator; G is the PWM generator matrix; $u_\varphi = [u_\phi, u_\vartheta, u_\psi]^T \in \mathbb{R}^3$ is attitude control inputs; $u_z \in \mathbb{R}$ is altitude control input. Employing (2.5) we map the generated control signals $u = [u_\varphi^T, u_z]^T$ to the actual PWM signals v for the four motors. Similar to (2.5), we define the effective altitude thrust T_z and attitude thrusts $T_\varphi = [T_\phi, T_\vartheta, T_\psi]^T$ as follows:

$$T_z \triangleq (T_1 + T_2 + T_3 + T_4)/4, \tag{2.6}$$
$$T_\phi \triangleq (T_1 - T_2)/2, \tag{2.7}$$
$$T_\vartheta \triangleq (T_3 - T_4)/2, \tag{2.8}$$
$$T_\psi \triangleq (T_1 + T_2 - T_3 - T_4)/4. \tag{2.9}$$

Combining the nonlinear dynamics (2.3), thrust-input model (2.4) and the relation (2.6)-(2.9), we derive the nonlinear state variable model in the form of (2.1) as

$$\dot{X} = F(X, u) = \begin{bmatrix} X_3 \\ X_4 \\ \frac{4}{m} f_1(X_2) X_6 - \zeta \\ \mathbf{A}_1 X_4 + \mathbf{A}_2 f_2(X_4) + \mathbf{B} X_5 \\ -b X_5 + K b u_\varphi \\ -b X_6 + K b u_z \end{bmatrix}, \tag{2.10}$$

with state and control input vectors of the quadrotor UAV

$$X = [X_1, X_2, X_3, X_4, X_5, X_6]^T \in \mathbb{R}^{16} \quad \text{and} \quad u = [u_\varphi^T, u_z]^T \in \mathbb{R}^4, \tag{2.11}$$

where $X_1 = p = [p_l^T, p_z]^T, X_2 = \varphi \triangleq [\phi, \vartheta, \psi]^T, X_3 = \dot{X}_1 = v, X_4 = \dot{X}_2 = w_\varphi, X_5 = T_\varphi \triangleq [T_\phi, T_\vartheta, T_\psi]^T$ are 3-D vectors; $X_6 = T_z$; $\zeta = [0, 0, g]^T$; $\mathbf{A}_1 = \text{diag}(d_\phi, d_\vartheta, d_\psi)$; $\mathbf{A}_2 =$

$\text{diag}(\frac{J_\vartheta - J_\psi}{J_\phi}, \frac{J_\psi - J_\phi}{J_\vartheta}, \frac{J_\phi - J_\vartheta}{J_\psi})$; $f_1(X_2) = \begin{bmatrix} \cos\phi\sin\vartheta\cos\psi + \sin\phi\sin\psi \\ \cos\phi\sin\vartheta\sin\psi - \sin\phi\cos\psi \\ \sin\phi\cos\vartheta \end{bmatrix}$; $f_2(X_4) = \begin{bmatrix} \dot{\vartheta}\dot{\psi} \\ \dot{\phi}\dot{\psi} \\ \dot{\phi}\dot{\vartheta} \end{bmatrix}$; $\mathbf{B} = \text{diag}(\frac{\sigma_\varphi}{J_\varphi}) = \text{diag}(\frac{2l}{J_\phi}, \frac{2l}{J_\vartheta}, \frac{4K_\psi}{J_\psi})$.

In order to have a more feasible problem setting for further advanced control design, we now present the separated dynamics of (2.10) as follows.

Lateral Position Model: The separated lateral position dynamics is

$$\dot{p}_l = v_l, \tag{2.12}$$

$$\ddot{p}_l = \frac{4T_z}{m} f_{1l}, \tag{2.13}$$

where $f_{1l} \triangleq \begin{bmatrix} \cos\phi\sin\vartheta\cos\psi + \sin\phi\sin\psi \\ \cos\phi\sin\vartheta\sin\psi - \sin\phi\cos\psi \end{bmatrix}$.

Altitude Model: The separated altitude dynamics is

$$\dot{p}_z = v_z, \tag{2.14}$$

$$\dot{v}_z = \frac{4}{m}(\cos\phi\cos\vartheta)T_z - g, \tag{2.15}$$

$$\dot{T}_z = -bT_z + Kbu_z, \tag{2.16}$$

Attitude Model: The separated attitude dynamics is

$$\dot{\varphi} = w_\varphi, \tag{2.17}$$

$$\dot{w}_\varphi = \mathbf{A}_1 w_\varphi + \mathbf{A}_2 f_2(w_\varphi) + \mathbf{B}T_\varphi, \tag{2.18}$$

$$\dot{T}_\varphi = -bT_\varphi + Kbu_\varphi. \tag{2.19}$$

Remark 2.1.1. *We are now able to design separated controllers to obtain more feasible control performances based on the self-control demands of the sub-models. In both altitude and attitude dynamics, an additional dynamics is defined to obtain u_z and u_φ which can be utilized to generate the PWM control inputs v_r of (2.4).*

2.1.2 Fixed-wing UAV Motion Dynamics

Fixed-wing UAV systems have the six-degree-of-freedom (DOF) and servo command inputs which are aileron (a), elevator (b), rudder (c), and throttle (d) as shown in Figure 2.2.

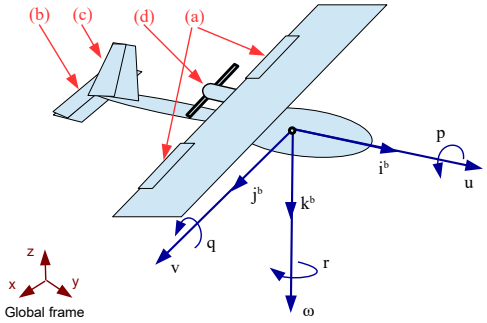

Figure 2.2: An example fixed-wing UAV and its motion axes.

The dynamics of fixed-wing UAVs consists of twelve-states which contain coupled states, model nonlinearities, nonlinear aerodynamics parameters, wind and other disturbances [23]. These complexities in the motion dynamics do not allow to develop advanced control methodologies, easily. On the other hand, small fixed-wing UAV systems are mainly considered to develop advanced control methods compared with large fixed-wing UAVs and conventional aircrafts. Small fixed-wing UAV's simplified equations of motion models (piccolo-controlled type) are suitable for advanced control solutions as studied in [20, 133].

In general, roll and yaw dynamics provide the lateral motion of the small fixed-wing UAV since there is a coupling between each other. In the piccolo-controlled type lateral motion, roll dynamics is ignored, and it is stabilized by autopilot devices. Hence, the simplified yaw and lateral velocity models provide lateral motion control [20, 133]. Since the angle of attack and pitch models are ignored and stabilized by autopilot devices, the altitude (longitudinal) motion only depends on the piccolo-controlled type height dynamics [20, 133]. Therefore, the simplified nonlinear equations of the small fixed-wing UAV motion (piccolo-controlled type) are considered for the position (lateral and altitude) and attitude as follows.

$$\dot{p}_x = v\cos(\psi), \tag{2.20}$$

$$\dot{p}_y = v\sin(\psi), \tag{2.21}$$

$$\ddot{p}_z = -\frac{1}{\alpha_{\dot{z}}}\dot{p}_z + \frac{1}{\alpha_z}(p_{zc} - p_z), \tag{2.22}$$

$$\dot{v} = \frac{1}{\alpha_v}(v_c - v), \tag{2.23}$$

$$\dot{\psi} = \omega, \tag{2.24}$$

$$\dot{\omega} = \frac{1}{\alpha_\omega}(\omega_c - \omega), \tag{2.25}$$

where $p = [p_x, p_y, p_z]^T$ are the position of O_g; v is lateral speed; ψ is heading angle; v_c, w_c and p_{zc} are lateral speed, heading and altitude control inputs. Then, the nonlinear state variable model in the form of (2.1) is derived as

$$\dot{X} = F(X,u) = \begin{bmatrix} X_3\cos(X_4) \\ X_3\sin(X_4) \\ -\frac{1}{\alpha_v}X_3 + \frac{1}{\alpha_v}v_c \\ X_5 \\ -\frac{1}{\alpha_w}X_5 + \frac{1}{\alpha_w}w_c \\ X_7 \\ -\frac{1}{\alpha_{\dot{z}}}X_7 - \frac{1}{\alpha_z}X_6 + \frac{1}{\alpha_z}p_{zc} \end{bmatrix}, \tag{2.26}$$

with state and control input vectors of the small fixed-wing UAV

$$X = [X_1, X_2, X_3, X_4, X_5, X_6, X_7]^T \in \mathbb{R}^7 \quad \text{and} \quad u = [v_c, w_c, p_{zc}]^T \in \mathbb{R}^3, \tag{2.27}$$

where $X_1 = p_x$, $X_2 = p_y$, $X_3 = v$, $X_4 = \psi$, $X_5 = w$, $X_6 = p_z$, and $X_7 = \dot{p}_z$; α_v, α_w $\alpha_{\dot{z}}$ and α_z are inertial related dynamical parameters.

For further control designs, (2.26) are separated to the lateral and the altitude motion models as follows.

Lateral Model: The separated lateral dynamics is

$$\dot{p}_x = v\cos(\psi), \tag{2.28}$$
$$\dot{p}_y = v\sin(\psi), \tag{2.29}$$
$$\dot{\psi} = \omega, \tag{2.30}$$
$$\dot{\omega} = \frac{1}{\alpha_\omega}(\omega_c - \omega), \tag{2.31}$$
$$\dot{v} = \frac{1}{\alpha_v}(v_c - v). \tag{2.32}$$

Altitude Model: The separated height dynamic is

$$\ddot{p}_z = -\frac{1}{\alpha_{\dot{z}}}\dot{p}_z + \frac{1}{\alpha_z}(p_{zc} - p_z). \tag{2.33}$$

2.2 Literature on Single-UAV Motion Control

In the literature, various control techniques and approaches have been studied extensively for quadrotor and fixed-wing UAV systems since both have different motion characteristics and control demands. This section presents a brief summary of the single-UAV motion control literature for both UAV systems. As discussed in the following subsections, it is noticed that some control methods have been studied for nonlinearity, uncertainty and optimality problems. However, the literature still needs advanced and feasible control solutions and analyses for realistic model issues such as model nonlinearities, parametric uncertainties, sensor noises and disturbances. By this motivation, new control strategies can be developed and combined with each other to design real-time implementable, optimal and robust controllers with guaranteed tracking error performance.

2.2.1 Quadrotor UAV Motion Control: Nonlinearities

It is well known that linear methods are easy and straightforward in terms of control designs and stability analyses. However, linear control schemes perform poorly for highly nonlinear systems since ignored dynamical terms affect linearized models, negatively. On the other hand, nonlinear control schemes have some disadvantages since they require more sophisticated hardware and equipment with larger memory and faster processor in real-time implementation. Also, their stability analysis is not easy for proof.

In the literature, the dynamics of quadrotor UAVs may consist of highly coupled states, nonlinear aerodynamic coefficients, external disturbances or uncertain parameters. To handle these effects, more advanced control designs are required. Before advanced methods were developed, there exist proportional-integral-derivative (PID) and linear quadratic (LQ) control based classical studies for simplified and linearized dynamics [29, 30, 36]. On the other hand, some earlier works [31, 107, 108] are studied solving nonlinear effects by using nonlinear control techniques such as feedback linearization, sliding mode, and backstepping control methods. These studies are partially implemented on quadrotor UAVs with restricted dynamics and without full autonomous flights. Using visual feedback without GPS and accelerometer, the approach described in [8] presents feedback linearization and backstepping-like control laws. The implementation of the study is not fully autonomous since the quadrotor UAV is restricted in vertical and yaw motion.

Unlike Newton-Euler modeling, [35] uses Lagrange approach to derive the motion dynamics for the control analyses. The authors use a nested saturation strategy to design the

proposed controllers, and the system is stabilized based on Lyapunov analysis. The experiment is technically not full autonomous flight since position and orientation sensing are provided via cables. In [41], the coupled dynamics derived by Lagrangian method is used to design backstepping control. The control structure is considered in two parts; attitude inner and position outer loop controllers. The control design is not easy and straightforward since position dynamics is bilinear. In the design, two neural networks are used for the estimation of system unknowns. In [107, 108], the dynamics is analyzed into three interconnected subsystems: under-actuated (for lateral and rotation), fully-actuated (for altitude and yaw) and propeller (for four rotors) subsystems. Then, the full-state backstepping methods are used for tracking control of the quadrotor UAV. The system stability is based on Lyapunov theorem. In [108], tests are lack of autonomous flight because of restricted yaw and altitude motions.

In contrast to the studies mentioned above, [145, 146] use the quaternion representation to define the attitude behavior. This helps to avoid singularities in the calculation of control laws comparing with Euler representation. In particular, [145] focuses on the attitude stabilization using the quaternion-based feedback control. Then, orientation is stabilized using PD^2 feedback control. This stabilized controller achieves a good transient and disturbance rejection performances during the high speed and large angle motions. [146] also contains the unit-quaternion, which is globally nonsingular, without velocity measurement to design a controller for tracking of desired attitude motion. Another control method is geometric tracking control to avoid singularities of Euler angles and ambiguities of quaternions in the attitude behavior during the complex and acrobatic maneuvers. This approach presents a global dynamic definition for the avoidances. Using the geometric method, [96] present nonlinear tracking controller which is used on the Euclidean group $SE(3)$. The study is extended to [97] which presents nonlinear output-tracking controllers for tracking of translational and rotational models. In this work, the authors consider that both dynamics contain the bounded uncertainties which are neglected in [96].

For robust nonlinear solutions on quadrotor UAVs, the sliding mode controllers (SMC) are designed in [142, 143] to track the desired position and yaw, and stabilization. For overall control design, the motion equations are considered in two parts: fully-actuated and under-actuated subsystems. The authors use a continuous approximation of sign function to avoid chattering effects in the controller. In [25], a feedback linearization-based controller is designed together with high order sliding mode (HOSM) observer against external disturbances such as wind and noise. The HOSM observer is also used for state measurements. Although the feedback linearization avoids nonlinearities, there still occurs the external disturbances. Hence, the HOSM observer is not only used to restraint the disturbances by estimation, but it also supports the stability and robustness of the closed-loop system.

[94] presents two nonlinear controllers based on either Feedback linearization (FL) and adaptive sliding mode (ASM) controllers. The FL controller is sensitive for external disturbances and sensor noises since it includes the high-order derivative terms. In the ASM, the controller has a robust structure to cancel model errors, external disturbances, and sensor noises. Without estimation of model uncertainties, sliding mode controller generates large input gains, and this causes application problems because of the motor-limitations of actual systems. Therefore, to avoid these uncertain effects, the authors use an adaptation in the SMC design. To make more easier analyses, the authors have simplified nonlinear dynamics for both control design.

For robust controllers against uncertainties and external disturbances, researchers have developed several control approaches such as robust nonlinear control methods, observers, robust compensators. In [27], the SMC based on disturbance observer is studied. This approach gives a robust continuous control in the presence of uncertainties and disturbances. The control design also avoids high control gains which cause inapplicable cases in practice. [139] presents a linear matrix inequality based controller gain synthesis. Using an approximate FL, the control gains are easily tuned. The design is not only achieved optimal gains for the cost function, but it also guarantees robust stability performance. [138] focuses on attitude performance. By using Lyapunov methodology, the nonlinear control design is developed to eliminate model uncertainties. The on-line estimation model is designed using a time-delay approach. Combining the anti-windup technique with the controller, the robustness of the system is proven.

Compared with the above mentioned robust designs, [102, 103, 104, 105] use a robust compensation approach combining with nominal control designs such as PD. The overall control design eliminates the effects of model nonlinearities, model uncertainties, and external disturbances. In these studies, nonlinearities and external disturbances are gathered into an uncertainty representation in the linear model, and they are taken as multiple uncertainties. Nonlinear dynamics are not ignored since they are taken into account as multiple uncertainties. Then, the robust decentralized control is designed within two control loops: the nominal control design which are position and attitude controllers, and the robust external compensator which deals with the control inputs. The nominal control design provides translational and rotational tracking. In the robust compensator, the system inputs are regulated. Combining the nominal control inputs and the compensator inputs, the effective control inputs are generated for the actual quadrotor UAV.

2.2.2 Quadrotor UAV Motion Control: Model Uncertainties

In some cases, quadrotor UAVs face model (dynamical) uncertainties while they operate to achieve trajectory tracking and stability objectives. These uncertainties come from unmeasurable or unknown parameters in the motion dynamics. One of the control techniques in the literature to solve dynamical uncertainties is adaptive control by using a direct method or estimating unknown parameters via an indirect method. Direct adaptive control approach updates uncertain parameters in control laws, directly. Indirect adaptive law is designed to estimate unknown parameters, separately and then calculating control gains.

In [115], the direct adaptive control is developed using backstepping methods for the tracking problem. Considering the unknown mass parameter, [73] uses an under-actuated model divided into three subsystems to design an adaptive backstepping controller. The authors use Lyapunov theorem to prove the stability of translational and yaw tracking. The stability analyses are considered to ensure adaptive control laws and estimation models. In [166], the authors develop on-line estimation laws to design a nonlinear adaptive regulation controller. In the proposed design, unknown parameters, moments of inertia, aerodynamic damping coefficients, length, and force-to-moment factor are estimated, then using estimated parameters, the effects of uncertainties are compensated via the control design. The stability of the system is proven by Lyapunov method under parametric uncertainties.

[45] presents a direct adaptive control application by using model reference adaptive control (MRAC) method. The control design is applied to the linearized model under parametric uncertainties. The authors also develop a nominal controller to compare performances of both design. The flight tests show that the MRAC design is more effective for robust responses than the nominal control design. In [46], nominal control, MRAC and combined/composite MRAC (CMRAC) design based on Lyapunov theorem are compared. The MRAC uses the direct adaptive method following [45]. In the CMRAC, the authors develop a combination of direct and indirect adaptive control. The proposed CMRAC aims to accomplish a smoother transient performance than others. All control designs are compared to each other using an indoor test facility. Both adaptive controllers give more robust responses against parametric uncertainties, in particular, actuator failure.

There are several studies on indirect adaptive control designs for linear models of quadrotor UAVs. A method proposed in [9] utilizes an indirect adaptive controller by using recursive least squares (LS) estimation for developing a linear parameter varying (LPV) controller. The study lacks altitude and yaw analyses. [89] presents an indirect adaptive linear quadratic controller (ALQC) considering inertial uncertainties for the pitch/roll dynamics. An on-line parameter identification (PI) is developed via the LS algorithm. In [33], an indirect mixing adaptive method is combined with the actuator failure problem.

Regarding intelligent estimation, [170] presents a neural network-based adaptive control under various uncertainties. In the design, the author uses a norm estimation approach instead of element-wise estimation to improve the real-time capability of the system, and the estimation method also saves the on-board computational resource. In [19], a radial basis function neural network (RBFNN) is used to approximate the perturbations and combined with backstepping. Adjustment of the RBFNN is based on on-line learning, and the RBFNN design does not need prior knowledge of uncertainties and disturbances.

Unlike most of the existing estimation based adaptive control literature, [119] develops a nonlinear function approximator, direct approximate, based on the Cerebellar Model Arithmetic Computer (CMAC). This method has fast adaptation and computation performance, and it is well-fit for applying with a direct adaptive controller. However, the control design has a weakness against sinusoidal disturbances. In the CMAC, the controller is adapted to the unknown payload and compensated disturbances. For the system robustness, the update method limits weight growth by catching large enough values to compensate the effects of unknown payloads. Under parametric and non-parametric uncertainties, a decentralized adaptive control method is presented in [114] to stabilize altitude and attitude dynamics and to cancel the effects of the uncertainties. The controller is asymptotically stabilized by a Lyapunov-based MRAC technique. Each dynamic channel is tuned by itself based on its error, and this model has a simple structure compared with existing adaptation methods. [63] uses a novel unified passivity-based adaption with the backstepping procedure to overcome the effects of the uncertain mass. The control approach consists of two main objectives which are velocity field following and timed trajectory tracking.

In some instances, uncertainties and disturbances are considered together to develop robust controllers. [167] presents a robust adaptive nonlinear control design to satisfy tracking performances. The robust integral of the signum of the error (RISE) method and the immersion/invariance-based adaptive control method are used in inner and outer loops of the quadrotor UAV to overcome the effects of parametric uncertainties and unknown external disturbances. Using Lyapunov and LaSalle's invariance-based analyses, the stability of the system is proven. In [76, 77], considering modeling error and disturbance uncertainties associated with aerodynamic and gyroscopic effects, payload mass, and other external forces/torques which come from the flying environment, the authors develop a robust adaptive tracking controller for nonlinear and linear models using the same control methodology. Using Lyapunov-energy function, the controllers are developed, and the stabilities are proven. For both, adaptive laws are designed to overcome modeling errors and disturbance uncertainties, and they do not need prior bound knowledge. In [77], PD-like control, gravity compensator, desired acceleration and desired angular acceleration models, and adaptive laws are combined to obtain position and attitude controllers.

In some cases, external uncertainties arise from disturbances such as external forces, wind, noises, etc. As a solution, disturbance rejection methods are used for these uncertainties. For constant wind disturbances, [34] present a globally stabilized robust path tracking controller by utilizing a disturbance rejection design. The control is based on Lyapunov-based backstepping methods to guarantee zero tracking error. Simulation and experimental results show the effectiveness and robustness of the design. In [148], the authors design a disturbance rejection control for internal and external disturbances in attitude dynamics. The design includes a robust disturbance-observer (DOB) and a nonlinear feedback control strategy. The DOB design uses an optimal approach, H_∞ theory, to overcome disturbance effects. The attitude tracking error model is developed using modified Rodrigues parameters (MRPs). The nonlinear feedback control is also based on backstepping techniques. In [147], the authors present another DOB based control strategy to overcome the effects of modeling error and external disturbances.

2.2.3 Quadrotor UAV Motion Control: Optimality

In the literature, one of the main control interests is to generate optimal control actions for quadrotor UAVs. These control methods provide effective control actions with optimal tracking and low energy consumption. Comparing with other control approaches, there are a few optimal control solutions applied to quadrotor UAVs. linear quadratic regulator (LQR), H_∞ and model predictive control (MPC) are generally used as earlier solutions.

In the earlier works, there firstly exist LQR implementations on linearized models [29, 30, 36]. The LQR method is combined with adaptive and fault tolerance solutions under parametric uncertainties in [33, 89]. These studies are experimentally validated, and the results show the effectiveness of adaptive LQR designs. Furthermore, H_∞ techniques are used in some studies. Despite several H_∞ strategies are developed using a linear model, there exists an H_∞ design for 2DOF based on the simplified nonlinear model in [37]. [125] present a nonlinear H_∞ control to stabilize rotation and to support backstepping strategy in translational, optimally. In [126], a robust nonlinear H_∞ control and integral MPC models are used for inner and outer loops in the overall design. As an optimal nonlinear control, [148] present a robust disturbance observer based on H_∞ strategy to provide a robust and optimal performance during the disturbance rejection.

Taking into account model constraints and disturbances, MPC is used as another optimal approach. [4] presents a robust and optimal MPC design under constraints and wind-gust disturbance for the attitude model. A set of Piecewise Affine (PWA) models is designed for each linearized subset attitude model. In [6], the authors extend the attitude

control [5] to the full motion control design. A switching MPC is used for translation and rotation dynamics. A robust MPC is designed in [7] to decrease the effects of disturbances for tracking performance. As existing optimal control methods, in [3], a constrained finite time optimal control (CFTOC) is designed to stabilize the experimental attitude model under constraints and wind disturbance. In another study, [156] uses L_1 optimal robust control for a quadrotor UAV system. The control strategies are developed using feedback linearization. The control design is implemented for no measurement noise and noise cases.

2.2.4 Fixed-wing UAV Motion Control

This subsection reviews control methodologies that are studied and applied to small fixed-wing UAVs in the earlier works. Regarding advanced nonlinear, optimal and adaptive approaches studied on the low-level control design of fixed-wing UAVs, the literature is restricted since the motion dynamics of fixed-wing UAVs are complicated and highly nonlinear [23, 55, 66, 106]. In some studies [20, 81, 133], fixed-wing UAVs are considered and studied as small vehicles with simplified kinematic and dynamic motion models to avoid highly nonlinearities. Therefore, by applying their control methods on the simplified models, the commanded heading angle, velocity, and altitude are generated for autopilot avionic devices which are inner-loop control equipment to generate actual motor inputs for aileron, elevator, rudder, and throttle. Furthermore, these control approaches can be efficiently utilized on unmanned ground vehicles (UGVs) for experimental validations in 2D since the simplified planar motion models of fixed-wing UAVs are well-suited to UGVs (since same non-holonomic motion characteristics). As a case study, [132] presents an experimental validation of the trajectory tracking control design by using a mobile robot platform as a fixed-wing UAV motion control at the fixed-level.

In [133], the authors develop a constrained nonlinear tracking control for the simplified kinematic and dynamic motion models of the fixed-wing UAV. The control model is designed with low-level altitude-hold, velocity-hold and heading-hold autopilots which are represented lateral and longitudinal motion. These autopilots reduce the 12-state strongly nonlinear model to 6-state equations of motion model which uses altitude, heading and velocity command inputs. Hence, using the 6-state motion model and considering system constraints, Control Lyapunov Function (CLF) approach is used for the overall control design. By the help of equipping low-level autopilots, [131] also uses an accurate 7-state kinematic model for nonlinear backstepping control to derive high-level velocity and roll angle control laws. In another study, [81] considers the kinematic model with the autopilots as low-level and develops a nonlinear model predictive control (NMPC) for the high-level controller before the low-level autopilot avionics. This study deals with solving

on-line an optimal trajectory tracking problem under limited turn. In [20], the authors use the Piccolo-controlled model, which is another simplified motion model with autopilots, to develop a Lyapunov-based backstepping controller in lateral and longitudinal motion. For lateral motion tasks, [61] presents a direct model reference adaptive approach with constant speed for the low-level heading control. As a realistic perspective, [18] presents the state estimation techniques via various methods and real-time sensors equipped with the fixed-wing UAV. It also discusses the control and stability details of autopilot avionics before the decoupled lateral and longitudinal dynamics controllers. As for adaptive, optimal and nonlinear control solutions at the high (guidance) control level, [55, 128, 160, 168] present path-following laws before the low-level control design.

2.3 Literature on Multi-UAV Formation Control

In the literature, various formation control architectures have been used. Regarding formation control schemes, there exist two main approaches: centralized and decentralized. The Centralized approach offers a global decision-making unit for multi-agent systems, and complexities may occur in mathematical analyses of large-scale systems. However, the Decentralized (distributed) approach provides a sub-decision making units for each agent in multi-agent systems. Hence, the distributed approach is more practical and easy to implement on real systems. In another categorization based on interaction topology of multi-agent systems, formation structures have been classified as hierarchical and non-hierarchical. For these structures, there are three main approaches used in the literature, namely, leader-follower, virtual-leader and behavioral-based [11, 15, 42]. The leader-follower approach works in a hierarchy and does not need sophisticated sensors in most cases. This approach depends on leader performance. The virtual-follower method uses a virtual leader for each agent to follow with non-hierarchy. This approach needs more complex communication capabilities; however, its performance is more robust than leader-follower. The behavioral-based approach needs predefined behaviors, such as formation-keeping and obstacle-avoidance. This approach mostly needs more complex computing capabilities. Moreover, symmetrical and asymmetrical information flows have been used in hierarchical and non-hierarchical patterns to ease the communication complexities.

A survey study [120] gives another overview of formation control for multi-agent systems based on sensing and interaction topology. So that, three categories are presented position-based, displacement-based, and distance-based controls. Position-based controls are usually not required interaction topologies, but they need long-range and more advanced sensors. Distance-based controls need interaction topology (rigid or persistence)

among members of multi-agent systems. The distance-based controls have sensing advantages since they only need inter-agent distances. In displacement-based controls, both sensing capabilities and interaction topologies of multi-agent systems are used equally. In the above categorizations, authors have been reviewed literature mostly depending on sensed variables, controlled variables, coordinate systems, and interaction topology.

In distanced-based control of an asymmetric (directed), hierarchical formation, a rigid or persistent interaction (communication) graph is needed to achieve desired positions and then maintain desired formation shape by controlling inter-agent distances. Hence, algebraic graph theory is used to design required communication topologies in this kind of formation structures. For graph theory analyses, the literature mostly considers single-integrator agents and lacks local (individual) control performance effects on formations. Graph rigidity and formation stabilization are discussed with detail in the earlier studies [12, 121, 163]. In particular, [20, 53] discuss cohesive motion control tasks using the distributed approach and present general characteristics of cohesive motion tasks.

In some of the recent works, formation control designs are studied for multi quadrotor and fixed-wing UAV systems. [123] examines a distributed formation control design with the robust local controller utilized on multi-quadrotor helicopters. In [59], using a nonlinear dynamic model in the leader-follower structure, a consensus-based formation control is designed for a two-quadrotor system. Using directed topology in the formation graph, [150] also studies a consensus problem for a multi-quadrotor system under bounded disturbance. [60] deals with the impact of communication design over information flows of directed and undirected graphs for the consensus task of the multi-quadrotor systems. [20] present a distributed cohesive motion control for multiple fixed-wing UAV and quadrotor systems. The study introduces solutions for the maintenance of rigid and persistent motion during trajectory tracking tasks. In [61], the authors present a distributed formation control using more realistic lateral motion dynamics for surveillance tasks of the multi fixed-wing UAV system. Using range-based measurement, [165] study a rigidity maintenance control for a multi-UAV system. Using simplified quadrotor motion dynamics, [38, 137] study nonlinear control approaches combined with formation level. As N-vehicle cases, [81, 82] present single-integrator model based formation control designs for a group of the quadrotor UAVs in 2D. The authors do not consider the performance effects of local controllers of the quadrotor UAVs on formation maintenance and robustness, especially, in case of modeling issues on actual quadrotor UAVs such as uncertainties or disturbances.

As discussed above the studies, literature mostly focuses on high-level control and stability using simple models such as single or double integrator dynamics. However, literature lacks low-level control design and analysis to study and compensate the effect of realistic model issues such as uncertainties and disturbances on formation maintenance.

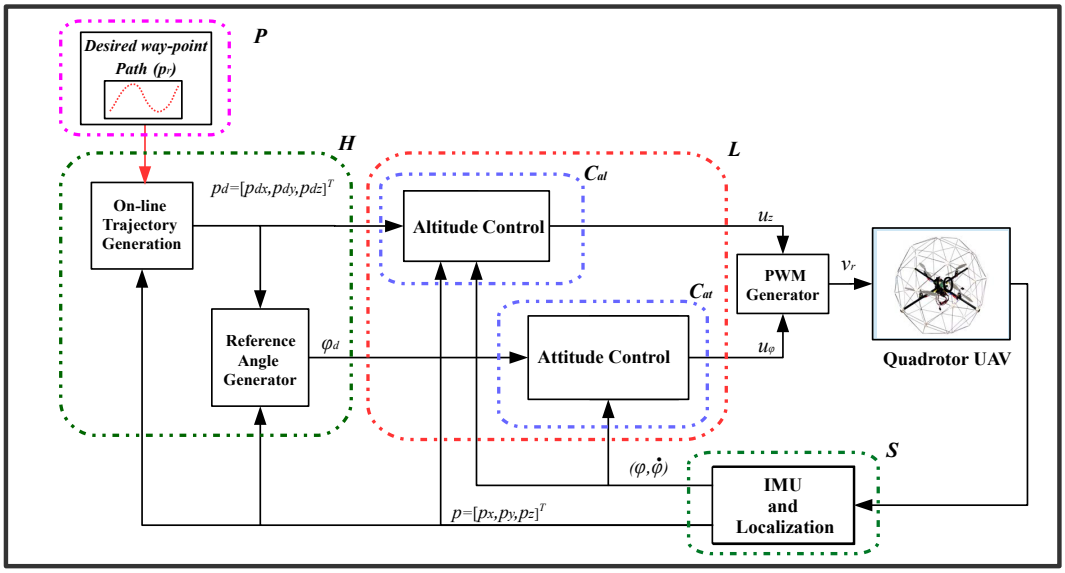

Figure 2.3: Motion control architecture of quadrotor UAVs [90].

2.4 Single UAV Motion Control Architecture

In this section, single UAV motion control architectures of quadrotor and small fixed-wing UAV systems are discussed and presented as follows.

2.4.1 Quadrotor UAVs

Motion control architecture of quadrotor UAVs within navigation, guidance, and control (NGC) systems consists of path planner (P), control schemes (H and L) and system sensors (S) as seen in Figure 2.3. The control system (CS) is considered in the two-level as high-level (H) and low-level (L). The separated dynamics (2.12)-(2.19) are located into the reference angle, altitude and attitude models to accommodate the proposed two-level control structure. In the CS, the on-line trajectory generator provides the desired positions $p_d(t)$. Reference angle model is responsible for generating the desired attitude angles $\varphi_d(t) = [\phi_d(t),\ \vartheta_d(t),\ \psi_d(t)]^T$. The reference angle generator and the attitude dynamics (C_{at}) provide lateral and attitude motion of the quadrotor UAV as a cascade control system. The altitude dynamics (C_{al}) controls the longitudinal motion. In the low-level, control laws generate control signals $u_z(t)$ and $u_\varphi(t)$. Then, the control signals are converted to actuator PWM motor inputs $v_r(t)$ by using the equation (2.5).

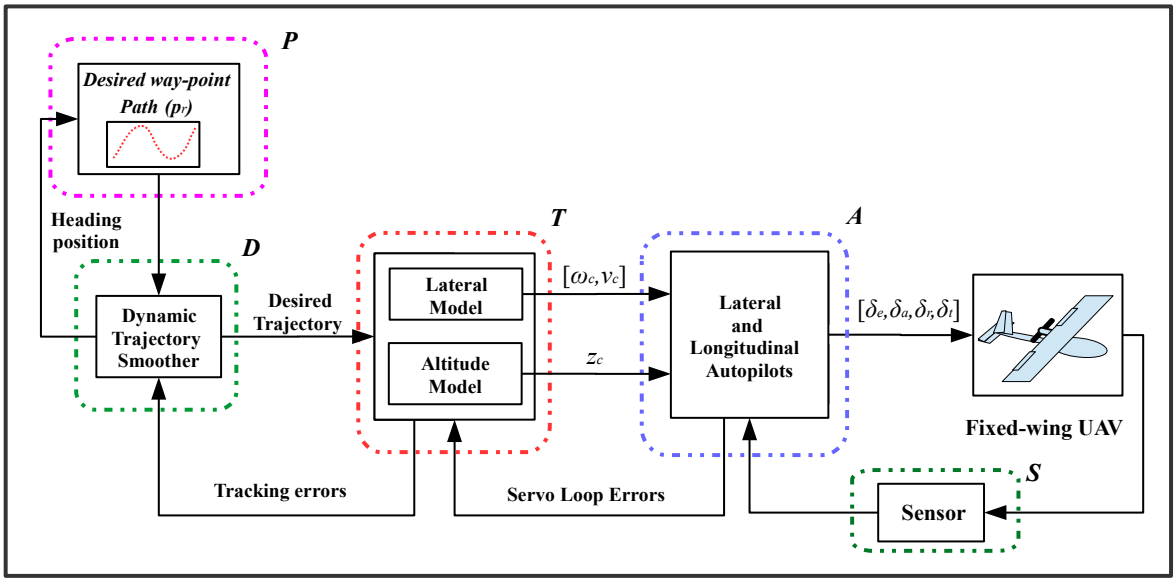

Figure 2.4: Motion control architecture of small fixed-wing UAVs [133].

2.4.2 Fixed-wing UAVs

As studied in [23, 133], motion control architecture of small fixed-wing UAVs within NGC systems consists of five main parts: path planner (P), trajectory smoother (D), trajectory tracker (T), low-level autopilots (A) and sensors (S) as shown in Figure 2.4. In the navigation system (NS), hardware equipment and estimation algorithms are used to sense system states. In the guidance system (GS), trajectory smoother generates a more smooth desired trajectory using generated way-points and tracking errors. Since fixed-wing UAV motion dynamics is represented by the highly nonlinear model, the control system (CS) is considered in two control parts. At the first part, the trajectory tracker T, the simplified motion model (2.26) is used to design controllers. The separated dynamics (2.28)-(2.32) of the simplified model are located into lateral and altitude models as presented in Section 2.1.2 to accommodate the proposed two-level control structure. Then, trajectory tracker T within the two-level control structure generates velocity, angular velocity and altitude commands to the autopilots. The second part is autopilot devices, and they are responsible for generating actual motor inputs of aileron, elevator, rudder, and throttle using control commands generated in the first control part.

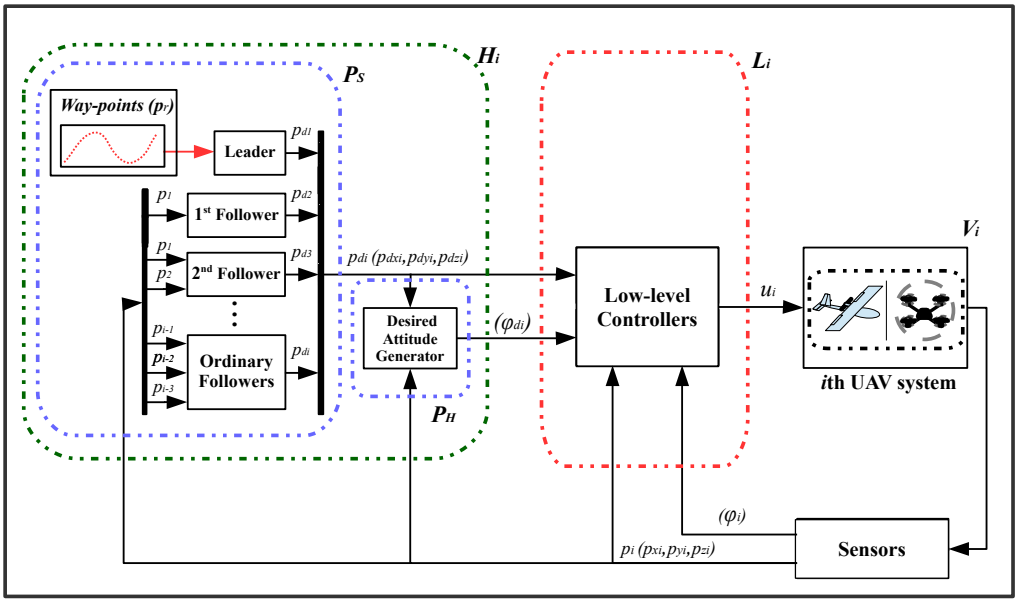

Figure 2.5: Formation control architecture of multi-UAV systems.

2.5 Multi-UAV Formation Control Architecture

This section presents a distributed formation control architecture of multi-UAV systems as shown in Figure 2.5 where high (formation) level control design is separated from low (individual) level motion control design via the proposed two-level control structure. In the two-level structure of the distributed formation control architecture, the high (formation) level controller (H_i) of ith UAV is designed using a hierarchal *leader-follower* formation, and it consists of two submodules. Formation supervisor (P_S) and desired attitude generator (P_H) generate the desired position and attitude to guide ith UAV for formation maintenance. In the low-level (L_i), proposed control laws are designed for ith individual UAV tracking control as well as maintaining desired formation shape via the guidance of the formation level module. Actual control inputs $u_i(t)$ of the ith UAV system are generated in this level control.

Chapter 3

Adaptive Linear Quadratic Attitude Tracking Control with Sensor Fusion

3.1 Introduction

In the literature, various control approaches have been proposed for quadrotor UAV systems as discussed in Chapter 2. For attitude tracking control and stabilization, researches have developed solutions such as quaternion-based feedback control for exponential attitude stabilization [145], robust adaptive attitude tracking control [95], robust attitude control for uncertain quadrotors with proportional-derivative (PD) controller combined with a robust compensator [102], robust nonlinear design under uncertainties and delays [105], and fractional sliding modes based attitude control [78].

One of the main control interests for quadrotors UAV is optimization of time and energy (battery) consumption by designing optimal path planning and optimal tracking control. For such optimal attitude tracking, [30] has designed a linear quadratic regulation (LQR) based attitude stabilization. For solving a more general form of the same problem under wind gust disturbances, a switching model predictive attitude controller is developed in [5]. [156] presents L_1 optimal robust tracking control to compensate persistent disturbances in translational and rotational (attitude) dynamics.

Linear-quadratic (LQ) based optimal control frameworks constitute a systematic toolset for calculating ideal control gains with guaranteed system stability under LQ design conditions. LQ-based control schemes provide robust and precise steady-state tracking while the performance index (quadratic cost function) adjusts optimality trade-off between track-

ing/regulator performance and battery consumption. A particular LQ-based control approach is infinite-horizon optimal regulation based on linear time-invariant (LTI) models. This approach is widely used in real-time applications since its solution does not have computational complexities for obtaining constant state-feedback control (Kalman) gains by solving algebraic Riccati Equation (ARE). The infinite-horizon LQR has been mostly used in many earlier works as studied for the quadrotor UAV in [30] for attitude state regulation and stability.

On the other hand, Linear-quadratic tracking (LQT) problems have gained less attention compared to LQR problems, since time-varying reference trajectories lead to further analysis and computational complexities. LQT control schemes typically consist of two state-feedback and feed-forward terms. The state-feedback terms guarantee system stability by state-feedback (Kalman) gains which are calculated off-line solving differential Riccati equation (DRE). The feed-forward terms provide optimal tracking of time-varying bounded reference trajectories utilizing differential auxiliary vector signal equation. In practice, computational complexities arise because of the time variations in the feed-forward terms. Accordingly, the literature on LQT control design and applications on real-time systems is limited. [17] presents an off-line solution to the infinite-horizon LQT problem by solving the feed-forward term based on calculating the initial condition of the auxiliary vector signal. The authors present a real-time implementation of this solution on flexible beams system in [2]. Other than the classical solution, [113] presents an on-line reinforcement learning algorithm to solve LQT problem without requiring the knowledge of the system drift dynamics or the command generator dynamics.

Regarding LQT of quadrotor UAV systems, [161] presents a finite-horizon LQT control design with time-varying control gains which are calculated solving off-line discrete time matrix Riccati equations for the linearized full dynamics of the quadrotor UAV. Consideration of finite-horizon LQT with known boundary conditions at the initial and final time instants prevents the computational complexity issues with implementation of this design. However, in many practical cases, including the cases considered in this chapter, since the boundary conditions are unknown, infinite-horizon LQT needs to be considered for designing an alternative optimal linear tracking controller.

In this chapter, by the motivations of LQ-based optimal control advantages as stated above and lack of infinite-horizon LQT control schemes with their applications on real-time systems in literature, we present an infinite-horizon LQT control design, its practical solution and its experimental validation on the real-time quadrotor UAV with inertial parametric uncertainties and Inertial Measurement Unit (IMU) sensor noises. Furthermore, to improve robustness against parametric uncertainties, the presented LQT control design is combined with an adaptive parameter identification (PI) scheme based on least-squares

(LS) estimation. Combining the LQT control design and the PI scheme, an adaptive LQT (ALQT) control scheme is developed for optimal attitude tracking of quadrotor UAVs, with reduced tracking error and battery consumption.

Reliable attitude estimation is one of the main challenges for quadrotor UAV tracking control. Euler angles (ϕ, ϑ and ψ) and Quaternions are two common types of attitude representation for UAV systems. IMUs, formed by 3-axis inertial sensors of gyroscopes, accelerometers and magnetometers, measures angular velocities, linear accelerations and the Earth's magnetic field. Ideally, accelerometer measurements or numerical integration of angular velocities of gyroscopes should be enough for ideal sensors to determine attitude angles. However, in real-world conditions, individual usage of these sensors is not sufficient to determine attitude angles due to large amounts of system noise, drift errors and vibrations.

To obtain fast and accurate attitude states, sensor fusion techniques have been applied to IMU measurements, including wide ranges of complementary filters [14, 26, 65, 101, 109, 110, 153, 158] and Kalman filters [49, 52, 54, 65, 67, 87, 98, 101, 111, 129, 145, 151, 154, 155]. A complementary filter typically combines accelerometer output for low-frequency attitude estimation with integrated gyroscope output for high-frequency estimation. Complementary filters are computationally less demanding, and due to their simplicity and efficiency, these filters are still used for attitude estimation. A variety of complementary filters has been used to estimate attitude quaternions [109, 110, 158] or Euler angles for relatively small roll and pitch aerial vehicle angles [14, 65, 101, 145]. Complex rotations of simultaneous roll, pitch and yaw angles require nonlinear complementary filter fusion techniques [130].

Kalman filter is an optimal recursive estimation scheme that uses a system's dynamic model, known control inputs, and multiple sequential measurements from sensors to form an estimate of the system states fusing prediction and measurement on-line [47, 52, 67, 129, 151]. The extended Kalman filter (EKF) is developed for nonlinear system state estimation and has been widely used for real-time UAV systems for Euler angle based attitude estimation [49, 54, 65, 101] as well as quaternion based attitude estimation [87, 98, 111, 154, 155]. Unscented Kalman filter (UKF) [29, 40, 43, 159] and adaptive Kalman filter (AKF) [100] are another widely used sensor fusion algorithms. In [49], a novel Kalman filter algorithm is proposed, which consists of an EKF and an inverse Φ-algorithm in a master-slave configuration to estimate reliable angular acceleration signals by fusing IMU sensor data. In [98], it is shown that even for applications with strong real-time constraints, EKF can properly estimate the UAV attitudes, even in the presence of data loss.

As discussed in Chapter 2 and the earlier work [90], we consider the quadrotor UAV con-

trol structure in two levels: high-level and low-level. High-level is mainly about guidance and position controlling in the autonomous motion tasks and generating the trajectories to be tracked by the low-level controller. Provided the trajectory from high-level, the low-level control is responsible for the quadrotor UAV's attitude and altitude tracking performance and stability. In this chapter, we focus on the low-level control design, following a decentralized approach, considering the three motion dynamics modes separately: adaptive LQT control for the attitude dynamics, proportional (P) control for the yaw dynamics, and proportional-integral-derivative (PID) control for the altitude dynamics, as shown in Figure 3.1. In the overall structure, the attitude measurement noises, which come from IMU sensors, are compensated using a Kalman filter to obtain a more reliable attitude estimation. The effectiveness of the employed Kalman filter is investigated over the experiments that compare the Kalman filter results with a complementary filter. In the next step, we developed an infinite-horizon ALQT controller and validated its effectiveness by performing two set of experiments.

3.2 Quadrotor UAV Dynamics

A nonlinear dynamic model of quadrotor UAV motion dynamics (2.10) is presented in Chapter 2. In this chapter, we have simplified and partitioned this nonlinear dynamic model to obtain separate linear models for each of attitude, yaw, and altitude dynamics.

3.2.1 Attitude Model

Ignoring inertial and drag effects, we obtain a linearized attitude (roll/pitch) dynamics from (2.17)-(2.19) of the nonlinear dynamic model (2.10). Hence, we write the attitude model in the state-space form as

$$\begin{aligned} \dot{x}_\varphi(t) &= A_\varphi x_\varphi(t) + B_\varphi u_\varphi(t), \quad \varphi \in \{\vartheta, \phi\}, \\ \varphi(t) &= C_\varphi x_\varphi(t), \end{aligned} \tag{3.1}$$

where $A_\varphi = \begin{bmatrix} 0 & 1 & 0 \\ 0 & 0 & \frac{2lK}{J_\varphi} \\ 0 & 0 & -b \end{bmatrix}$, $B_\varphi = \begin{bmatrix} 0 \\ 0 \\ b \end{bmatrix}$, $C_\varphi = \begin{bmatrix} 1 \\ 0 \\ 0 \end{bmatrix}^T$ and $x_\varphi = \begin{bmatrix} \varphi \\ \dot{\varphi} \\ T_\varphi \end{bmatrix}$. x_φ, u_φ, φ, $\dot{\varphi}$, T_φ, J_φ, K, b and l represent states, control inputs, Euler angles, angular velocities, thrust forces, rotational inertias, positive armature gain, the actuator bandwidth in attitude (roll/pitch) dynamics and the distance between the center of gravity O_b and each propeller, respectively.

Remark 3.2.1. *Attitude (φ) dynamics represents roll (ϑ) and pitch (ϕ) dynamics, and yaw (ψ) is separated from attitude dynamics for the proposed control design.*

3.2.2 Yaw Model

We obtain linearized yaw dynamic as

$$\ddot{\psi} = \frac{4K_{\psi}K}{J_{\psi}} \frac{b}{(s+b)} u_{\psi}, \tag{3.2}$$

where u_{ψ} is the yaw control input, K_{ψ} is thrust-to-moment gain and J_{ψ} is the rotational inertia in yaw motion. Finally, we write the linearized yaw model in form of an input-output transfer function as:

$$\psi = \frac{4K_{\psi}Kb}{s^2(s+b)J_{\psi}} u_{\psi}. \tag{3.3}$$

3.2.3 Altitude Model

We have linearized the nonlinear altitude model (2.14)-(2.16) by the use of small angle approximation and taking the effect of gravity as an offset in the linearized model. Accordingly, we obtain the simplified linear altitude model as

$$\ddot{p}_z = \frac{4K}{m} \frac{b}{(s+b)} u_z, \tag{3.4}$$

where p_z is z-position of O_b, u_z is the altitude control input and m is the total mass of the quadrotor UAV system. Finally, we obtain the linearized altitude model in the form of an input-output transfer function as

$$p_z = \frac{4Kb}{s^2(s+b)m} u_z. \tag{3.5}$$

3.3 Problem Statement

Considering a quadrotor UAV with attitude (roll/pitch) dynamics (3.1), yaw dynamics (3.3), and altitude dynamics (3.5), as illustrated in Figure 3.1, the objectives of this chapter are threefold:

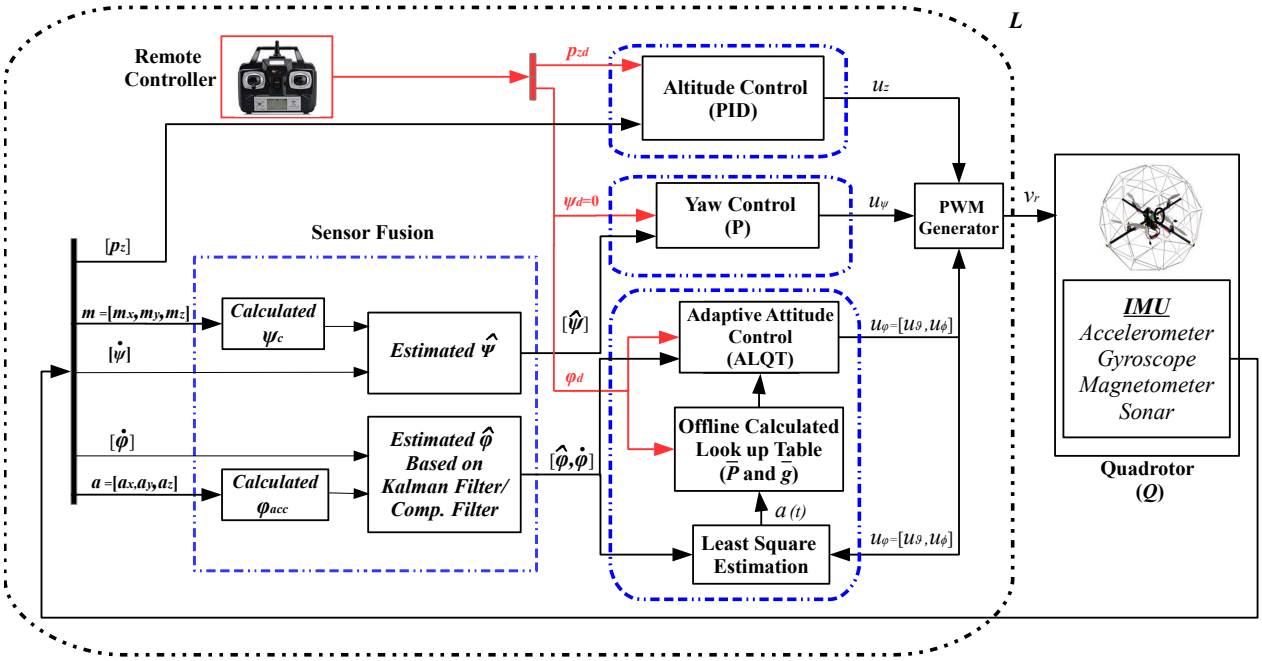

Figure 3.1: The overall quadrotor UAV control block diagram.

1. Given the IMU sensor measurements of the attitude angles, design a data fusion algorithm based on (i) Kalman filtering and , for comparative analysis purposes, (ii) complementary filtering, to cancel the IMU sensor noise effects and produce accurate attitude state estimates

2. Design the control units to generate the command signals u_z, u_ψ, u_ϑ, u_ϕ for feeding the PWM generator that generates the motor control input signal v_r, per the diagram in Figure 3.1: (a) Design an infinite-horizon ALQT controller to generate the optimal attitude control signal $u_\varphi(t) = u^*_\varphi(t)$ so that $\varphi(t)$ tracks its desired trajectory $\varphi_d(t)$, minimizing the predefined quadratic performance optimal tracking and energy consumption *cost function*

$$J = \frac{1}{2}\int_0^\infty (Qe^2_\varphi(t) + Ru^2_\varphi(t))dt, \tag{3.6}$$

where Q and R are positive constant weighting terms and

$$e_{\varphi}(t) = \varphi(t) - \varphi_d(t) \tag{3.7}$$

is the attitude tracking *error*. (b) Design a P yaw controller to generate $u_{\psi}(t)$ and a PID altitude controller to generate $u_z(t)$.

3. Combining the designs in 1 and 2, above, real-time implement and experimentally validate the overall control scheme

3.4 Control Approach

In our infinite-horizon ALQT control design, the optimal control law consists of two terms: the state-feedback and the feed-forward. The state-feedback term maintains the stability of the attitude dynamics. This term is obtained solving an algebraic Riccati equation (ARE). The feed-forward term depends on the desired trajectory and is used for establishing trajectory tracking performances. The above optimal control law is combined with an LS based adaptive PI algorithm to make it robust, adaptive and avoid inertial uncertainties in the attitude dynamics. After this combination, because of the uncertainties, the ARE needs to be solved on-line as well. In the implementation, by comparing the on-line estimates of the uncertain parameters with some critical parameters calculated and stored in a look-up table, the time-varying state-feedback (from the PI) and then the time-varying feed-forward (from slowly-varying desired attitude and the PI) terms are calculated on-line. In the real-time implementation of the designed ALQT scheme, we utilize a practical real-time computation technique based on parameterized analytical solutions of the state-feedback and the feed-forward terms.

3.5 IMU Sensor Data Fusion

The quadrotor UAV needs a robust estimation scheme for denoising the attitude angle measurements to provide reliable feedbacks to the proposed ALQT control scheme. The attitude angles are measured using an ADIS16405 IMU as shown in Figure 3.2. Then a Kalman filter is employed to attenuate the effect of measurement noises. The IMU contains a 3-axis gyroscope to measure angular velocities $(\dot{\vartheta}, \dot{\phi}, \dot{\psi})$, a 3-axis accelerometer to measure accelerations due to Earth's gravity (a_x, a_y, a_z) and a 3-axis magnetometer to measure the magnetic field intensities (m_x, m_y, m_z). The specifications are listed in Table 3.1.

Table 3.1: The ADIS16405 IMU Specifications [171].

	Gyroscope	Accelerometer	Magnetometer
Range	$\pm 305(deg/s)$	$\pm 18(g)$	$\pm 3.5(gauss)$
Sensitivity	$0.05(deg/s/LSB)$	$3.33(mg/LSB)$	$0.5(mgauss/LSB)$

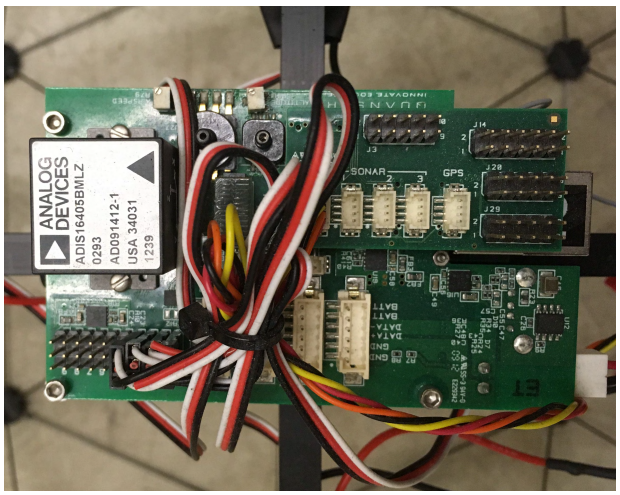

Figure 3.2: The ADIS16405 IMU Module on the Qball-X4 quadrotor UAV.

3.5.1 Attitude Determination from IMU Sensors

Roll and pitch angles are obtained based on accelerometer and gravity vector relation. The rotation matrix from the body frame to the inertial frame is defined with the Euler angles as:

$$R_{b2i} = \begin{bmatrix} \cos\psi\cos\vartheta & -\sin\psi\cos\phi + \cos\psi\sin\vartheta\sin\phi & \sin\psi\sin\phi + \cos\psi\sin\vartheta\cos\phi \\ \sin\psi\cos\vartheta & \cos\psi\cos\phi + \sin\psi\sin\vartheta\sin\phi & -\cos\psi\sin\phi + \sin\psi\sin\vartheta\cos\phi \\ -\sin\vartheta & \cos\vartheta\sin\phi & \cos\vartheta\cos\phi \end{bmatrix}. \tag{3.8}$$

Assuming constant translational velocities [49, 152], i.e., ignoring translational accelerations, we obtain the following relation between the accelerometer output, rotation matrix

and earth gravity:

$$\begin{bmatrix} a_x \\ a_y \\ a_z \end{bmatrix} = R_{i2b} \begin{bmatrix} 0 \\ 0 \\ g \end{bmatrix} = \begin{bmatrix} -\sin\vartheta \\ \cos\vartheta\sin\phi \\ \cos\vartheta\cos\phi \end{bmatrix} g, \tag{3.9}$$

where $R_{i2b} = R_{b2i}^T$. From (3.9), attitude angles are calculated as

$$\varphi_{acc} = \begin{bmatrix} \vartheta_{acc} \\ \phi_{acc} \end{bmatrix} = \begin{bmatrix} \text{atan2}(-a_x, \sqrt{a_y^2 + a_z^2}) \\ \text{atan2}(a_y, a_z) \end{bmatrix}, \tag{3.10}$$

where $\text{atan2}(a_y, a_z)$ denotes arc tangent of a_x and a_y while it uses the signs of both arguments to determine the quadrant of the result. By determining the roll and pitch angles, the rotation matrix from the body frame to the magnetometer local (NED:North-East-Down) frame is rearranged as

$$\begin{bmatrix} m_x \\ m_y \\ m_z \end{bmatrix} = \begin{bmatrix} \cos\vartheta & \sin\vartheta sin\phi & \sin\vartheta\cos\phi \\ 0 & \cos\phi & -\sin\phi \\ -\sin\vartheta & \cos\vartheta\sin\phi & \cos\vartheta\cos\phi \end{bmatrix} \begin{bmatrix} m_{xb} \\ m_{yb} \\ m_{zb} \end{bmatrix}. \tag{3.11}$$

Hence, yaw (heading) is calculated as

$$\psi_c = \left[\text{atan2}(m_y, m_x)\right]. \tag{3.12}$$

In practice, the yaw (heading) is updated by gyroscope data integration instead of a Kalman filter or a complementary filter since the laboratory environment has magnetic (metallic) disturbances on the heading calculation (3.12). Solution methods of magnetic disturbances on heading calculation are discussed with the details in [50].

3.5.2 Attitude Estimation Using Kalman Filter

To filter IMU accelerometer noises, a linear Kalman filter is employed in this chapter. At each time step k, this Kalman filter first predicts the state propagation using the dynamic model of the quadrotor UAV, the control inputs applied at step $k-1$ and the state measurement at step $k-1$. Then, it incorporates new measurement data of step k, to determine the state estimate.

Consider the following discrete-time linear time-invariant model of the attitude dynamics, with additive Gaussian measurement noise and disturbance, based on (3.1):

$$x[k+1] = A_{\mathrm{d}}x[k] + B_{\mathrm{d}}u[k] + w, \tag{3.13}$$
$$y[k] = C_{\mathrm{d}}x[k] + v, \tag{3.14}$$

where w is zero mean Gaussian disturbance noise with covariance Q_{K}, v is zero mean Gaussian measurement noise with covariance R_{K}, and

$$A_d = \begin{bmatrix} 1 & T_s & 0 \\ 0 & 1 & \frac{2lK}{J_\varphi}T_s \\ 0 & 0 & 1 - bT_s \end{bmatrix}, B_d = \begin{bmatrix} 0 \\ 0 \\ bT_s \end{bmatrix}, C_d = \begin{bmatrix} 1 & 0 & 0 \\ 0 & 1 & 0 \end{bmatrix}, \tag{3.15}$$

with sampling time T_s. Note that in implementation of (3.15), since the value of the rotational inertia J_φ is uncertain, the nominal value of this parameter is used, as detailed in Remark 3.6.1 in Section 3.6.1. For this system model, the Kalman filter prediction and update equations are as follows.
Prediction:

$$\hat{x}[k+1|k] = A_{\mathrm{d}}x[k|k] + B_{\mathrm{d}}u[k], \tag{3.16}$$
$$P[k+1|k] = A_{\mathrm{d}}P[k|k]A_{\mathrm{d}}^T + Q_{\mathrm{K}}, \tag{3.17}$$

Update:

$$\bar{y}[k] = y[k] - C_{\mathrm{d}}\hat{x}[k|k-1], \tag{3.18}$$
$$M[k] = P[k|k-1]C_{\mathrm{d}}^T(C_{\mathrm{d}}P[k|k-1]C_{\mathrm{d}}^T + R_{\mathrm{K}})^{-1}, \tag{3.19}$$
$$\hat{x}[k|k] = \hat{x}[k|k-1] + M[k]\bar{y}[k], \tag{3.20}$$
$$P[k|k] = (I - M[k]C_{\mathrm{d}})P[k|k-1]. \tag{3.21}$$

where $P[k+1|k]$ and $M[k]$ are the predicted error covariance and the optimal Kalman gain, respectively.

Remark 3.5.1. *Measurement covariance matrix is specified by calculating the variance of the sensor noise from off-line sample measurement of IMU sensors. Disturbance covariance matrix is tuned by trial and error method via experimental tests. The states are initialized at zero and the sampling time is selected same as used in overall experiment design.*

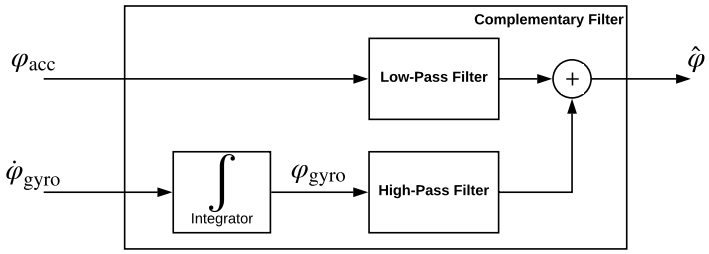

Figure 3.3: Complementary Filter.

3.5.3 Attitude Estimation by Complementary Filter

As an alternative to Kalman filtering, we also study the utilization of complementary filter in denoising and fusion of measurement data from accelerometers and gyroscopes. Typically, an accelerometer based orientation estimation works better in static conditions, and on the other hand a gyroscope based orientation estimation gives better results in dynamic conditions. A complementary filter passes the accelerometer signals through a low-pass filter and the gyroscope signals integral through a high-pass filter. Then, the resulting signals are summed up to estimate the attitude angles more reliably in both dynamic and static condition cases. The schematic complementary filter block diagram is depicted in Figure 3.3.

3.6 Adaptive Optimal Attitude Tracking Control Design

In this section, the proposed ALQT control scheme for attitude tracking of a quadrotor UAV is presented.

3.6.1 Adaptive Parameter Identification Scheme

We employ an LS based PI scheme to estimate the uncertain inertial parameters. From the attitude dynamics equation (3.1), following the procedure in [74, 89], we first define a linear parametric model avoiding the need for signal differentiation and the associated

noise sensitivity issue by use of the stable filter $\frac{1}{(s+\lambda)},\ \lambda > 0$, as follows:

$$z_\varphi = \theta_\varphi^* \Phi_\varphi, \tag{3.22}$$
$$z_\varphi = \frac{s}{(s+\lambda)}\dot{\varphi}, \theta_\varphi^* = \frac{1}{J_\varphi}, \Phi_\varphi = \frac{2lKb}{(s+\lambda)(s+b)}u_\varphi,$$

noting that the Euler rate $\dot{\varphi}$ (obtained using the IMU and the filters in Section 3.5) and the control signal u_φ are measurable, and l, K, b are known constant parameters.

Assumption 3.6.1. *The upper and lower limits of $\theta_\varphi^*(t)$ are known, i.e. $0 < \underline{\theta}_\varphi \leq \theta_\varphi^*(t) \leq \bar{\theta}_\varphi$ for some known $\underline{\theta}_\varphi, \bar{\theta}_\varphi > 0$.*

Remark 3.6.1. *For the setup used in this chapter, the limits of $\hat{\theta}_\varphi(t)$ are taken $10 \leq \hat{\theta}_\varphi(t) \leq 49$. Accordingly, the nominal value of J_φ is calculated as $J_{\varphi 0} = \frac{2}{\underline{\theta}_\varphi + \bar{\theta}_\varphi} \approx 0.03$.*

To generate the estimate $\hat{\theta}_\varphi$ of the uncertain inertia parameter θ_φ^*, we apply the following recursive LS algorithm [74] based on the parametric model (3.22):

$$\dot{\hat{\theta}}_\varphi(t) = Pr(\mathbf{P}(t)\epsilon(t)\Phi_\varphi(t)) = \begin{cases} \mathbf{P}(t)\epsilon(t)\Phi_\varphi(t), & \text{if } \underline{\theta}_\varphi < \hat{\theta}_\varphi < \bar{\theta}_\varphi \\ 0, & \text{otherwise} \end{cases}, \quad \hat{\theta}_\varphi(0) = \hat{\theta}_{\varphi 0}, \tag{3.23}$$
$$\dot{\mathbf{P}}(t) = \begin{cases} \beta \mathbf{P}(t) - \frac{\Phi_\varphi^2(t)}{m_n^2(t)}\mathbf{P}^2(t), & \text{if } \underline{\theta}_\varphi < \hat{\theta}_\varphi < \bar{\theta}_\varphi \\ 0, & \text{otherwise} \end{cases},$$
$$\epsilon(t) = \frac{z_\varphi(t) - \hat{\theta}_\varphi(t)\Phi_\varphi(t)}{m_n^2(t)}, \qquad m_n^2(t) = 1 + \alpha_n \Phi_\varphi^2(t), \quad 1 \gg \alpha_n > 0,$$

where $\mathbf{P}(t)$ is the positive covariance (time varying gain) term with $\mathbf{P}(0) = \mathbf{P}_0 > 0$, m_n is the normalizing signal, and ϵ is the estimation error. $Pr(.)$ is a projection operator which maintains $\hat{\theta}_\varphi \in [\underline{\theta}_\varphi, \bar{\theta}_\varphi]$.

Lemma 3.6.2 (Stability and Convergence)**.** *Consider the LS based PI scheme (3.23), applied to the attitude dynamics (3.1). It is guaranteed that all the signals in (3.23), including $\mathbf{P}$ and $\mathbf{P}^{-1}$, are bounded and $\hat{\theta}_\varphi \in [\underline{\theta}_\varphi, \bar{\theta}_\varphi]$. Further, if $\Phi_{\varphi n} = \frac{\Phi_\varphi}{m_n}$ is persistently exciting, i.e. if $\frac{1}{T}\int_t^{t+T} \Phi_{\varphi n}^2 d\tau \geq \alpha_0$ for all $t \geq 0$ and some $T, \alpha_0 > 0$, then (3.23) ensures that $\theta_\varphi(t) \to \theta_\varphi^*$ as $t \to \infty$. The convergence of $\theta_\varphi(t) \to \theta_\varphi^*$ is exponential for $\beta > 0$.*

Proof. The result is a direct corollary of the more general Theorem 3.7.4 and 3.10.1 in [74]. □

3.6.2 Generic Linear Quadratic Tracking Control Design

To construct the base optimal control law of the proposed ALQT scheme, we follow an infinite-horizon LQT control design approach [116], explained in the sequel for a linear system in the generic state-space form

$$\begin{aligned} \dot{x}(t) &= Ax(t) + Bu(t), \\ y(t) &= Cx(t), \end{aligned} \tag{3.24}$$

where $x \in \Re^n$, $u \in \Re^r$ and $y \in \Re^m$ are state, control input and output vectors. $A \in \Re^{n\times n}$, $B \in \Re^{n\times r}$ and $C \in \Re^{m\times n}$ are state, input and output matrices. m, n, and r are generic system dimensions. The objective is to generate $u(t)$ so that $y(t)$ tracks a given desired continuous and differentiable output trajectory $z(t) \in \Re^m$ as close as possible with minimum consumption of control effort for all t. Thus, let us define the *error vector*

$$e(t) = z(t) - y(t), \tag{3.25}$$

and the *cost function*

$$J = \frac{1}{2}\int_0^\infty (e^T(t)Qe(t) + u^T(t)Ru(t))dt, \tag{3.26}$$

where $Q \in \Re^{m\times m}$ and $R \in \Re^{r\times r}$ are symmetric, positive definite weighting matrices.

In order to generate the optimal control signal $u(t) = u^*(t)$ that minimizes the cost function (3.26), following *Hamiltonian* calculation [116], at first, the following DRE is formed:

$$\dot{P} = -PA - A^TP + PBR^{-1}B^TP - C^TQC, \tag{3.27}$$

where $P \in \Re^{n\times n}$ is a symmetric, positive definite matrix. Since the infinite-horizon LQT design [116] is studied, there is no terminal $F(t_f) = 0$ in *cost function* (3.26). Therefore, $P(t)$ tends to its steady-state value $\lim_{t_f\to\infty}(P(t_f)) = \bar{P}$ as the solution of the following ARE:

$$-\bar{P}A - A^T\bar{P} + \bar{P}BR^{-1}B^T\bar{P} - C^TQC = 0, \tag{3.28}$$

where $\bar{P} \in \Re^{n\times n}$ is a symmetric, positive definite matrix calculated by the analytical solution of the ARE (3.28).

Then, as the next step in the LQT design steps with *Hamiltonian* approach a vector signal $g(t) \in \Re^n$ is generated via the differential equation

$$\dot{g}(t) = -[A^T - PBR^{-1}B^T]g(t) - C^TQz(t). \tag{3.29}$$

The final optimal control signal is generated as

$$u^*(t) = -R^{-1}B^T\bar{P}x(t) + R^{-1}B^T g(t), \tag{3.30}$$

where $-R^{-1}B^T\bar{P}x(t)$ is the state feedback term and $R^{-1}B^T g(t)$ is the feedforward term. Note that the control law (3.30) is established in [116] to bear the following optimal tracking property:

Proposition 3.6.3. *[116]: The control law (3.30) guarantees that (3.24) is closed loop stable and (3.26) is minimized, for any given slowly-varying desired output trajectory $z(t)$.*

To simplify and ease the calculation of the vector signal $g(t)$, we use an approximation [10] as follows:

Approximate vector signal $\bar{g}(t)$*:* It is established in [10], if $z(\cdot)$ is slowly varying then $\dot{g}(t)$ in (3.29) can be approximated as $\dot{g}(t) \approx 0$ leading to the approximate solution

$$g(t) \approx \bar{g}(t) = [A^T - \bar{P}BR^{-1}B^T]^{-1}[-C^T Q z(t)]. \tag{3.31}$$

3.6.3 Adaptive Linear Quadratic Tracking (ALQT) Control Design

For attitude control, our approach is to apply the control law (3.28), (3.30), (3.31) to the system (3.1). Note that the implementation of the control law (3.30) requires $\bar{P}$ from (3.28) and $\bar{g}(t)$ from (3.31), and hence requires knowledge of the system matrices A, B, C. In our case, in (3.1), although B_φ, C_φ are known, A_φ is unknown. Hence, following the certainty equivalence approach [74, 116], the following adaptive version of the LQT control law (3.28), (3.30), (3.31) for the *cost function* (3.6) and the attitude tracking *error* (3.7) is designed.

The time-varying adaptive ARE, the approximate vector signal $\bar{g}(t)$ and the adaptive optimal control signal are obtained, respectively as

$$-\bar{P}\hat{A}_\varphi(t) - \hat{A}_\varphi^T(t)\bar{P} + \bar{P}B_\varphi R^{-1}B_\varphi^T\bar{P} - C_\varphi^T Q C_\varphi = 0, \tag{3.32}$$

$$\bar{g}(t) = [\hat{A}_\varphi^T(t) - \bar{P}B_\varphi R^{-1}B_\varphi^T]^{-1}[-C_\varphi^T Q z(t)], \tag{3.33}$$

$$\hat{u}_\varphi^*(t) = -R^{-1}B_\varphi^T\bar{P}x_\varphi(t) + R^{-1}B_\varphi^T\bar{g}(t), \tag{3.34}$$

where $\hat{A}_\varphi(t) = \begin{bmatrix} 0 & 1 & 0 \\ 0 & 0 & 2lK\hat{\theta}_\varphi(t) \\ 0 & 0 & -b \end{bmatrix}$, $B_\varphi = \begin{bmatrix} 0 \\ 0 \\ b \end{bmatrix}$, $C_\varphi = \begin{bmatrix} 1 \\ 0 \\ 0 \end{bmatrix}^T$. Solving (3.32) for $\bar{P} = \begin{bmatrix} \bar{P}_1 & \bar{P}_2 & \bar{P}_3 \\ \bar{P}_2 & \bar{P}_4 & \bar{P}_5 \\ \bar{P}_3 & \bar{P}_5 & \bar{P}_6 \end{bmatrix} \in \Re^{3\times 3}$, we obtain

$$0 = -(\bar{P}_3^2 b^2/R) + Q, \tag{3.35a}$$
$$0 = -\bar{P}_1 + ((\bar{P}_3\bar{P}_5 b^2)/R), \tag{3.35b}$$
$$0 = -(2lK\hat{\theta}_\varphi \bar{P}_2) + \bar{P}_3 b + (\bar{P}_3\bar{P}_6 b^2/R), \tag{3.35c}$$
$$0 = -2\bar{P}_2 + (\bar{P}_5^2 b^2/R), \tag{3.35d}$$
$$0 = -(2lK\hat{\theta}_\varphi \bar{P}_4) + \bar{P}_5 b - \bar{P}_3 + (\bar{P}_5\bar{P}_6 b^2/R), \tag{3.35e}$$
$$0 = -(4lK\hat{\theta}_\varphi \bar{P}_5) - 2\bar{P}_6 b + (\bar{P}_6^2 b^2/R). \tag{3.35f}$$

Solving (3.33) for $\bar{g}(t) = [\bar{g}_1(t)\ \bar{g}_2(t)\ \bar{g}_3(t)]^T \in \Re^3$, we obtain

$$\bar{g}_1(t) = [(\bar{P}_5 Q)/(\bar{P}_3 R)]\varphi_d(t), \tag{3.36a}$$
$$\bar{g}_2(t) = [(\bar{P}_6 bQ + RQ)/(2lK\hat{\theta}_\varphi \bar{P}_3)]\varphi_d(t), \tag{3.36b}$$
$$\bar{g}_3(t) = [(RQ)/(\bar{P}_3 b^2)]\varphi_d(t). \tag{3.36c}$$

Remark 3.6.4. *There is also no constraint on the control signal $\hat{u}_\varphi(t)$ considered in the control design. However, we consider a limit $-0.025 \leqslant u_\varphi(t) \leqslant 0.025$ to prevent damages on the quadrotor motors due to high torque commands.*

3.7 Yaw and Altitude Control

To provide the overall motion in experiments, P and PID controllers are designed respectively, for yaw and altitude dynamics as follows.

3.7.1 Yaw Control

Since yaw dynamics is not directly affecting the lateral motion of the quadrotor UAV system, the yaw motion control is considered independently. Therefore, the following P

control law is used based on the dynamic model (3.3):

$$u_\psi = K_{p\psi} e_\psi, \tag{3.37}$$

where $e_\psi = (\psi_d - \psi)$.

3.7.2 Altitude Control

Altitude controller is derived for keeping the quadrotor UAV system in its desired altitude and providing stability at the longitudinal motion. The following PID control law is used based on the dynamic model (3.5):

$$u_z = K_{pz}(e_z) + K_{iz} \int_0^t (e_z)dt + K_{dz}(\dot{e}_z), \tag{3.38}$$

where $e_z = (p_{zd} - p_z)$.

Remark 3.7.1. *With the attitude, yaw and altitude control schemes as designed above, the control inputs $\hat{u}^*_\varphi$, u_ψ and u_z are generated. Then, we combine these inputs [90] to generate each motor PWM inputs v_r. for flight control of the Qball-X4 quadrotor UAV system.*

3.8 Experimental Tests and Comparative Simulations

3.8.1 Test Platform

The test platform consists of a Qball-X4 quadrotor UAV and a ground control and communication station (host computer) as illustrated in Figure 3.4. The Qball-X4 is developed by Quanser Inc. and equipped with a sonar sensor and an IMU to provide altitude, acceleration, angular rate and magnetometer measurements [172]. It has an on-board avionics data acquisition card (DAQ) and Gumstix embedded computer for interfacing with on-board sensors and driving the four rotor motors. Each motor is linked to one of the four PWM servo output channels on the DAQ. The Qball-X4 dynamic parameters as specified in [172] are presented in Table 3.2. The ground station computer is used for coding the designed control algorithms, and embedding on the Qball-X4 on-board computers before tests as well as generating the high-level control inputs in the form of desired attitude and altitude trajectories on-line during the tests. For control algorithm coding and embedding, Quarc, a MATLAB/*Simulink*® based interface software developed by Quanser Inc., is used.

Table 3.2: The Qball-X4 quadrotor UAV dynamic parameters [172].

m (kg)	l (m)	K (N)	K_ψ (Nm)	b (rad/sec)	$J_{\varphi 0}$ (kgm^2)	J_ψ (kgm^2)
1.4	0.2	120	4	15	0.03	0.04

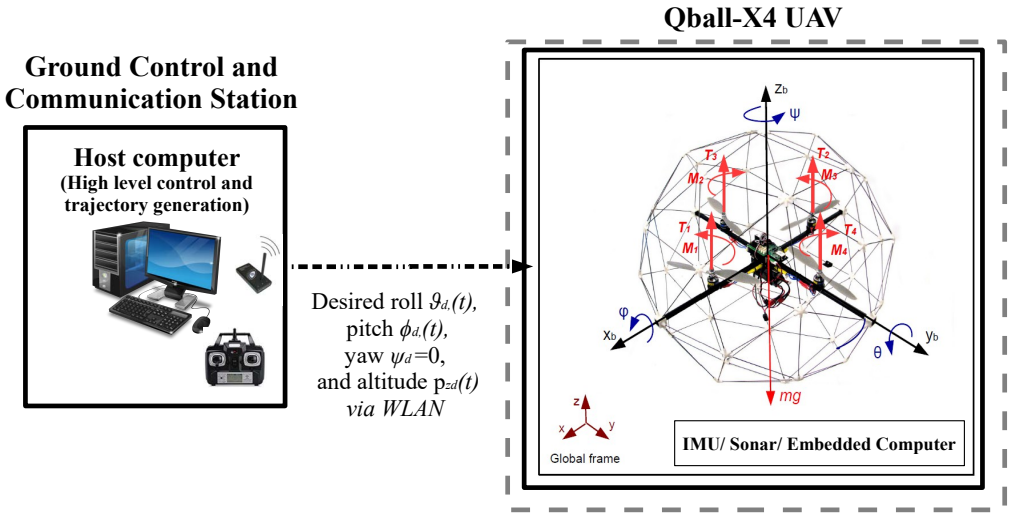

Figure 3.4: The Qball-X4 quadrotor UAV test platform.

3.8.2 Control Design Specifications and On-line Calculation of Control Parameters

In the implementation of the ALQT control design explained in detail in Section 3.6.3, the error and the control weighting parameters are chosen as $Q = 100$ and $R = 30000$. Following (3.35a), the constant entry $\bar{P}_3$ of $\bar{P}(t)$ is calculated as $\bar{P}_3 = \sqrt{(QR)}/b = 115.4701$. The other entries of $\bar{P}(t)$ are calculated solving (3.35) online, noting the dependence of these entries to each other and the parameter estimate $\hat{\theta}_\varphi$. From (3.35d), the entry $\bar{P}_2$ is found in the form of the entries $\bar{P}_5$ and written in (3.35c). Then, the equations (3.35c) and (3.35f) are obtained in the form of the entries $\bar{P}_5$ and $\bar{P}_6$ as follows:

$$0 = -(lK\hat{\theta}_\varphi \bar{P}_5^2 b^2/R) + \bar{P}_3 b + (\bar{P}_3 \bar{P}_6 b^2/R), \tag{3.39a}$$

$$0 = -(4lK\hat{\theta}_\varphi \bar{P}_5) - 2\bar{P}_6 b + (\bar{P}_6^2 b^2/R). \tag{3.39b}$$

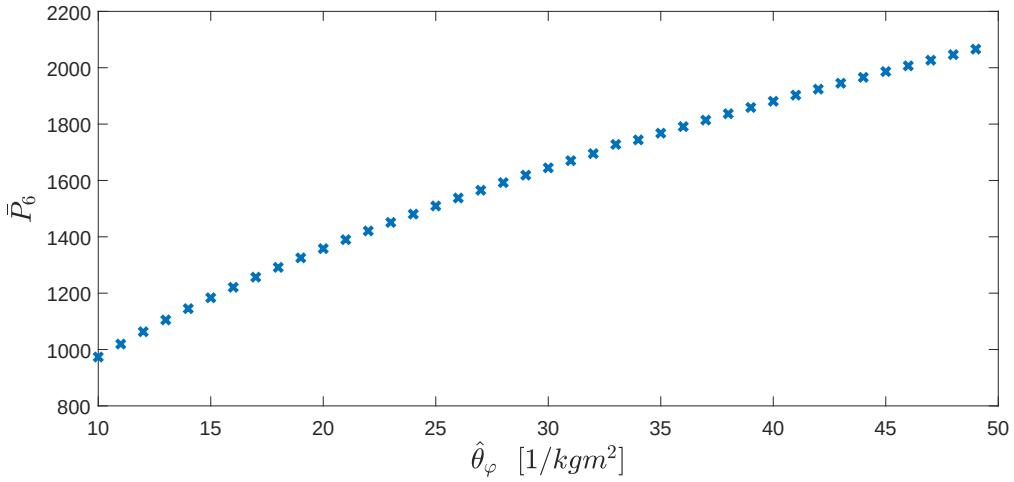

Figure 3.5: Off-line calculation of $\bar{P}_6$ for the estimate $\hat{\theta}_\varphi \in [\underline{\theta}_\varphi, \overline{\theta}_\varphi]$.

Solving the equations (3.39a) and (3.39b) by using Maple® and MATLAB® softwares, $\bar{P}_6$, which is chosen as a critical parameter, is off-line calculated for the estimate $\hat{\theta}_\varphi \in [\underline{\theta}_\varphi, \overline{\theta}_\varphi]$ of θ^*_φ. Then, a lookup table is prepared as plotted in Figure 3.5. The remaining entries of $\bar{P}$ are simultaneously calculated using $\bar{P}_6$ and the estimate $\hat{\theta}_\varphi$ as follows:

$$\bar{P}_5 = ((2\bar{P}_6 b) + ((\bar{P}_6^2 b^2)/R))/(4lK\hat{\theta}_\varphi), \tag{3.40a}$$

$$\bar{P}_2 = (\bar{P}_5^2 b^2)/(2R), \tag{3.40b}$$

$$\bar{P}_1 = (\bar{P}_3 \bar{P}_5 b^2)/R, \tag{3.40c}$$

$$\bar{P}_4 = ((-\bar{P}_3)/2lK\hat{\theta}_\varphi) + ((\bar{P}_5 b)/2lK\hat{\theta}_\varphi) + ((\bar{P}_5 \bar{P}_6 b^2)/2lK\hat{\theta}_\varphi R). \tag{3.40d}$$

After obtaining $\bar{P}$, by (3.36) and the reference input $\varphi_d(t)$, the vector signal $\bar{g}(t)$ is found at each time instant, as well. For example, for the nominal value $\hat{\theta}_{\varphi 0} = 33\ [1/kgm^2]$, the Riccati coefficient matrix $\bar{P}$ is obtained using (3.39a), (3.39b), (3.40a), (3.40b), (3.40c), (3.40d) as follows:

$$\bar{P} = \begin{bmatrix} 20.0886934 & 2.0177780 & 115.4700538 \\ 2.01777802 & 480969.75 & 23.19642512 \\ 115.470053 & 23.196425 & 1727.886987 \end{bmatrix}. \tag{3.41}$$

After that, the vector signal $\bar{g}(t)$ is found by (3.41) and (3.36) as follows:

$$\bar{g}(t) = \begin{bmatrix} 20.08869343750145\ \varphi_d(t) \\ 2.017798199381859\ \varphi_d(t) \\ 115.4700538758503\ \varphi_d(t) \end{bmatrix}. \tag{3.42}$$

The ALQT control design with specifications above is used for pitch and roll control. For yaw tracking a P controller is used with gain $K_{p\psi} = 0.015$, and for altitude tracking a PID controller is used with gains $K_{pz} = 0.006$, $K_{iz} = 0.008$ and $K_{dz} = 0.002$.

In implementation of the adaptive PI scheme (3.23), the forgetting factor, the initial covariance, and the initial parameter estimate, are selected as, respectively, $\beta = 0.001$, $\mathbf{P}_0 = 10^5$ and $\theta_0 = 10\ [1/kgm^2]$. In the Kalman filter implementation, Q_{K} and R_{K} matrices are taken as $Q_{\mathrm{K}} = 10^{-3} I_3$ and $R_{\mathrm{K}} = 2\mathrm{x}10^{-4} I_2$. A_d, B_d and C_d matrices are numerically obtained for the nominal value of $J_{\varphi 0} = 0.03\ [kgm^2]$ and the sampling time $T_s = 0.005$ as

$$A_d = \begin{bmatrix} 1 & 0.005 & 0 \\ 0 & 1 & 8 \\ 0 & 0 & 0.925 \end{bmatrix}, B_d = \begin{bmatrix} 0 \\ 0 \\ 0.075 \end{bmatrix}, C_d = \begin{bmatrix} 1 & 0 & 0 \\ 0 & 1 & 0 \end{bmatrix}.$$

For the complementary filter, φ_{acc} is passed through a low pass filter with transfer function $G_a(s) = (20s+1)/(100s^2+20s+1)$, and $\dot{\varphi}$ is passed through a high pass filter with transfer function $G_g(s) = (100s)/(100s^2 + 20s + 1)$.

3.8.3 Experimental Results

After setting all control parameters with the sampling rate 200 $[Hz]$ by using MATLAB/ *Simulink*® and Quarc interface in the host computer, as explained in Sections 3.8.1 and 3.8.2, we have implemented the proposed control scheme on the Qball-X4 as seen in Figure 3.6 for the following two cases:
Test 1. ALQT with complementary filter: The video of the experiment is presented in URL: https://www.youtube.com/watch?v=OVZ_zg4SSOY.
Test 2. ALQT with Kalman filter: The video of the experiment is presented in URL: https://www.youtube.com/watch?v=wsKiPJJjj68.

In both tests, the Qball-X4 starts to perform the tracking control task after hovering for 15 *seconds*. The real-time IMU data measurements in Test-2 from the gyroscope, the accelerometer and the magnetometer are presented in Figures 3.7, 3.8 and 3.9, respectively.

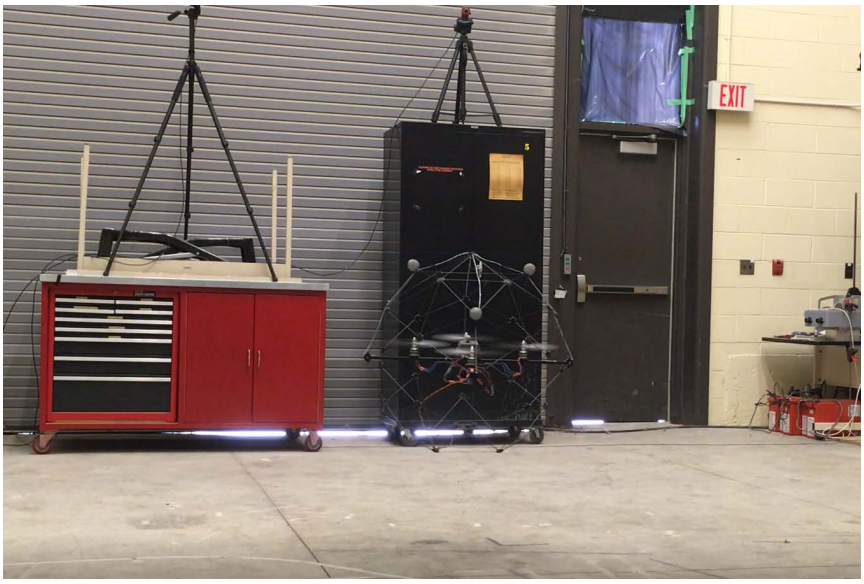

Figure 3.6: The Qball-X4 quadrotor during the experiment.

Applying the methodology explained in Section 3.5.1, the IMU measurements shown in Figure 6 are used to obtain the raw calculation of the roll and pitch parameters (yellow plots), and then to generate the estimates by complementary filter (blue plots) and Kalman filter (red plots) shown in Figures 3.11 and 3.12. Kalman filter provides more reliable data less sensitive to noise. For the yaw estimation, gyroscope data integration is used instead, due to distortion effects by metallic objects of the test environment, as explained in Section 3.5.1.

The tracking error performances of both tests verify that the control objective is satisfied as seen in Figure 3.13 and 3.14. In both tests, the controllers maintain attitude angles close to their desired angles with small attitude tracking errors $\pm 0.1[rad]$. However, as seen in 3.14, ALQT control with Kalman filter is more robust to sensor noises and uncertainties, and results in smaller tracking errors.

As seen in Tables 3.3 and 3.4, ALQT control with Kalman filter gives significantly smaller mean-square error and consumes less battery (energy). It is also observed in additional simulations that the proposed controller consumes less battery energy with more robust control action compared to other classical controllers such as PID.

In real-time, the motor PWM control inputs have the constraint $-0.1 \leqslant v_r(t) \leqslant 0.1$ since they work with limited voltage to prevent damages due to high torque commands.

Table 3.3: Mean square error of e_φ.

ALQT	Roll [rad]	Pitch [rad]
with Kalman filter	0.0012	0.0012
with comp. filter	0.0027	0.0029

Table 3.4: Average battery consumption by $\hat{u}^*_\varphi$.

ALQT	Roll [voltage/sec]	Pitch [voltage/sec]
with Kalman filter	0.00071	0.00066
with comp. filter	0.00086	0.00140

Hence, a limit is applied for the optimal attitude control inputs as mentioned in Remark 3.6.4 even though LQT design procedure does not have any constraints. As seen in Figures 3.15, 3.16 and 3.17, the proposed controller satisfies admissible and optimal control actions for all $t > 0$ during the tests. Figures 3.15, 3.16 and 3.17 show that the motor PWM and the optimal attitude control inputs are kept within the allowed limits.

The LS based estimation of the uncertain inertia parameters $\hat{\theta}_\vartheta$ and $\hat{\theta}_\phi$ is presented in Figure 3.10. The estimates, which are purposely initialized at values away from the nominal values (to test the expected convergence), successfully converge to the vicinity of the nominal value 33 $[1/kgm^2]$ in around 40 $[sec]$. The convergence rate of the estimation can be adjusted easily adjusting the design parameters of the LS based adaptive law.

3.8.4 Comparative Simulations and Observations

For optimal performance comparison with the existing literature, in ideal simulation conditions without noises, we simulate the ALQT control design and compare with a classical PID controller with control gains $K_p = 0.0017$; $K_i = 8.98$; $K_d = 0.005$. As seen in Figure 3.18 and 3.19, the ALQT controller gives smaller tracking errors with less control action. Therefore, in the actual settings with noises, it is expected that the ALQT with a reliable filter will give us better tracking and control input performances compared to a PID controller. Figure 3.20 presents the estimates of the simulation. It is also observed from the literature that the proposed controller gives a good control performance in terms of optimal attitude tracking compared to the attitude tracking errors of [5, 156].

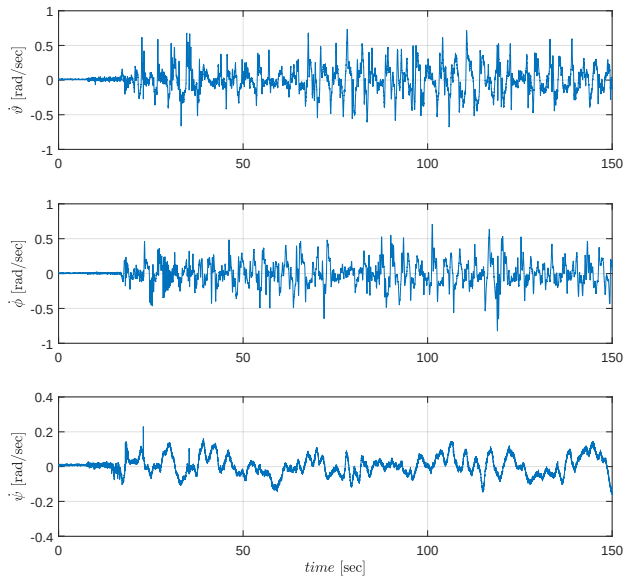

Figure 3.7: IMU data measurements from gyroscope.

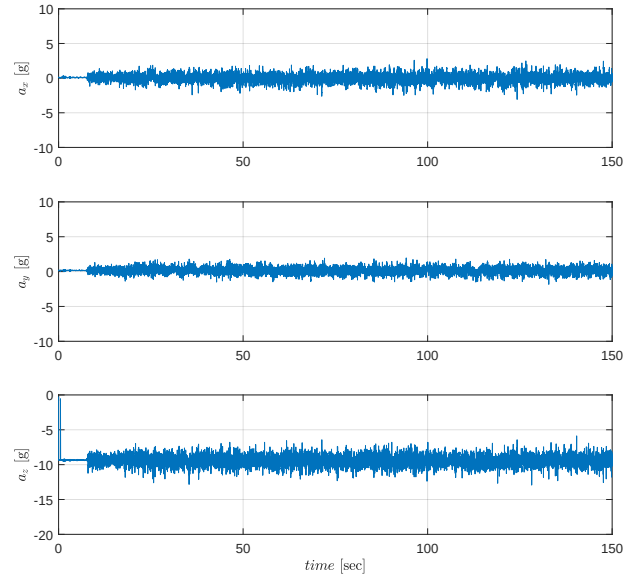

Figure 3.8: IMU data measurements from accelerometer.

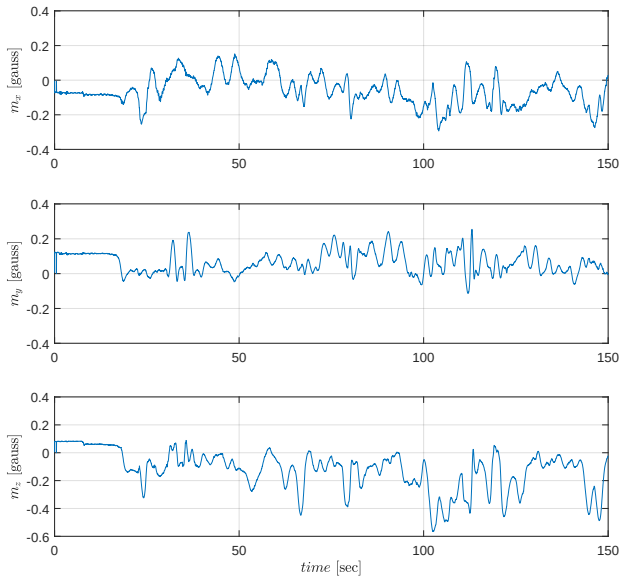

Figure 3.9: IMU data measurements from magnetometer.

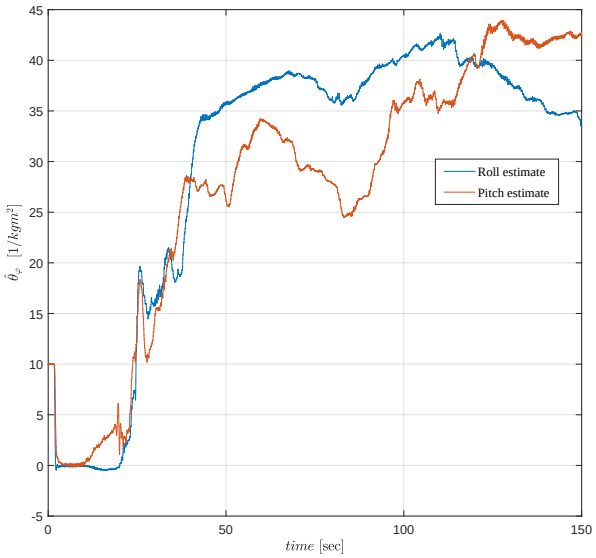

Figure 3.10: LS based estimate $\hat{\theta}_\varphi$ of the uncertain inertia parameter θ^*_φ.

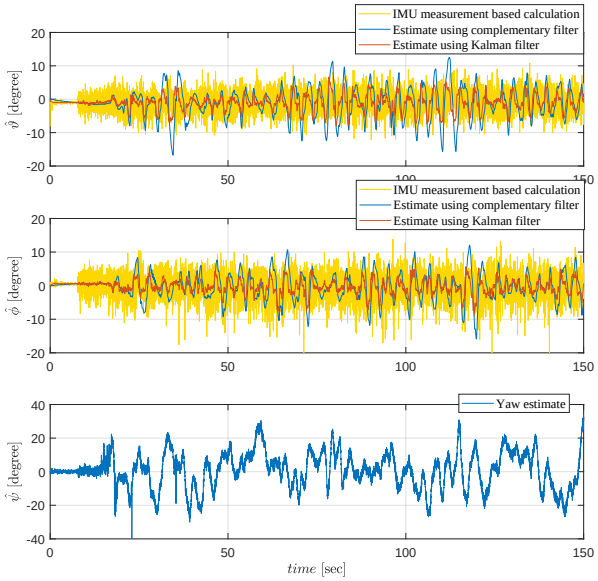

Figure 3.11: Attitude estimation of the Qball-X4.

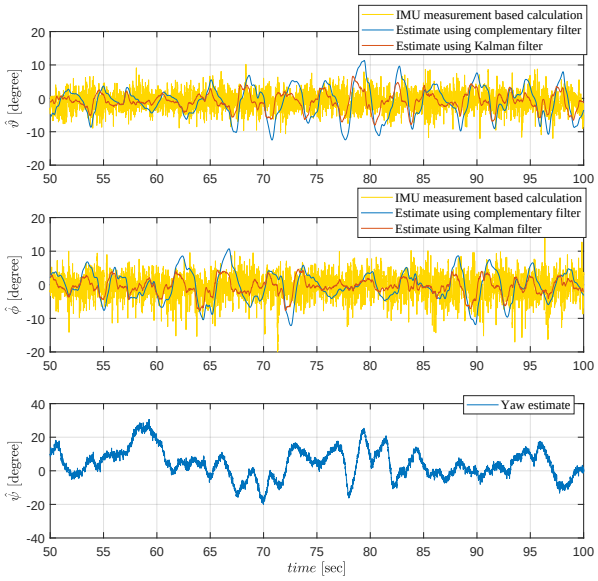

Figure 3.12: Attitude angle estimation of the Qball-X4 from 50 to 100 [sec].

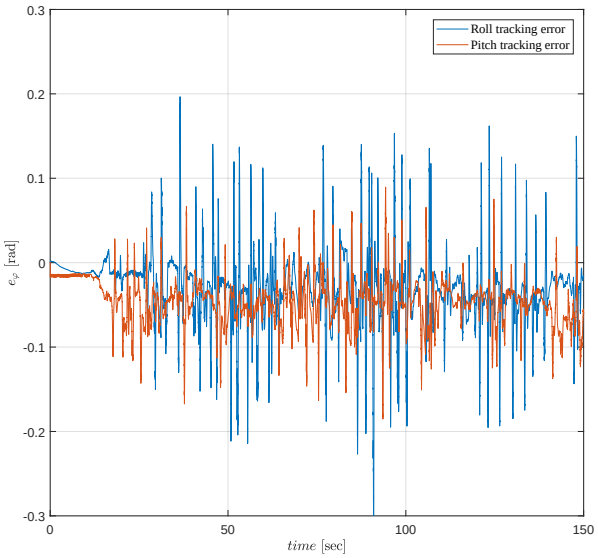

Figure 3.13: Attitude tracking error of the Qball-X4 using complementary filter.

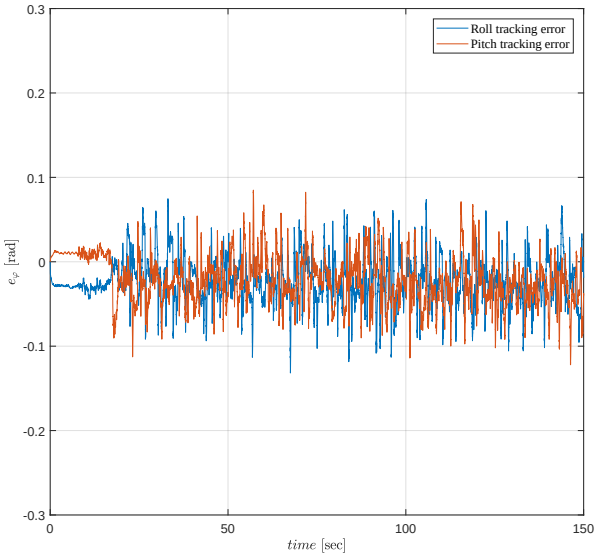

Figure 3.14: Attitude tracking error of the Qball-X4 using Kalman filter.

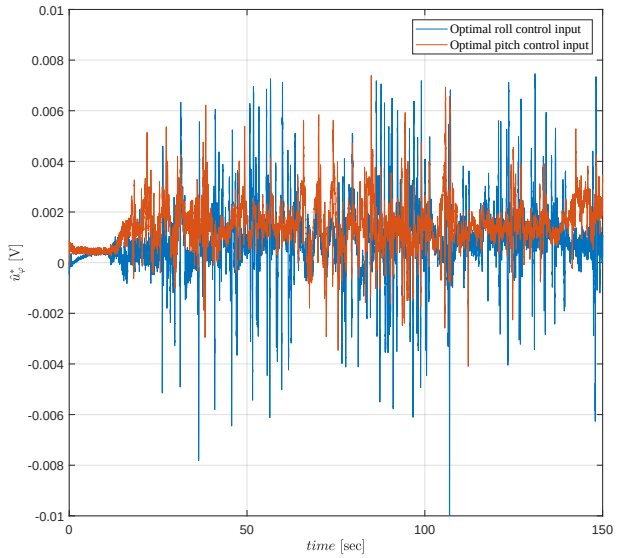

Figure 3.15: Optimal attitude control inputs for the complementary filter.

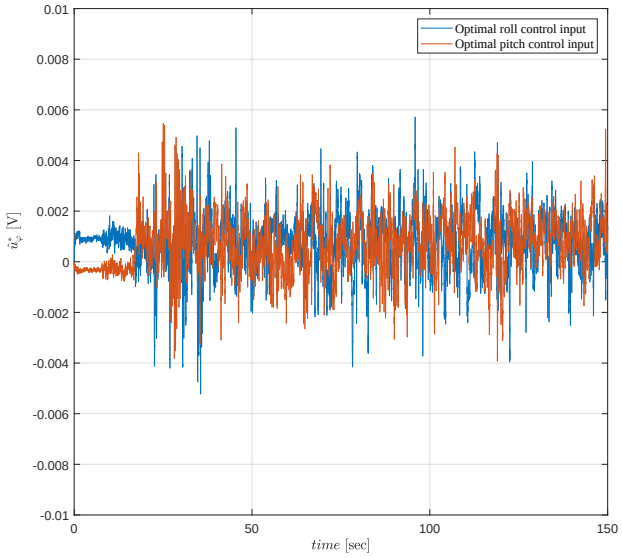

Figure 3.16: Optimal attitude control inputs for Kalman filter.

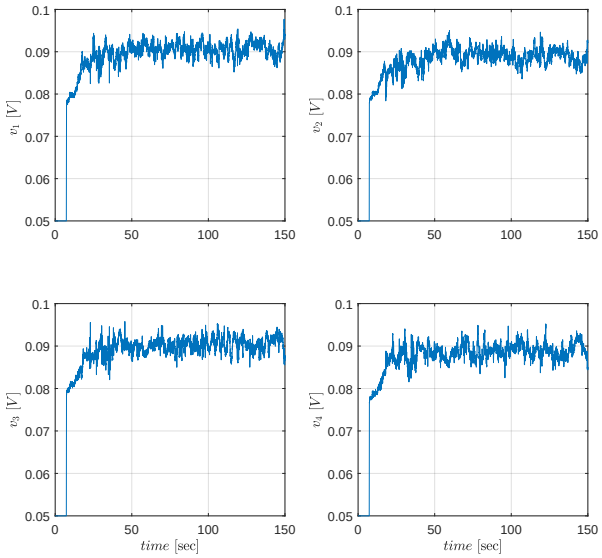

Figure 3.17: Motor PWM control inputs v_r.

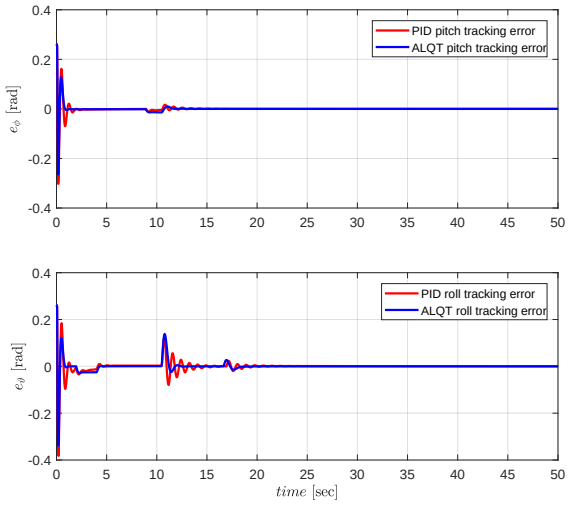

Figure 3.18: PID vs ALQT performance comparison: attitude tracking error.

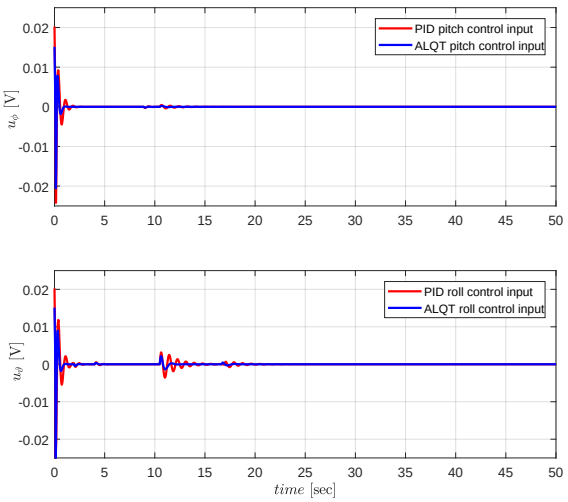

Figure 3.19: PID vs ALQT performance comparison: attitude control input.

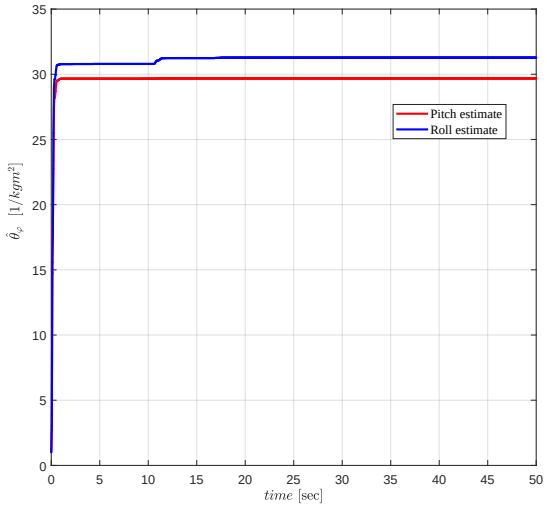

Figure 3.20: LS based estimate $\hat{\theta}_\varphi$ of the uncertain inertia parameter θ^*_φ for the simulation.

3.9 Summary and Remarks

The adaptive linear quadratic tracking (ALQT) scheme has been developed to control and stabilize the attitude of the Qball-X4 quadrotor UAV system in an optimal sense. The proposed adaptive controller is designed by indirect approach and combined with the LS based parameter identification (PI) to eliminate the influences of inertial uncertainties. Additionally, Kalman filter has been designed for canceling noise effects on the attitude estimation data to provide more reliable feedbacks to the controller and it is compared with Complementary filter. All analytical analyses and designs are verified by the two experimental tests. We witness that the ALQT design in experiments works satisfactorily in terms of the optimal tracking performance. In Kalman filter vs Complementary filter, although both filter designs are good to canceling noise effects on the estimated attitude data, Kalman filter gives a better accuracy and reliable attitude estimation. Thus, the experimental results show that the quadrotor UAV has more robust behavior and better tracking error with the estimated attitude data by Kalman filter comparing with the Complementary filter.

Chapter 4

Robust Adaptive Control of a Quadrotor UAV with Guaranteed Tracking Performance

4.1 Introduction

In the literature, some advanced nonlinear control methods have been studied for tracking problem of the quadrotor UAV, including the backstepping, sliding-mode and feedback linearization based ones [13, 39, 90, 107]. The above mentioned studies rely on the full knowledge of dynamics for robust tracking performances. For the purpose of ensuring the control robustness in case of model uncertainties and disturbances, [103] introduces a robust three-loop design, which comprises of the nominal position and attitude controllers with a robust compensator, to deal with nonlinearities, parametric uncertainties and disturbances. In [127], a robust backstepping control scheme based on integral sliding modes is used to compensate bounded disturbances, including wind gust, side-slip aerodynamics, and drags in both position and the attitude dynamics. In [141], terminal sliding mode control (TSMC) is studied for position and attitude tracking, subject to such disturbances. [140] extends the TSMC approach to the globally fast dynamic TSMC, which not only provides finite-time position and attitude tracking control and eliminates the chattering, but also rejects the external disturbances.

Guaranteeing transient and steady-state tracking performances for highly nonlinear systems with model uncertainties and disturbances is a challenging and important control task. The earlier studies [24, 149] have introduced a prescribed performance function based

error transformation approach, which is capable of transferring the original constrained tracking error system to an unconstrained form. As a big advantage of this approach, the unconstrained system is capable of guaranteeing prescribed performance when the stability of the unconstrained system is proven. Hence, the maximum overshoot/undershoot, the convergence rate and steady-state error are easily tunable.

In [124], a fault tolerant control is studied and prescribed performance bound (PPB) technique is also used to improve the transient attitude tracking performance of UAV system. In [169], a robust controller with guaranteed certain predefined transient performance is designed for the attitude of the rigid spacecraft system on SO(3). [157] studies the backstepping based adaptive compensation control strategy with guaranteed transient attitude tracking performance for the quadrotor UAV with partial loss of rotational speed, limited air flow disturbance and inertial uncertainties. In [72], a robust adaptive control strategy based on sliding mode and PPB techniques for time-varying payload and wind gust disturbance. In [71], a PPB based formation control scheme is designed for systems of multiple quadrotor UAVs.

In this chapter, inspired by [24, 149], we design and implement a robust adaptive controller with guaranteed transient and steady-state tracking error performances in case of under-actuated dynamics, nonlinearities and model uncertainties. To achieve this goal, we design a backstepping based position controller using a PPB based error transformation approach which ensures bounded trajectory tracking errors, and a backstepping based adaptive attitude controller combined with a least squares (LS) based parameter identification (PI) algorithm.

4.2 Quadrotor UAV Dynamics

A nonlinear dynamic modeling of the quadrotor UAV motion dynamics (2.10) is considered from Chapter 2. The nonlinear dynamics is separated into three strict-feedback sub-systems as follows:

a) Lateral position dynamics is

$$\dot{p}_l = [\dot{p}_x, \dot{p}_y]^T = [v_x, v_y]^T, \tag{4.1}$$

$$\dot{v}_l = [\dot{v}_x, \dot{v}_y]^T = \frac{4T_z}{m}[f_{1x}, f_{1y}]^T, \tag{4.2}$$

$$f_{1x} = \{\cos\phi \sin\vartheta \cos\psi + \sin\phi \sin\psi\},$$
$$f_{1y} = \{\cos\phi \sin\vartheta \sin\psi - \sin\phi \cos\psi\},$$

where p_l, v_l and T_z are lateral position, lateral velocity and thrust in the body frame O_b; m is total mass; $\{\phi, \vartheta, \psi\}$ are Euler angles.

b) Altitude dynamics is

$$\dot{p}_z = v_z, \tag{4.3}$$

$$\dot{v}_z = \frac{4}{m}(\cos\phi\cos\vartheta)T_z - g, \tag{4.4}$$

$$\dot{T}_z = -bT_z + Kbu_z, \tag{4.5}$$

where p_z and v_z are position and velocity in longitudinal motion of the O_b; g is gravity; b is actuator bandwidth; K is positive armature gain.

c) Attitude dynamics is

$$\dot{\varphi} = w_\varphi, \tag{4.6}$$

$$\dot{w}_\varphi = \mathbf{A}_1 w_\varphi + \mathbf{A}_2 f_2(w_\varphi) + \mathbf{B}T_\varphi, \tag{4.7}$$

$$\dot{T}_\varphi = -bT_\varphi + Kbu_\varphi, \tag{4.8}$$

where $\mathbf{A}_1 = diag(\mathbf{a}_{11}, \mathbf{a}_{12}, \mathbf{a}_{13}) = diag(d_\phi, d_\vartheta, d_\psi)$; $\mathbf{A}_2 = diag(\mathbf{a}_{21}, \mathbf{a}_{22}, \mathbf{a}_{23}) = diag(\frac{J_\vartheta - J_\psi}{J_\phi}$, $\frac{J_\psi - J_\phi}{J_\vartheta}, \frac{J_\phi - J_\vartheta}{J_\psi})$; $f_2(w_\varphi) = [f_{21}(w_\varphi), f_{22}(w_\varphi), f_{23}(w_\varphi)]^T = \begin{bmatrix} \dot{\vartheta}\dot{\psi} \\ \dot{\phi}\dot{\psi} \\ \dot{\phi}\dot{\vartheta} \end{bmatrix}$; $\mathbf{B} = diag(\mathbf{b}_1, \mathbf{b}_2, \mathbf{b}_3) = diag(\frac{2l}{J_\phi}, \frac{2l}{J_\vartheta}, \frac{4K_\psi}{J_\psi})$; $\varphi \triangleq [\varphi_1, \varphi_2, \varphi_3]^T = [\phi, \vartheta, \psi]^T$, $w_\varphi = [w_{\varphi 1}, w_{\varphi 2}, w_{\varphi 3}]^T = [\dot{\phi}, \dot{\vartheta}, \dot{\psi}]^T$, $T_\varphi \triangleq [T_{\varphi 1}, T_{\varphi 2}, T_{\varphi 3}]^T = [T_\phi, T_\vartheta, T_\psi]^T$, $u_\varphi \triangleq [u_{\varphi 1}, u_{\varphi 2}, u_{\varphi 3}]^T = [u_\phi, u_\vartheta, u_\psi]^T$, $J_\varphi \in (J_\phi, J_\vartheta, J_\psi)$ and $d_\varphi \in (d_\phi, d_\vartheta, d_\psi)$ are Euler angles, angular velocities, attitude thrusts, attitude control inputs, inertias and drags in the O_b, respectively.

4.3 Control Problem

Consider the position (lateral and altitude) dynamics (4.1)-(4.5) and the attitude dynamics (4.6)-(4.8). The following practical assumptions are made.

Assumption 4.3.1. *Attitude angles are bounded as*

$$-\frac{\pi}{2} < \phi < \frac{\pi}{2}, \quad -\frac{\pi}{2} < \vartheta < \frac{\pi}{2}, \quad -\frac{\pi}{2} < \psi < \frac{\pi}{2}. \tag{4.9}$$

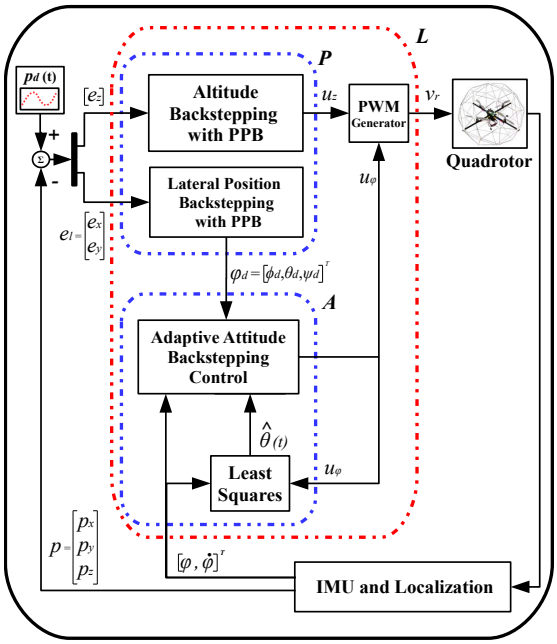

Figure 4.1: The overall control structure for the quadrotor UAV

Assumption 4.3.2. *The desired trajectory $p_d(t) \in \mathbb{R}^3$ and its derivatives are known and bounded function of time.*

Assumption 4.3.3. *The states p_l, v_l, p_z, v_z, T_z, φ, w_φ, T_φ of the quadrotor UAV are measurable.*

The control problem of the chapter is stated as follows:

Problem 4.3.1. *Design the control units to generate the command signals u_z and u_φ for feeding the PWM generator that generates the motor control input signal v_r, per the diagram in Figure 4.1 such that the system output $p(t) = [p_x(t), p_y(t), p_z(t)]^T$ tracks the desired trajectory $p_d(t) = [p_{xd}(t), p_{yd}(t), p_{zd}(t)]^T$:*

(a) Design a backstepping based position controller using a PPB based error transformation to generate φ_d and u_z so that the transient and steady-state behaviors of the tracking error

$$e(t) = p(t) - p_d(t) = [e_x(t), e_y(t), e_z(t)]^T \tag{4.10}$$

are guaranteed within the prescribed bounds.

(b) Design a backstepping based adaptive attitude controller combined with a least squares (LS) based parameter identification (PI) algorithm to generate u_φ so that φ_d tracks the desired attitude φ_d and robustness is increased in presence of the model uncertainties.

4.4 Robust Adaptive Tracking Control Design with Guaranteed Error Performance

The low-level closed-loop system (L) is considered in the two-layer: position (P) and attitude (A) control schemes for the three sub-systems of the quadrotor UAV as seen in Figure 4.1. As formally stated in Problem 4.3.1, the proposed control scheme is designed in the following sections.

4.4.1 Position Control Design with Guaranteed Error

The position control scheme is designed by using backstepping procedures combined with the PPB based error transformation system [24, 149]. The following subsection first introduces the error transformation for each component $e_j,\ j \in x, y, z$ of the tracking *error* (4.10). Then, the lateral and the altitude control designs are presented.

Error Transformed System

a) Performance function: To transform the prescribed performance characteristics into e_j similar to [24, 149], a decreasing smooth performance function $\rho_j(t) : \mathbb{R}_+ \to \mathbb{R}_+ \backslash \{0\}$ with $\lim_{t\to\infty} \rho_j(t) = \rho_{j\infty} > 0$ is defined. In this thesis, the function is chosen as

$$\rho_j(t) = (\rho_{j0} - \rho_{j\infty})e^{(-k_j t)} + \rho_{j\infty}, \tag{4.11}$$

where $\rho_{j0} > \rho_{j\infty}$ and $k_j > 0$ are design parameters. Then, the control performance condition is defined as satisfaction of

$$\overline{\delta}_j \rho_j(t) > e_j(t) > -\underline{\delta}_j \rho_j(t), \quad \forall t \geq 0, \tag{4.12}$$

where $1 \geq \overline{\delta}_j$ and $\underline{\delta}_j > 0$ are prescribed scalars. $\overline{\delta}_j \rho_j(0)$ and $-\underline{\delta}_j \rho_j(0)$ are the upper and the lower bounds of the overshoot and the undershoot of $e_j(t)$. Use of (4.12) is illustrated in Figure 4.2.

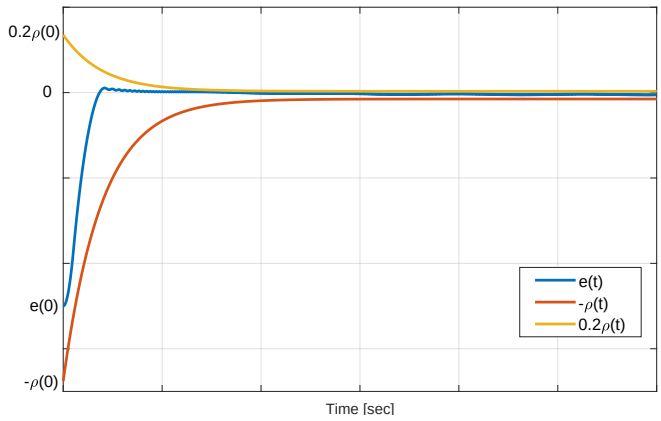

Figure 4.2: Graphical representation of (4.12) for prescribed tracking error behavior with $\overline{\delta} = 0.2$ and $\underline{\delta} = 1$.

b) Error transformation: To solve the control Problem 1-(a), tracking error transformation will be established by transforming condition (4.12) into an equivalent unconstrained one. For this purpose, we define a smooth, strictly increasing and invertible function $\mathcal{S}_j(.)$ with following properties:

(i) $\overline{\delta}_j > \mathcal{S}_j(\varepsilon) > -\underline{\delta}_j$, for any $\varepsilon \in \mathbb{R}$

(ii) $\lim_{\varepsilon \to +\infty} \mathcal{S}_j(\varepsilon) = \overline{\delta}_j$ and $\lim_{\varepsilon \to -\infty} \mathcal{S}_j(\varepsilon) = -\underline{\delta}_j$,

(iii) $\mathcal{S}_j(0) = 0$.

A function satisfying these properties is $\mathcal{S}_j(\varepsilon) = \frac{\bar{\delta}_j e^{(\varepsilon+c)} - \underline{\delta}_j e^{-(\varepsilon+c)}}{e^{(\varepsilon+c)} + e^{-(\varepsilon+c)}}$ where $c = \frac{ln(\underline{\delta}_j / \bar{\delta}_j)}{2}$ [149]. The condition (4.12) is satisfied [24, 149] if

$$\begin{aligned} \varepsilon_j &= \mathcal{S}_j^{-1}(\Lambda_j(t)) \\ &= \frac{1}{2} ln(\bar{\delta}_j \Lambda_j(t) + \bar{\delta}_j \underline{\delta}_j) - \frac{1}{2} ln(\bar{\delta}_j \underline{\delta}_j - \bar{\delta}_j \Lambda_j(t)), \end{aligned} \tag{4.13}$$

where $\Lambda_j(t) = \frac{e_j(t)}{\rho_j(t)}$, is guaranteed to be bounded.

The time derivative of ε_j is in (4.13) computed as

$$\begin{aligned}\dot{\varepsilon}_j &= \frac{\partial \varepsilon_j}{\partial \Lambda_j}\dot{\Lambda}_j \\ &= \frac{1}{2}\left(\frac{1}{\Lambda_j + \underline{\delta}_j} - \frac{1}{\Lambda_j - \bar{\delta}_j}\right)\left(\frac{\dot{e}_j}{\rho_j} - \frac{e_j\dot{\rho}_j}{\rho_j^2}\right) \\ &= \Theta_j\left(\dot{e}_j - \frac{e_j\dot{\rho}_j}{\rho_j}\right),\end{aligned} \tag{4.14}$$

where $\Theta_j = \frac{1}{2\rho_j}\left(\frac{1}{\Lambda_j+\underline{\delta}_j} - \frac{1}{\Lambda_j-\bar{\delta}_j}\right) \neq 0$ is well defined by (i) and (4.13).

To guarantee the transient and steady-state tracking performances, we now combine the PPB based error transformation (4.11)-(4.14) with the lateral position and the altitude dynamics (4.1)-(4.5) by replacing the error dynamics of the equations (4.1) and (4.3) with $\dot{\varepsilon}_j$ in (4.14) for $j \in \{x, y, z\}$.

Lateral Position Backstepping Control with PPB

The reference angle φ_d is generated to drive the quadrotor UAV to the desired lateral position $p_{jd} \in \{p_{xd}, p_{yd}\}$. The backstepping procedure is combined with the PPB based transformation as presented in subsection 4.4.1 to guarantee the prescribed lateral tracking error performance.

For each of $j \in \{x, y\}$, first define

$$z_{j1} = \varepsilon_j \text{ and } z_{j2} = v_j - \alpha_{j1}, \tag{4.15}$$

where α_{j1} is to be chosen in the sequel.

From (4.14) and the definition of z_{j2} in (4.15), we have

$$\begin{aligned}\dot{z}_{j1} &= \Theta_j\left(\dot{p}_j - \dot{p}_{jd} - \frac{e_j\dot{\rho}_j}{\rho_j}\right) \\ &= \Theta_j\left(z_{j2} + \alpha_{j1} - \dot{p}_{jd} - \frac{e_j\dot{\rho}_j}{\rho_j}\right).\end{aligned} \tag{4.16}$$

To stabilize (4.16), α_{j1} is chosen

$$\alpha_{j1} = \left(-\frac{k_1 z_{j1}}{\Theta_j} + \dot{p}_{jd} + \frac{e_j\dot{\rho}_j}{\rho_j}\right), \quad k_1 > 0, \tag{4.17}$$

so that

$$\dot{z}_{j1} = \Theta_j z_{j2} - k_1 z_{j1}. \tag{4.18}$$

This leads to

$$\dot{z}_{j2} = \dot{v}_j - \dot{\alpha}_{j1} = \frac{4T_z}{m} f_{1j} - \dot{\alpha}_{j1}. \tag{4.19}$$

To stabilize (4.19), choosing f_{1l} such that

$$f_{1j} = \frac{m}{4T_z} \left(-\Theta_j z_{j1} - k_2 z_{j2} + \dot{\alpha}_{j1} \right), \quad k_2 > 0, \tag{4.20}$$

where $\dot{\alpha}_{j1} = \frac{\partial \alpha_{j1}}{\partial p_j} v_j + \frac{\partial \alpha_{j1}}{\partial p_{jd}} v_{jd} + \frac{\partial \alpha_{j1}}{\partial v_{jd}} \dot{v}_{jd} + \frac{\partial \alpha_{j1}}{\partial \rho_j} \dot{\rho}_j + \frac{\partial \alpha_{j1}}{\partial \dot{\rho}_j} \ddot{\rho}_j$, we have

$$\dot{z}_{j2} = -\Theta_j z_{j1} - k_2 z_{j2}. \tag{4.21}$$

Using the equations (4.2) and (4.20), the desired pitch and roll angles are generated as

$$\phi_d = \arcsin \left(\sin\psi f_{1x} - \cos\psi f_{1y} \right), \tag{4.22}$$

$$\vartheta_d = \arcsin \left(\frac{f_{1x} - \sin\phi \sin\psi}{\cos\phi \cos\psi} \right), \tag{4.23}$$

and to prevent yaw motion's direct effect on the lateral motion of the quadrotor UAV, the desired yaw angle is set to zero; as $\psi_d(t) = 0$ for all $t \geq 0$. Therefore, the desired attitude angle is designed as $\varphi_d = [\varphi_{d1}, \varphi_{d2}, \varphi_{d3}]^T = [\phi_d, \vartheta_d, 0]^T$.

Remark 4.4.1. *The total thrust force is $T_z > 0$, $\forall t \geq 0$ so that the system avoids singularity during the operation.*

Altitude Backstepping Control with PPB

The backstepping technique is utilized to design the altitude controller with the PPB by defining

$$z_3 = \varepsilon_z, \;\; z_4 = v_z - \alpha_4, \text{and } z_5 = T_z - \alpha_5. \tag{4.24}$$

where α_5 is to be chosen in the sequel.

From (4.14) and the definition of z_4 in (4.24), we then write

$$\begin{aligned}\dot{z}_3 &= \Theta_z \left(\dot{p}_z - \dot{p}_{zd} - \frac{e_z \dot{\rho}_z}{\rho_z} \right) \\ &= \Theta_z \left(z_4 + \alpha_4 - \dot{p}_{zd} - \frac{e_z \dot{\rho}_z}{\rho_z} \right). \end{aligned} \tag{4.25}$$

To stabilize (4.25), α_4 is chosen as

$$\alpha_4 = \left(-\frac{k_3 z_3}{\Theta_z} + \dot{p}_{zd} + \frac{e_z \dot{\rho}_z}{\rho_z} \right), \quad k_3 > 0, \tag{4.26}$$

so that

$$\dot{z}_3 = \Theta_z z_4 - k_3 z_3. \tag{4.27}$$

This leads to

$$\begin{aligned}\dot{z}_4 = \dot{v}_z - \dot{\alpha}_4 &= \frac{4 \cos\phi \cos\vartheta}{m} T_z - g - \dot{\alpha}_4 \\ &= \frac{4 \cos\phi \cos\vartheta}{m} (z_5 + \alpha_5) - g - \dot{\alpha}_4. \end{aligned} \tag{4.28}$$

To stabilize (4.28), α_5 is chosen as

$$\alpha_5 = \frac{m}{4 \cos\phi \cos\vartheta} \left(g - k_4 z_4 + \dot{\alpha}_4 - \Theta_z z_3 \right), \quad k_4 > 0, \tag{4.29}$$

where $\dot{\alpha}_4 = \frac{\partial \alpha_4}{\partial p_z} v_z + \frac{\partial \alpha_4}{\partial p_{zd}} v_{zd} + \frac{\partial \alpha_4}{\partial v_{zd}} \dot{v}_{zd} + \frac{\partial \alpha_4}{\partial \rho_z} \dot{\rho}_z + \frac{\partial \alpha_4}{\partial \dot{\rho}_z} \ddot{\rho}_z$, so that

$$\dot{z}_4 = -\Theta_z z_3 + \frac{4 \cos\phi \cos\vartheta}{m} z_5 - k_4 z_4. \tag{4.30}$$

We further have

$$\dot{z}_5 = \dot{T}_z - \dot{\alpha}_5 = -b T_z + K b u_z - \dot{\alpha}_5. \tag{4.31}$$

To stabilize (4.31), the altitude control input is designed as

$$u_z = \frac{1}{Kb} \left[b T_z - k_5 z_5 - \frac{4 \cos\phi \cos\vartheta}{m} z_4 + \dot{\alpha}_5 \right], \quad k_5 > 0, \tag{4.32}$$

where $\dot{\alpha}_5 = \frac{\partial \alpha_5}{\partial p_z} v_z + \frac{\partial \alpha_5}{\partial v_z} \dot{v}_z + \frac{\partial \alpha_5}{\partial p_{zd}} v_{zd} + \frac{\partial \alpha_5}{\partial v_{zd}} \dot{v}_{zd} + \frac{\partial \alpha_5}{\partial \dot{v}_{zd}} \ddot{v}_{zd} + \frac{\partial \alpha_5}{\partial \rho_z} \dot{\rho}_z + \frac{\partial \alpha_5}{\partial \dot{\rho}_z} \ddot{\rho}_z + \frac{\partial \alpha_5}{\partial \ddot{\rho}_z} \rho_z^{(3)}$, so that (4.31) becomes

$$\dot{z}_5 = -\frac{4 \cos\phi \cos\vartheta}{m} z_4 - k_5 z_5. \tag{4.33}$$

Remark 4.4.2. *Assumption 4.3.1 guarantees that the designed control law (4.32) is always well-defined with the coefficient* $-\frac{4\cos\phi\cos\vartheta}{m}$ *of* z_4 *always negative.*

4.4.2 Adaptive Attitude Control Design

The proposed backstepping based adaptive control scheme is composed of two-parts: a parameter identification (PI) algorithm and an indirect adaptive backstepping control law as follows.

Parameter Identification Algorithm

The attitude dynamics equation (4.7) can be rewritten for each of $i \in \{1, 2, 3\}$ in the form of

$$\mathbf{b}_i^{-1}\dot{w}_{\varphi i} = \mathbf{b}_i^{-1}\mathbf{a}_{1i}w_{\varphi i} + \mathbf{b}_i^{-1}\mathbf{a}_{2i}f_{2i}(w_\varphi) + T_{\varphi i}, \tag{4.34}$$

which leads to the equation

$$T_{\varphi i} = \bar{\mathbf{a}}_{1i}w_{\varphi i} + \bar{\mathbf{a}}_{2i}f_{2i}(w_\varphi) - \bar{\mathbf{a}}_{3i}\dot{w}_{\varphi i}, \tag{4.35}$$

where $\bar{\mathbf{a}}_{1i} = \mathbf{b}_i^{-1}\mathbf{a}_{1i}$, $\bar{\mathbf{a}}_{2i} = \mathbf{b}_i^{-1}\mathbf{a}_{2i}$ and $\bar{\mathbf{a}}_{3i} = \mathbf{b}_i^{-1}$.

To avoid numerical differentiation, (4.35) is rewritten using the stable filter $\frac{1}{(s+\lambda)}$, $\lambda > 0$, as

$$\frac{1}{(s+\lambda)}[T_{\varphi i}] = \bar{\mathbf{a}}_{1i}\frac{1}{(s+\lambda)}[w_{\varphi i}] + \bar{\mathbf{a}}_{2i}\frac{1}{(s+\lambda)}[f_{2i}(w_\varphi)] - \bar{\mathbf{a}}_{3i}\frac{s}{(s+\lambda)}[w_{\varphi i}], \tag{4.36}$$

where the Euler rates in $w_{\varphi i} \in \mathbb{R}$ and the control thrust inputs in $T_{\varphi i} = \frac{Kb}{(s+b)}u_{\varphi i} \in \mathbb{R}$ are measurable; K and b are constant parameters. Based on (4.36), a parametric model is defined

$$z_{\varphi i} = \theta_{\varphi i}^{*T}\Phi_{\varphi i}, \tag{4.37}$$

$$z_{\varphi i} = \frac{1}{(s+\lambda)}[T_{\varphi i}] \in \mathbb{R}, \theta_{\varphi i}^* = [\bar{\mathbf{a}}_{1i}, \bar{\mathbf{a}}_{2i}, \bar{\mathbf{a}}_{3i}]^T \in \mathbb{R}^3, \Phi_{\varphi i} = \begin{bmatrix} \frac{1}{(s+\lambda)}[w_{\varphi i}] \\ \frac{1}{(s+\lambda)}[f_{2i}(w_\varphi)] \\ -\frac{s}{(s+\lambda)}[w_{\varphi i}] \end{bmatrix} \in \mathbb{R}^3.$$

Assumption 4.4.1. *The upper and lower limits of* $\theta_{\varphi i3}^*(t)$ *are known, i.e.* $0 < \underline{\theta}_{\varphi i3} \leq \theta_{\varphi i3}^*(t) \leq \bar{\theta}_{\varphi i3}$ *for some known* $\underline{\theta}_{\varphi i3}, \bar{\theta}_{\varphi i3} > 0$.

Next, the recursive LS algorithm [74] is applied with forgetting factor to (4.37) to produce the estimate $\hat{\theta}_{\varphi i}(t) = [\hat{\bar{\mathbf{a}}}_{1i}, \hat{\bar{\mathbf{a}}}_{2i}, \hat{\bar{\mathbf{a}}}_{3i}]^T$ of $\theta^*_{\varphi i}$ as follows:

$$\dot{\hat{\theta}}_{\varphi i}(t) = Pr(\mathbf{P}(t)\Phi_{\varphi i}(t)\epsilon_i(t)), \quad \hat{\theta}_{\varphi i}(0) = \hat{\theta}_{\varphi 0}, \tag{4.38}$$

$$\dot{\mathbf{P}}(t) = \begin{cases} \beta\mathbf{P} - \mathbf{P}\frac{\Phi_{\varphi i}\Phi_{\varphi i}^T}{m_{ni}^2}\mathbf{P}, & \text{if} \underline{\theta}_{\varphi i3} < \hat{\theta}_{\varphi i3} < \bar{\theta}_{\varphi i3} \\ 0, & \text{otherwise} \end{cases},$$

$$\epsilon_i(t) = \frac{z_{\varphi i}(t) - \hat{z}_{\varphi i}(t)}{m_{ni}^2(t)}, \quad m_{ni}^2(t) = 1 + \Phi_{\varphi i}^T(t)\Phi_{\varphi i}(t),$$

$$\hat{z}_{\varphi i}(t) = \hat{\theta}_{\varphi i}^T(t)\Phi_{\varphi i}(t), \tag{4.39}$$

where $\mathbf{P}(0) = \mathbf{P}_0 \in \mathbb{R}^{3\times 3}$ is a positive definite (covariance) matrix, m_n is the normalizing signal and ϵ is the estimation error, and $Pr(.)$ is the parameter projection operator [74] used to guarantee that $\hat{\theta}_{\varphi i3} \in [\underline{\theta}_{\varphi i3}, \bar{\theta}_{\varphi i3}]$.

Lemma 4.4.3 (Stability and Convergence)**.** *Consider the LS based PI algorithm (4.38), applied to the attitude dynamics (4.6)-(4.8). It is guaranteed that all the signals in (4.38), including* $\mathbf{P}$ *and* $\mathbf{P}^{-1}$*, are bounded. Further, if* $\Phi_{\varphi ni} = \frac{\Phi_{\varphi i}}{m_{ni}}$ *persistently exciting, i.e. if* $\frac{1}{T}\int_t^{t+T} \Phi_{\varphi ni}^T\Phi_{\varphi ni}d\tau \geq \alpha_0$ *for all* $t \geq 0$ *and some* $T, \alpha_0 > 0$*, then (4.38) ensures that* $\theta_{\varphi i}(t) \to \theta^*_{\varphi i}$ *as* $t \to \infty$*. The convergence of* $\theta_{\varphi i}(t) \to \theta^*_{\varphi i}$ *is exponential for* $\beta > 0$*.*

Proof. The result is a direct corollary of the more general Theorem 3.7.4 in [74]. □

Adaptive Control Design

A backstepping based indirect adaptive controller is proposed for tracking the desired attitude angles. For each of $i \in \{1, 2, 3\}$, we first define the error system

$$z_{6i} = \varphi_i - \varphi_{di} \in \mathbb{R}, \ \bar{z}_{7i} = w_{\varphi i} - \alpha_{7i} \in \mathbb{R}. \tag{4.40}$$

where α_7 is to be selected in the sequel.

From (4.40) and (4.6), we have

$$\dot{z}_{6i} = \dot{\varphi}_i - \dot{\varphi}_{di} = \bar{z}_{7i} + \alpha_{7i} - \dot{\varphi}_{di}. \tag{4.41}$$

To stabilize (4.41), α_7 is chosen as

$$\alpha_{7i} = -k_6 z_{6i} + \dot{\varphi}_{di}, \quad k_6 > 0, \tag{4.42}$$

so that

$$\dot{z}_{6i} = \bar{z}_{7i} - k_6 z_{6i}. \tag{4.43}$$

At the second step, from (4.40), we define

$$z_{7i} = \mathbf{b}_i^{-1}\bar{z}_{7i} = \mathbf{b}_i^{-1}w_{\varphi i} - \mathbf{b}_i^{-1}\alpha_{7i}, \tag{4.44}$$

then from (4.34), (4.35) and (4.44), we obtain

$$\begin{aligned}\dot{z}_{7i} &= \mathbf{b}_i^{-1}\dot{w}_{\varphi i} - \mathbf{b}_i^{-1}\dot{\alpha}_{7i} \\ &= \mathbf{b}_i^{-1}\mathbf{a}_{1i}w_{\varphi i} + \mathbf{b}_i^{-1}\mathbf{a}_{2i}f_{2i}(w_\varphi) + T_{\varphi i} - \mathbf{b}_i^{-1}\dot{\alpha}_{7i} \\ &= \bar{\mathbf{a}}_{1i}w_{\varphi i} + \bar{\mathbf{a}}_{2i}f_{2i}(w_\varphi) - \bar{\mathbf{a}}_{3i}\dot{\alpha}_{7i} + T_{\varphi i}.\end{aligned} \tag{4.45}$$

To stabilize (4.45), $T_{\varphi i}$ is chosen as

$$T_{\varphi i} = -\hat{\bar{\mathbf{a}}}_{1i}w_{\varphi i} - \hat{\bar{\mathbf{a}}}_{2i}f_{2i}(w_\varphi) + \hat{\bar{\mathbf{a}}}_{3i}\dot{\alpha}_{7i} - k_7\hat{\bar{\mathbf{a}}}_{3i}z_{7i} - z_{6i}, \tag{4.46}$$

where $\dot{\alpha}_{7i} = \frac{\partial\alpha_{7i}}{\partial\varphi_i}\dot{\varphi}_i + \frac{\partial\alpha_{7i}}{\partial\varphi_{di}}\dot{\varphi}_{di} + \frac{\partial\alpha_{7i}}{\partial\dot{\varphi}_{di}}\ddot{\varphi}_{di}$ and $k_7 > 0$, so that

$$\dot{z}_{7i} = -k_7 z_{7i} - z_{6i} - \tilde{\bar{\mathbf{a}}}_{1i}w_{\varphi i} - \tilde{\bar{\mathbf{a}}}_{2i}f_{2i}(w_\varphi) + \tilde{\bar{\mathbf{a}}}_{3i}\dot{\alpha}_{7i}, \tag{4.47}$$

where $\tilde{\bar{\mathbf{a}}}_{1i} = \hat{\bar{\mathbf{a}}}_{1i} - \bar{\mathbf{a}}_{1i}$; $\tilde{\bar{\mathbf{a}}}_{2i} = \hat{\bar{\mathbf{a}}}_{2i} - \bar{\mathbf{a}}_{2i}$; $\tilde{\bar{\mathbf{a}}}_{3i} = \hat{\bar{\mathbf{a}}}_{3i} - \bar{\mathbf{a}}_{3i}$.

Remark 4.4.4. *Since the actuator dynamics have been fully considered in the altitude and attitude design process, the control laws (4.32) and (4.46) can be regarded as the actual PWM control signals of the motors, which makes an easier way to application in practice. After all, the altitude u_z and the attitude u_φ control inputs generated via $T_{\varphi i}$ are mixed and converted to the actuator motor PWM inputs $v_r(t), r = 1, .., 4$ as discussed in [90] for providing the overall motion.*

4.5 System Stability Analysis

The stability of the overall closed-loop system is analyzed in this section, where the analysis results are summarized in the following theorem.

Theorem 4.5.1. *Consider the adaptive control scheme (4.15), (4.20), (4.24), (4.32), (4.38), (4.39), (4.40), (4.46) applied to Problem 4.3.1. Assume that $\Phi_{\varphi ni}$ in Lemma 1 is persistently exciting. It is guaranteed that all the signals are bounded and the tracking error $e(t) = [e_x(t), e_y(t), e_z(t)]^T$ asymptotically converges to zero. Further, pre-defined control performance condition (4.12) is satisfied.*

Proof. For proving the stability of the lateral position control system, define the Lyapunov function

$$V_{la}(z_1, z_2) = \frac{1}{2}\sum_{i=1}^{2} z_i^2. \tag{4.48}$$

From (4.17) and (4.20), the time derivative of (4.48) is obtained as

$$\begin{aligned}\dot{V}_{la}(z_1, z_2) =& z_1(\Theta_l z_2 - k_1 z_1) + z_2(-\Theta_l z_1 - k_2 z_2) \\ =& -k_1 z_1^2 - k_2 z_2^2 \leq -2min\{k_1, k_2\}V_{la}.\end{aligned} \tag{4.49}$$

Therefore, the origin $z_1 = z_2 = 0$ of the error system (4.15)-(4.21) is exponentially stable.

Then, by defining the Lyapunov function for the altitude as

$$V_{al}(z_3, z_4, z_5) = \frac{1}{2}\sum_{i=3}^{5} z_i^2. \tag{4.50}$$

From (4.26), (4.29) and (4.32), the time derivative of (4.50) is obtained as

$$\begin{aligned}\dot{V}_{al}(z_3, z_4, z_5) &= \Theta_z z_3 z_4 - k_3 z_3^2 - \Theta_z z_3 z_4 + \frac{4\cos\phi\cos\vartheta}{m} z_4 z_5 - k_4 z_4^2 - \frac{4\cos\phi\cos\vartheta}{m} z_4 z_5 - k_5 z_5^2 \\ &= -k_3 z_3^2 - k_4 z_4^2 - k_5 z_5^2 \leq -2min\{k_3, k_4, k_5\}V_{al}.\end{aligned} \tag{4.51}$$

Therefore, the origin $z_3 = z_4 = z_5 = 0$ of the error system (4.24)-(4.33) is exponentially stable.

The stability of the attitude motion is established by defining the Lyapunov function as

$$V_{at}(z_{6i}, z_{7i}) = \frac{1}{2} z_{6i}^2 + \frac{1}{2}\mathbf{b}_i z_{7i}^2. \tag{4.52}$$

From (4.42) and (4.46), the time derivative of (4.52) is obtained as

$$\begin{aligned}\dot{V}_{at}(z_{6i}, z_{7i}) &= z_{6i}\dot{z}_{6i} + z_{7i}\mathbf{b}_i\dot{z}_{7i} \\ &= -k_6 z_{6i}^2 - k_7 \mathbf{b}_i z_{7i}^2 - \tilde{\theta}_{\varphi i}^T [w_{\varphi i}\bar{z}_{7i}, f_{2i}(w_\varphi)\bar{z}_{7i}, -\dot{\alpha}_{7i}\bar{z}_{7i}]^T,\end{aligned} \tag{4.53}$$

where $\mathbf{b}_i$ is positive inertial based parameter under Assumption 4.4.1 and by Lemma 4.4.3 with the boundedness of the PI algorithm (4.38) guarantees that $\tilde{\theta}_{\varphi i}$ asymptotically converges to zero, which implies that as $t \to \infty$

$$\dot{V}_{at}(z_{6i}, z_{7i}) \to -k_6 z_{6i}^2 - k_7 \mathbf{b}_i z_{7i}^2 \leq -2min\{k_6, k_7\}V_{at}. \tag{4.54}$$

Hence, the origin $z_{6i} = z_{7i} = 0$ of the error system (4.40)-(4.47) is asymptotically stable. □

4.6 Alternative Adaptive Attitude Control Design

To design an alternative adaptive attitude control scheme that does not require persistent excitation for solving Problem 4.3.1, we redefine the Lyapunov function (4.52) as

$$V_{at}(z_{6i}, z_{7i}, \tilde{\theta}_{\varphi i}) = \frac{1}{2}z_{6i}^2 + \frac{1}{2}\mathbf{b}_i z_{7i}^2 + \frac{\gamma^{-1}}{2}\tilde{\theta}_{\varphi i}^T\tilde{\theta}_{\varphi i}, \tag{4.55}$$

where γ is positive design parameter.

The time derivative of (4.55) is obtained, similarly to Section 4.5, as

$$\begin{aligned}\dot{V}_{at}(z_{6i}, z_{7i}, \tilde{\theta}_{\varphi i}) &= z_{6i}\dot{z}_{6i} + z_{7i}\mathbf{b}_i\dot{z}_{7i} + \gamma^{-1}\tilde{\theta}_{\varphi i}^T\dot{\tilde{\theta}}_{\varphi i} \\ &= -k_6 z_{6i}^2 - k_7\mathbf{b}_i z_{7i}^2 - \tilde{\theta}_{\varphi i}^T[w_{\varphi i}\bar{z}_{7i}, f_{2i}(w_\varphi)\bar{z}_{7i}, -\dot{\alpha}_{7i}\bar{z}_{7i}]^T + \gamma^{-1}\tilde{\theta}_{\varphi i}^T\dot{\tilde{\theta}}_{\varphi i}.\end{aligned} \tag{4.56}$$

Choosing the update law $\dot{\tilde{\theta}}_{\varphi i} = \dot{\hat{\theta}}_{\varphi i}$ in (4.56) as

$$\dot{\hat{\theta}}_{\varphi i} = -\gamma[w_{\varphi i}\bar{z}_{7i}, f_{2i}(w_\varphi)\bar{z}_{7i}, -\dot{\alpha}_{7i}\bar{z}_{7i}]^T, \tag{4.57}$$

we obtain

$$\dot{V}_{at}(z_{6i}, z_{7i}, \tilde{\theta}_{\varphi i}) = -k_6 z_{6i}^2 - k_7\mathbf{b}_i z_{7i}^2, \tag{4.58}$$

which implies that z_{6i} and z_{7i} asymptotically converge to zero and $\dot{\hat{\theta}}_{\varphi i}$ asymptotically converges to a constant. Therefore, we have the following result.

Theorem 4.6.1. *Consider the adaptive control scheme (4.15), (4.20), (4.24), (4.32), (4.40), (4.46), (4.57) applied to Problem 4.3.1. It is guaranteed that all the signals are bounded and the tracking error $e(t) = [e_x(t), e_y(t), e_z(t)]^T$ asymptotically converges to zero. Further, pre-defined control performance condition (4.12) is satisfied.*

4.7 Simulations and Experimental Tests

4.7.1 Testbed Platform and Benchmark Controllers

In simulations and experiments, the quadrotor UAV testbed platform is Qball-X4, developed by Quanser Inc. [172]. Designed controllers are implemented via MATLAB

Table 4.1: The Qball-X4 quadrotor UAV dynamic parameters

Parameter	Definition	Value
m	Total mass	1.4 [Kg]
l	Distance between O_b and the motor	0.2 [m]
g	Gravity	9.81 [m/s^2]
K	Positive armature gain	120 [N]
K_ψ	Thrust-to-moment gain	4 [Nm]
b	Actuator bandwidth	15 [rad/s]
$J_{\phi 0}$	Nominal pitch inertia	0.03 [Kgm^2]
$J_{\theta 0}$	Nominal roll inertia	0.03 [Kgm^2]
$J_{\psi 0}$	Nominal yaw inertia	0.04 [Kgm^2]
$d_{\phi 0}$	Nominal drag on pitch	-0.01 [Nms^2]
$d_{\theta 0}$	Nominal drag on roll	-0.012 [Nms^2]
$d_{\psi 0}$	Nominal drag on yaw	-0.009 [Nms^2]

Simulink® and Quanser Quarc interfaces. The dynamic parameters of the Qball-X4 are specified as shown in Table-4.1. The nominal values of inertias and drags are used for non-adaptive designs. Detailed description of the platform can be found in Section 3.8.1.

Three different benchmark controllers are used in comparison with the proposed control design as follows. Benchmark controller-1 is composed of a PID position control with $K_{pb} = 0.006$, $K_{ib} = 0.01$ and $K_{db} = 0.008$, and a LQR attitude control with $K_L = [0.0616,\ 0.0126,\ 1.1066]$. Benchmark controller-2 is composed of a full backstepping control by using backstepping gains with $k_1 = 0.1$, $k_2 = 0.4$, $k_3 = 5$, $k_4 = 20$, $k_5 = 100$, $k_6 = 5$ and $k_7 = 5$. Benchmark controller-3 is composed of a full backstepping control with guaranteed tracking error by using specified PPB parameters and same control settings as used in benchmark controller-2. The proposed adaptive backstepping control with guaranteed tracking error is designed by using PI model parameters which are specified as the forgetting factor $\beta = 0.001$, the initial covariance matrix $\mathbf{P}_0 = 10^5 I_{3\times 3}$ and the initial parameter matrix $\theta_{\varphi 0} = [-0.75; -0.5; 0.05]$, and same control and PPB settings as used in benchmark controller-3.

4.7.2 Simulation Tests

In simulations, a spiral trajectory is considered as

$$p_d(t) = [10\cos(0.04t), 10\sin(0.04t), 0.025t]^T, \tag{4.59}$$

with the initial position $p(0) = [9, 1, 0.2]^T$. The PPB parameters are specified as $\rho_{l0} = 3.58$, $\rho_{l\infty} = 0.08$, $k_l = 0.2$, $\overline{\delta}_l = 0.7$, $\underline{\delta}_l = 0.7$, $\rho_{z0} = 1.25$, $\rho_{z\infty} = 0.04$, $k_z = 0.3$, $\overline{\delta}_z = 1$ and $\underline{\delta}_z = 0.4$.

The simulation results of the proposed controller compared with benchmark controllers are presented in Figures 4.3-4.4. The proposed design works successfully; the tracking errors remain within the intended bounds while the attitude dynamics model uncertainties are compensated. As seen in Figure 4.4, it is verified that PPB based error transformation gives flexibility in tuning transient and steady-state behaviors of the nonlinear system. The maneuvering, tracking and parameter estimation details with the proposed controller are shown in Figures 4.5-4.7. Next, the alternative direct adaptive controller in Section 4.6 is simulated and compared with the proposed control scheme in Section 4.4.2 in Figures 4.8. Both design methods work effectively to satisfy attitude tracking.

4.7.3 Experimental Tests

In experiments, a sinusoidal altitude trajectory is considered as

$$p_d(t) = [0, 0, 0.5 + 0.2\sin(0.05t)]^T, \tag{4.60}$$

with the initial position $p(0) = [0, 0, 0.2]^T$. The PPB parameters are specified as $\rho_{l0} = 2.3$, $\rho_{l\infty} = 0.3$, $k_l = 0.2$, $\overline{\delta}_l = 0.9$, $\underline{\delta}_l = 1$, $\rho_{z0} = 2.3$, $\rho_{z\infty} = 0.3$, $k_z = 0.2$, $\overline{\delta}_z = 1$ and $\underline{\delta}_z = 0.9$.

Transient and steady-state tracking errors with the proposed controller, compared with the benchmark controllers, are presented in Figure 4.9. The video of the experimental tests is presented in URL: https://www.youtube.com/watch?v=KsILES17DDk. The proposed controller is observed to guarantee bounded error performances with adjustable error convergence rates. The error convergence rate is clearly improved around 20 [sec] using tuning flexibility of the proposed control design. The experimental results of the proposed controller are shown in Figures 4.10-4.13, indicating high tracking performance and robustness to modeling uncertainties. While sinusoidal altitude motion is performing, lateral tracking is freely worked within the specified bound 0.3 [m] as shown in Figure 4.10.

Two different motion cases are tested at the fixed-level altitude to investigate hovering performance of the proposed indirect adaptive control design. The results of the circular

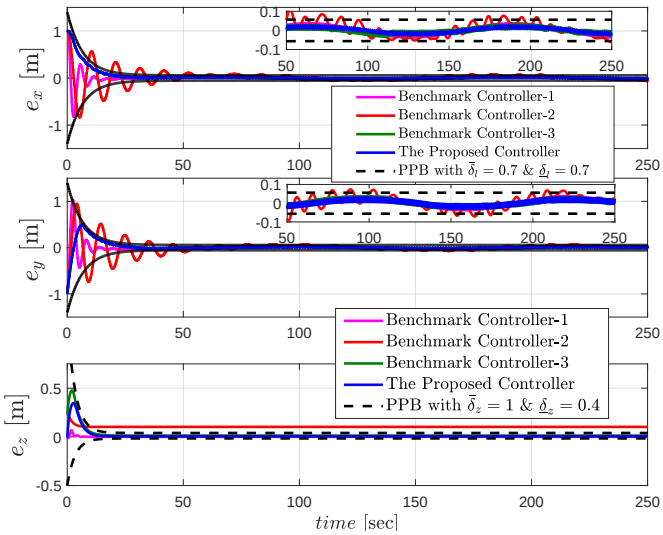

Figure 4.3: Spiral trajectory tracking errors of the proposed control design, compared with the benchmark controllers.

trajectory tracking test are shown in Figures 4.14-4.17 and the video of the circular hovering experiment is presented in URL: https://www.youtube.com/watch?v=fuTXh-JeRyk. The results of the square-waypoint tracking test are shown in Figures 4.18-4.21, and the video of the square hovering experiment is presented in URL: https://www.youtube.com/watch?v=G1x4r-hDU48. The proposed controller works successfully for both motion cases.

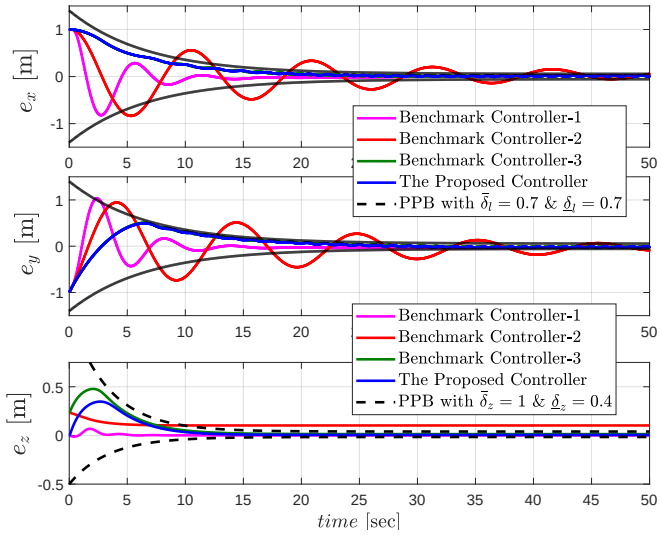

Figure 4.4: Transient error performances for 0-50[sec].

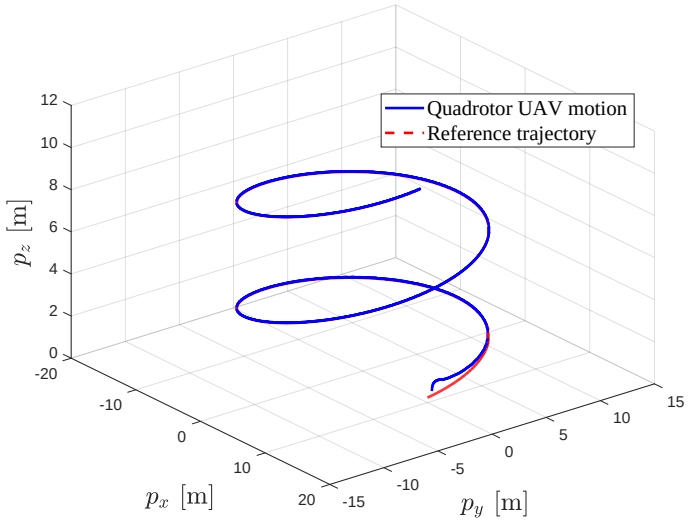

Figure 4.5: Spiral motion with proposed control design.

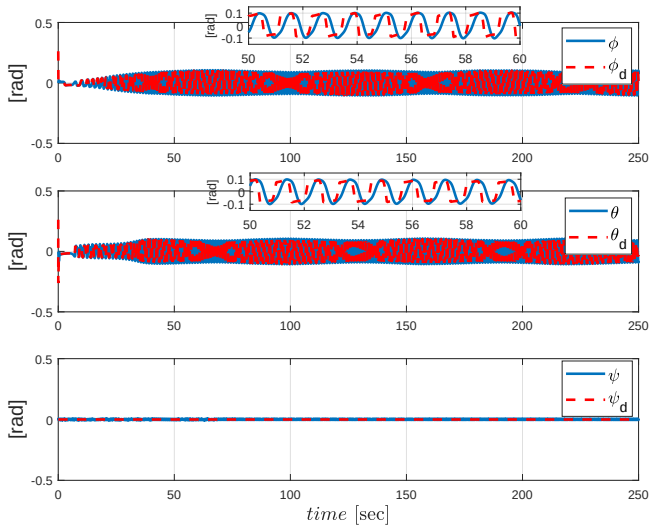

Figure 4.6: Attitude tracking of the proposed control design.

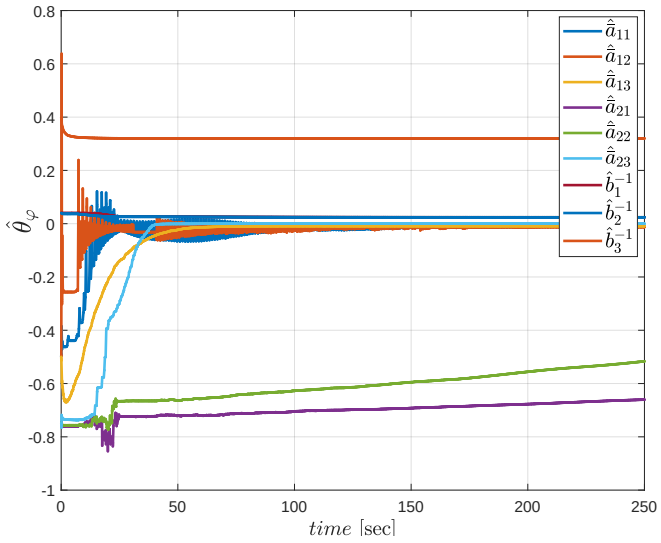

Figure 4.7: LS based estimation $\hat{\theta}_\varphi$ of θ_φ^*.

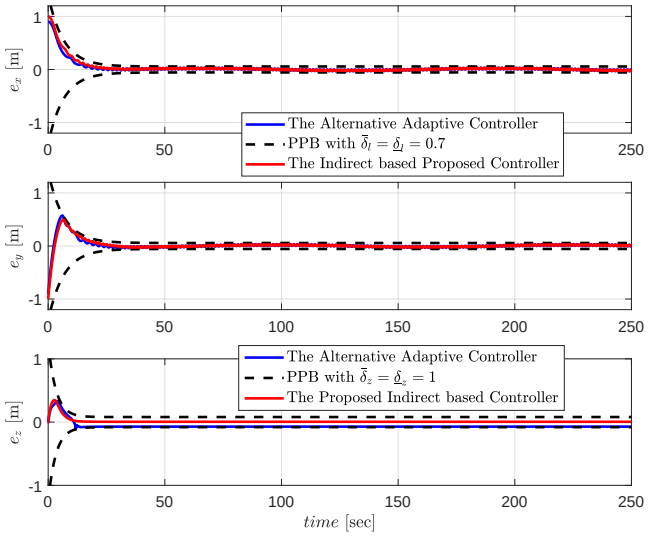

Figure 4.8: Tracking errors with the proposed indirect adaptive control design Section 4.4.2 and the direct adaptive control in Section 4.6.

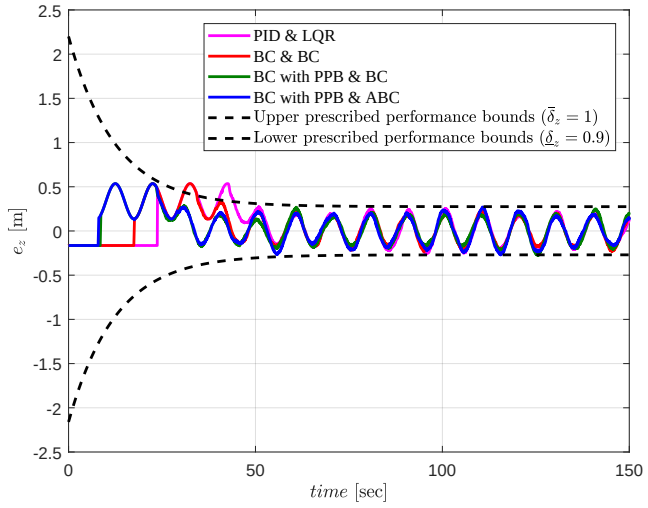

Figure 4.9: Altitude tracking errors of the proposed control design, compared with the benchmark controllers.

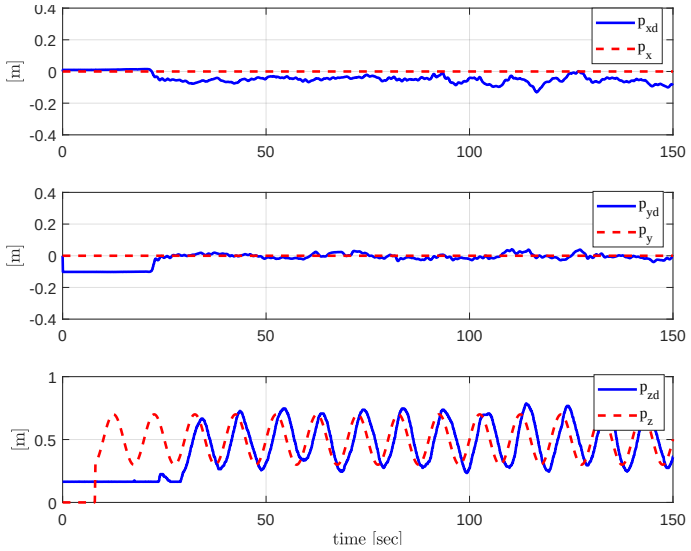

Figure 4.10: Trajectory tracking of the proposed control design.

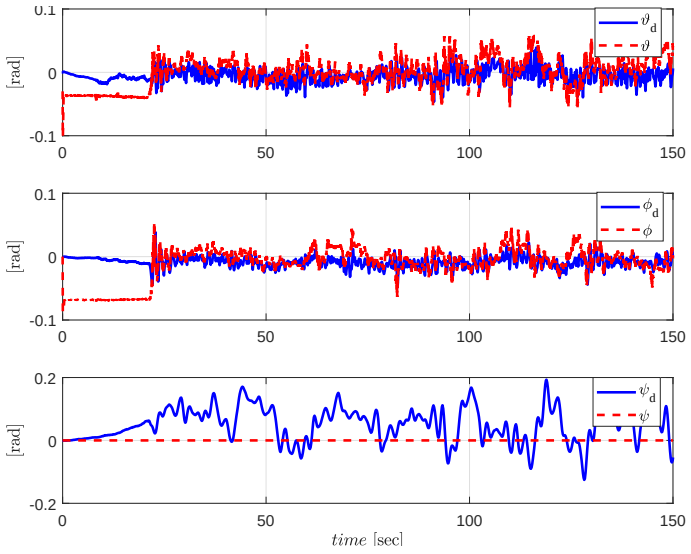

Figure 4.11: Attitude tracking of the proposed control design.

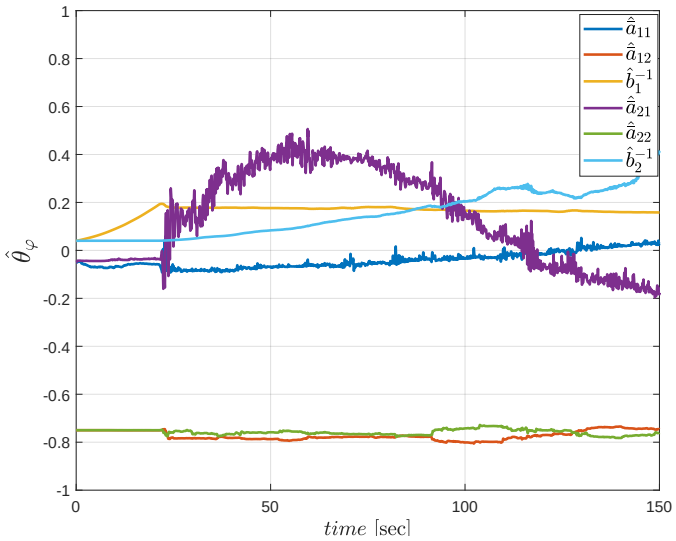

Figure 4.12: LS based estimation $\hat{\theta}_\varphi$ of θ^*_φ.

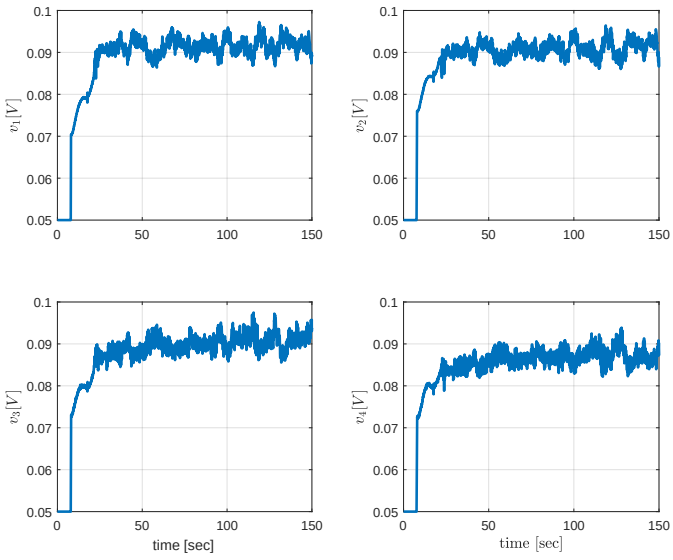

Figure 4.13: Motor PWM inputs v_r for the proposed control design.

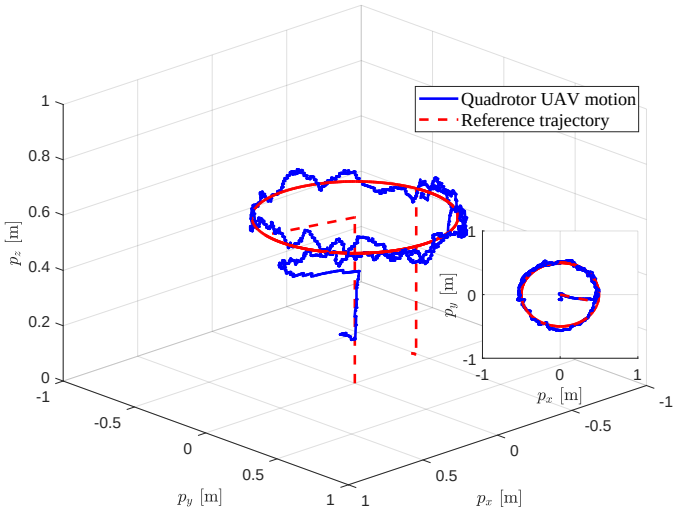

Figure 4.14: Circular hovering test motion.

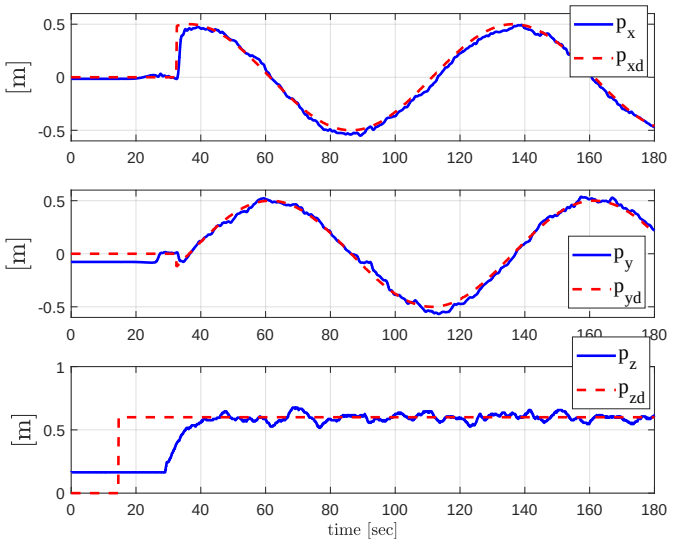

Figure 4.15: Trajectory tracking for the circular hovering test.

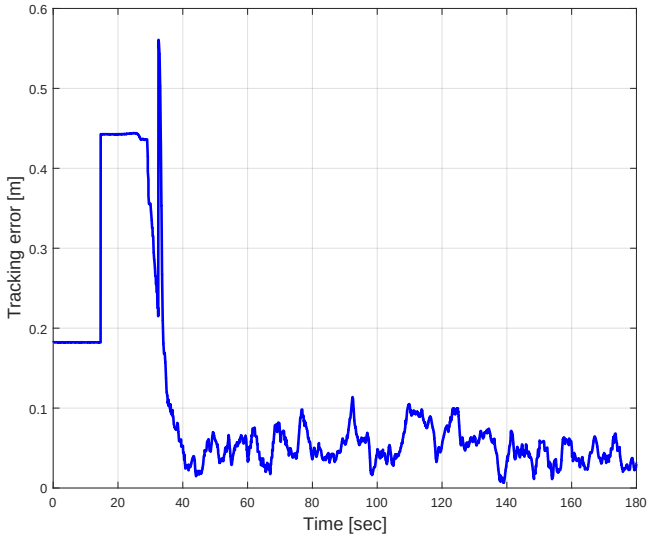

Figure 4.16: Mean Square tracking error for the circular hovering test.

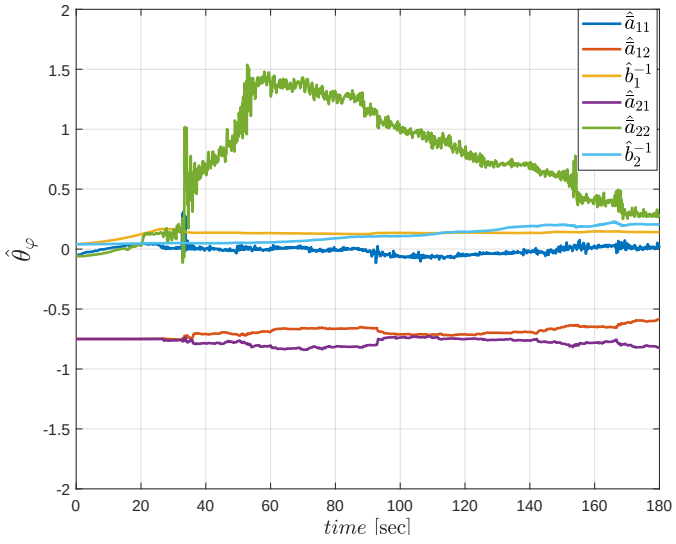

Figure 4.17: LS based estimation $\hat{\theta}_\varphi$ of θ_φ^* for the circular hovering test.

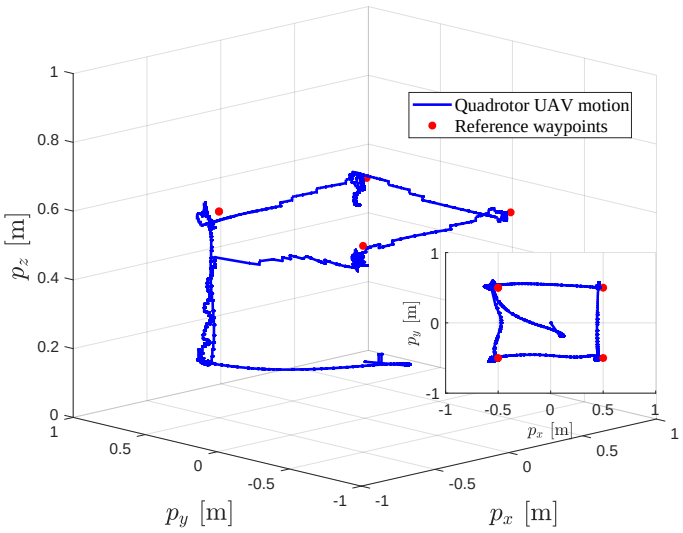

Figure 4.18: Square hovering test motion.

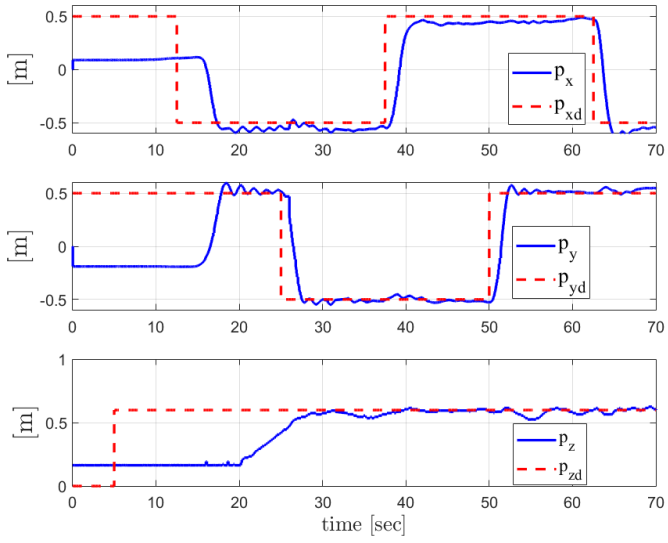

Figure 4.19: Waypoint tracking for the square hovering test.

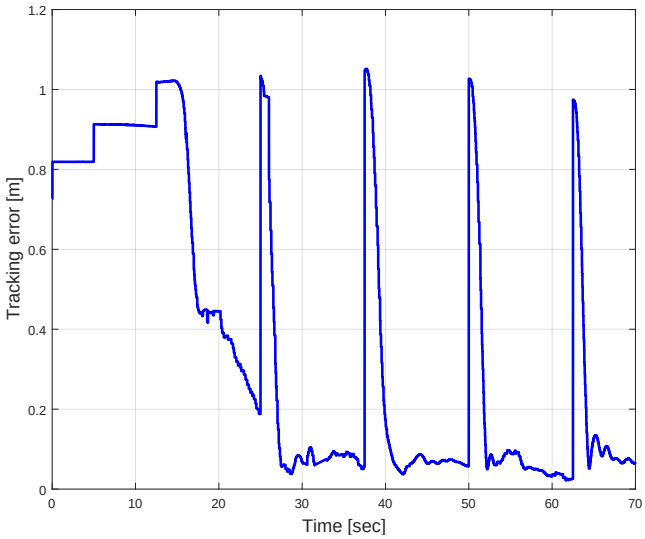

Figure 4.20: Mean Square tracking error for the square hovering test.

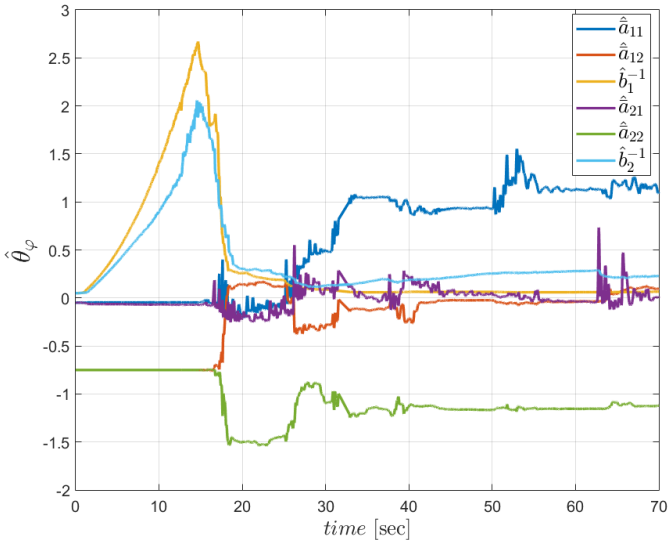

Figure 4.21: LS based estimation $\hat{\theta}_\varphi$ of θ^*_φ for the square hovering test.

4.8 Summary and Remarks

Robust adaptive motion control of quadrotor UAVs with guaranteed tracking error performance has been studied and tested on a Qball-X4 quadrotor testbed. The proposed control schemes have been developed for position (lateral position and altitude) and attitude dynamics, separately. The position control schemes have been designed utilizing prescribed performance bound (PPB) based error transformation and backstepping techniques. These control schemes have ensured bounded trajectory tracking error with tunable transient and steady-state behaviors. Effects of nonlinearities and model (inertia and drag) uncertainties in attitude dynamics are compensated making the control design adaptive via use of LS based PI algorithms. The overall stability and convergence of the closed-loop system have been proved. The effectiveness of the proposed design has been verified via simulations and experiments.

Chapter 5

Adaptive Mixing Formation Control of a Multi-UAV System

5.1 Introduction

In formation, several architectures have been studied e.g., decentralized (distributed) vs. centralized, hierarchical vs. non-hierarchical and symmetric vs. asymmetric [22, 53, 89] as high-level designs. Hierarchical architectures are more practical and better suited for real-time implementation in multi-UAV systems without long-range sensors. In this chapter, a distributed formation control scheme is designed for a system of $N \geq 4$ quadrotor UAVs in the asymmetric and hierarchical ($leader$-$follower$) structure with $leader$, $first$, $second$ and $ordinary$ followers, for a robust maintenance of predefined formation geometry , utilizing tools of rigid graph theory [12, 163] for performing cohesive motion in 3D.

Formation control literature works mostly use simple dynamical models such as single-integrator, point-mass (double integrator) or kinematic UAV model [11, 56, 70]. A single integrator model based formation control design is presented in [82] for a group of quadrotor UAVs in 2D. [83] extends the study to a global convergence in formation. In both studies, the authors do not deal with low-level control design of the quadrotor UAVs and its performance effects on the formation maintenance and robustness. In [89], an adaptive formation control of a multi quadrotor UAV system considering the realistic dynamic modeling is studied for parametric uncertainties. The quadrotor UAV dynamics is considered in three separated sub-models: reference angle, altitude, and attitude dynamics to make more proper and effective low-level control analyses, separately. In this chapter, the main contribution is to design an adaptive mixing controller (AMC) to enhance tracking perfor-

mance and robustness at the low-level while using rigid graph theory tools for formation maintenance of a multi quadrotor UAV system in 3D.

The quadrotor UAV dynamics consists of highly coupled states, aerodynamic coefficients, disturbances, and uncertainties. To compensate these effects, more advanced control designs are required. In the literature, there exist proportional-integral-derivative (PID) and linear quadratic (LQ) control based classical studies for simplified and linearized dynamics [30, 36] as well as advanced control schemes [25, 27, 39, 90, 103] that use nonlinear effects by utilizing nonlinear control techniques such as feedback linearization, sliding mode and backstepping control methods.

To compensate the effects of parametric uncertainties, there exist two main adaptive control approaches: direct and indirect [74]. Indirect approaches calculate controller gains using estimated system parameters at each instant time [33, 46, 89], while direct methods update controller parameters directly [46, 53]. In this chapter, we develop indirect adaptive controllers using the least squares (LS) based parameter identification (PI) algorithm to cancel the effects of inertial uncertainties in the attitude of quadrotor UAVs. This approach gives us some advantages, e.g. avoiding negative effects of adaptation time on control performances. By this approach, control performances can be adjusted easily. An integral state is also added into the controllers for dealing with disturbances which come from ignored terms, e.g. drag and Coriolis.

Although there are many theoretical accomplishments and successful applications of PI based indirect adaptive control designs, this area still needs an effort to solve difficulties in robustness performance [92]. Since PI algorithms need a time to converge uncertain parameters to actual values, indirect adaptive control schemes perform poorly for transient tracking performance with overshoot/undershoot and more chattering during the convergence time. By this motivation, as the main contribution of the chapter, the AMC scheme is designed to improve the individual tracking of each quadrotor UAV by providing smoother control action as well as formation maintenance performance. In the proposed scheme, the multiple model adaptive control approach [16, 32, 33, 92] is used for quadrotor UAVs. Based on inertial changes, the proposed scheme is aimed to blend outputs of a set of controllers, each of which is pre-designed to provide desirable stability and performance properties for a certain parametric setting of the system environment. Since mixing strategies provide a smooth transition between control gains based on the estimated parameters, the AMC scheme aims to increase the robustness of tracking performances and formation maintenances. The proposed AMC is compared with the adaptive linear quadratic controller (ALQC) design. In both cases, PD controller is used for reference angle generation and PID controller is used for the altitude model to complete the motion of the multi quadrotor UAV system.

5.2 Quadrotor UAV Dynamics

The full nonlinear dynamic model of quadrotor UAV motion dynamics (2.10) is presented in Chapter 2. Then, the nonlinear dynamics is parted into the lateral position (reference angle), the altitude and the attitude dynamics. In this chapter, we have reconsidered the sub-models to obtain their separate linear models as following:

a) *Reference Angle Dynamics:* The reference angle φ_d is defined for the quadrotor UAV to drive on the desired lateral position $p_{ld} = [p_{xd}, p_{yd}]^T$ by using the dynamics as

$$\dot{p}_l = v_l, \tag{5.1}$$

$$\dot{v}_l = \frac{4T_z}{m} f_{1l}, \tag{5.2}$$

$$f_{1l} \triangleq \begin{bmatrix} \cos\phi \sin\vartheta \cos\psi + \sin\phi \sin\psi \\ \cos\phi \sin\vartheta \sin\psi - \sin\phi \cos\psi \end{bmatrix} \approx \begin{bmatrix} \vartheta \\ -\phi \end{bmatrix} \approx \begin{bmatrix} \vartheta_d \\ \phi_d \end{bmatrix},$$

where the approximation is valid for small angles ϑ, ϕ, ψ.

b) *Altitude Dynamics:* The altitude dynamics is

$$\dot{p}_z = v_z, \tag{5.3}$$

$$\dot{v}_z = \frac{4}{m}(\cos\phi \cos\vartheta) T_z - g, \tag{5.4}$$

$$\dot{T}_z = -bT_z + Kbu_z. \tag{5.5}$$

Since the rotational angles are close to zero by the small angle approximation, the linearized altitude model is obtained as

$$\ddot{p}_z = \left(\frac{4Kb}{m(s+b)} u_z - g \right). \tag{5.6}$$

c) *Attitude Dynamics:* Consider the attitude dynamics from (2.10), and for further design, let us redefine the attitude dynamics properly for controllable canonical form as

$$\dot{\varphi} = w_\varphi, \tag{5.7}$$

$$\dot{w}_\varphi = \varsigma_\varphi, \tag{5.8}$$

$$\dot{\varsigma}_\varphi = -b\varsigma_\varphi + Kb\frac{\sigma_\varphi}{J_\varphi} u_\varphi, \quad \varphi \in \{\phi, \vartheta, \psi\}. \tag{5.9}$$

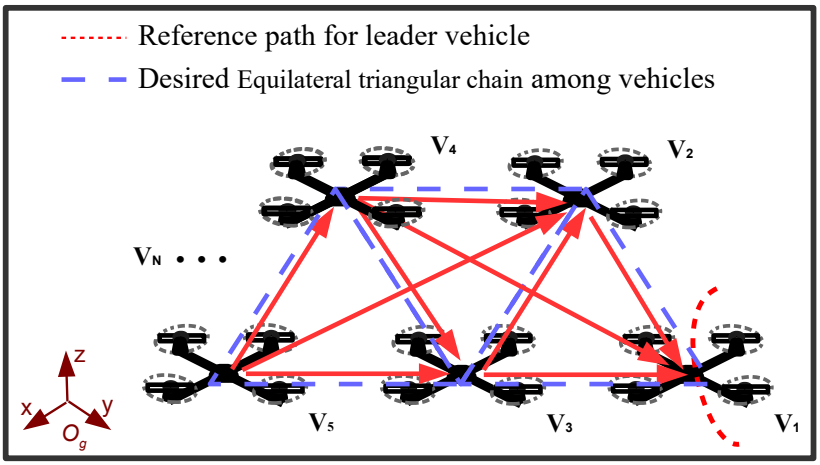

Figure 5.1: Directed underlying graph of a leader-follower persistent 3D formation F_S with N vehicles.

where ς_φ is the fictitious state. For the disturbance rejection, we also augment an integrator to the attitude dynamics. Then, we write the state-space form of the attitude dynamics as follows:

$$\dot{x} = Ax + Bu_\varphi + d, \tag{5.10}$$

where $x = [\int(\varphi - \varphi_d),\ (\varphi - \varphi_d),\ \dot{\varphi},\ \varsigma_\varphi]^T$,

$$A = \begin{bmatrix} 0 & 1 & 0 & 0 \\ 0 & 0 & 1 & 0 \\ 0 & 0 & 0 & 1 \\ 0 & 0 & 0 & -b \end{bmatrix}, B = \begin{bmatrix} 0 \\ 0 \\ 0 \\ \frac{\sigma_\varphi K b}{J_\varphi} \end{bmatrix}, \text{ and } d = \begin{bmatrix} 0 \\ -\dot{\varphi}_d \\ 0 \\ 0 \end{bmatrix}$$

with assuming that $\dot{\varphi}_d : \mathbb{R} \longrightarrow \mathbb{R}$ is bounded since there exists a desired angular velocity limit ε such that $|\dot{\varphi}_d(t)| \leq \varepsilon$.

5.3 Rigid Graph Modeling of the Multi-UAV System

In this chapter, a 3D asymmetric, hierarchical (*leader-follower*) formation architecture [20, 163] is considered as illustrated in Figure 5.1 for a multi quadrotor UAV system S that

consists of N vehicles indexed as $V_1, ..., V_N$, where the position of each vehicle V_i is denoted as $p_i(t) = [x_i(t)\ y_i(t)\ z_i(t)]^T \in \mathbb{R}^3$. The sensing and distance constraint network within the system S is represented by a directed underlying graph $G_S = (V_S, E_S)$ [20, 53, 163], where each quadrotor UAV V_i is represented by a vertex $i \in V_S$ and each directed edge $\overrightarrow{(i,j)} \in E_S$ represents a sensing and distance constraint link from V_i to V_j, indicating that V_i senses its distance $d_{ij} = \|p_i - p_j\|$ from V_j and is required to keep this distance at a pre-defined desired value of d^*_{ij}. The 3D formation is represented by $F_S = (S, G_S, D_S)$ as a combination of the multi quadrotor UAV system S, the underlying directed graph $G_S = (V_S, E_S)$ and the desired distance set $D_S = \{d^*_{ij} | \overrightarrow{(i,j)} \in E_S\}$.

In the high-level (formation) control design of this chapter, the notion of *persistence* [20, 163] is used to accommodate *cohesive* motion. A 3D formation is called *rigid* if the distance d_{ij} between corresponding quadrotor UAV pair (V_i, V_j) remains constant during any formation scenario. If each quadrotor UAV satisfies the distance constraint in the formation, it is called *constraint consistent*. If a formation satisfies both *rigidity* and *constraint consistence*, it is called *persistent*. For the formation $F_S = (S, G_S, D_S)$ to be persistent in 3D, the underlying graph $G_S = (V_S, E_S)$ needs to have at least $|E_S| = 3|V_S| - 6$ edges, in which case F_S is called *minimally persistent*. Formal definitions of *rigidity*, *constraint consistence* and *persistence* are presented with more details in [163].

5.4 Problem Statement

Given a system S of $N \geq 4$ quadrotor UAVs in a predefined persistent formation F_S and a desired trajectory to follow, the high-level (formation) control objective is to maintain the predefined formation during trajectory maneuvering, and, for each quadrotor UAV V_i, the low level (individual) control objective is to guarantee accurate trajectory tracking, robustly to inertial uncertainties and disturbances, under the following assumptions:

Assumption 5.4.1. *Reference way-points are known for the leader V_1 as a sequence of M way-points:*

$$p_r^k \in \{p_r^1, \ldots, p_r^M\}. \tag{5.11}$$

Assumption 5.4.2. *Each quadrotor UAV V_i can measure the position p_i of itself in O_g and the relative position $R_{(j,i)} = (p_j - p_i)$ of each neighbor agent V_j, for which $\overrightarrow{(i,j)} \in E_S$ and sensing d_{ij}.*

Assumption 5.4.3. *Desired relative positions of first V_2, second V_3 and ordinary V_i followers are known as $R^*_{(1,2)}$, $R^*_{(1,3)}$, $R^*_{(2,3)}$ and $R^*_{(j,i)}$, $j \in \{i-1, i-2, i-3\}$ for establishing d^*_{ij} and formation geometry.*

Next, the corresponding formal control problem is stated.

Problem 5.4.1. *Consider a system S of $N \geq 4$ quadrotor UAVs moving in $\mathbb{R}^3$, with agent motion dynamics (5.2), (5.6), (5.10) and let $F_S = (S, G_S, D_S)$ be a 3D minimally persistent formation in leader-follower structure. Design a distributed formation control scheme in the two-level as following:*

1. *At the formation level, design an on-line distributed supervisor P_s, under Assumptions 5.4.1-5.4.3, to generate the desired positions $p_{di}(t)$. Then, design a PD controller to generate desired angles $\varphi_{di} = (\phi_{di},\ \vartheta_{di},\ \psi_{di})$.*
2. *At the individual level, for attitude and altitude dynamics, design control laws to generate the control signals $\hat{u}^*_{\varphi i}(t)$ and $u_{zi}(t)$ such that the position $p_i(t)$ tracks the desired trajectory $p_{di}(t)$ generated at the formation level while maintaining desired distances d^*_{ij} and keeping the predefined formation shape without deforming during trajectory maneuvering.*

5.5 Distributed Control Design

High (formation) and low (individual) levels of the control scheme to address Problem 5.4.1 are designed as described in the following two subsections.

5.5.1 High-level Control Design

The high-level module H_i of each agent V_i's controller within the proposed distributed control scheme consists of two submodules as shown in Figure 5.2:

On-line Distributed Formation Supervisor

Desired trajectory $p_{di}(t)$ of V_i is generated on-line by this submodule, depending on whether V_i is the *leader* ($i = 1$), *first* or *second* follower ($i = 2$ or $i = 3$), or *ordinary* follower ($i \geq 4$), as follows:

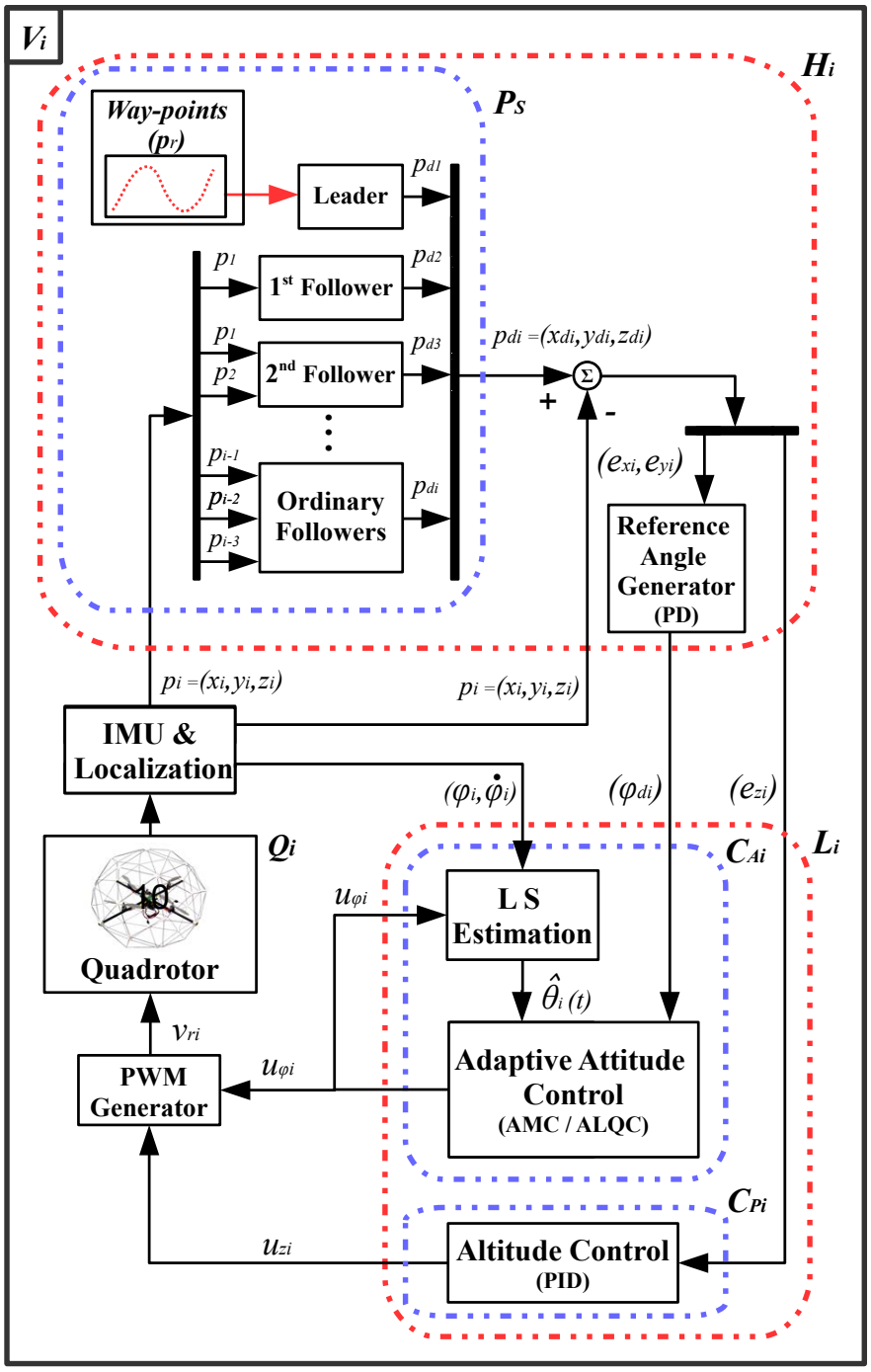

Figure 5.2: The Overall Control Structure for ith quadrotor UAV.

Leader: V_1 is responsible for tracking the predefined way-points defined in (19). To address this task, Algorithm 1 is used to generate $p_{d1}(t)$ at each time instant t.

Algorithm 1 Leader Way-point Based Trajectory Generation

Set $p_{d1}(0) = p_r^1$; $k = 1$
At each time instant $t > 0$:
$p_{d1}(t) = p_r^k$;
if $k < M$ and $\|p_1(t) - p_r^k\| \leq \delta$,
$k = k + 1$;
end

First Follower: V_2 only follows the *leader*. Its desired trajectory $p_{d2}(t)$ is generated as

$$p_{d2}(t) = \left[p_1(t) + R^*_{(1,2)}\right]. \tag{5.12}$$

Second Follower: V_3 follows the *leader* and $first$ follower. Its desired trajectory $p_{d3}(t)$ is generated as

$$p_{d3}(t) = \frac{1}{2}\left[p_1(t) + R^*_{(1,3)} + p_2(t) + R^*_{(2,3)}\right]. \tag{5.13}$$

Ordinary Followers: $V_i,\ i = 4, .., N$ follows previous three neighbors. The desired trajectory $p_{di}(t)$ of V_i is obtained as

$$p_{di}(t) = \frac{1}{3}\sum_j \left[p_j(t) + R^*_{(j,i)}\right]. \tag{5.14}$$

Note that the sensed and the desired distance sets among quadrotor UAVs are obtained by the relative and the pre-defined relative position knowledge under Assumption 5.4.2-5.4.3. To achieve *cohesive* motion for the *leader-follower* formation as discussed in Section 5.3, $first$, *second* and *ordinary* followers need to sense *leader*, *leader* and $first$ follower, and previous three neighbors, respectively. Thus, these required interactions are provided via $first$ (5.12), *second* (5.13) and *ordinary* (5.14) follower formation rules. Moreover, the above formation rules are derived to increase the robustness of the $leader - follower$ formation when the number of *ordinary* followers enlarges.

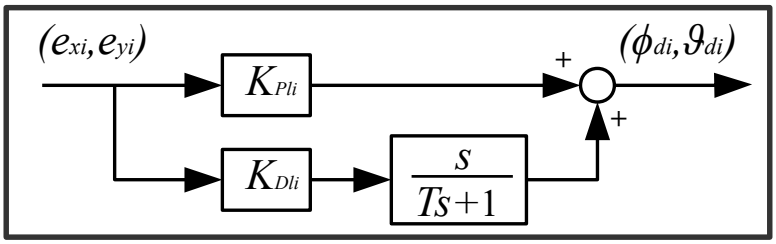

Figure 5.3: Low-pass filter for reference angle generator

Reference Angle Generation

Using desired position information, desired angles $\varphi_{di} = [\vartheta_{di},\ \phi_{di},\ \psi_{di}]^T$ is generated by a PD controller before the low-level scheme as

$$f_{1li} = K_{Pli}(p_{ldi} - p_{li}) + K_{Dli}(\dot{p}_{ldi} - \dot{p}_{li}). \tag{5.15}$$

It is considered that yaw motion does not affect directly the lateral motion of quadrotor UAVs. Thus, assumed that the desired yaw angle is $\psi_{di} = 0$ for $\forall t$. Then, $\varphi_{di} = [f_{1li},\ \psi_{di}]^T = [\vartheta_{di},\ \phi_{di},\ \psi_{di}]^T$. Since the derivative term of (5.15) has high frequency, this action can generate large control input variations in high-frequency error signals. To limit high-frequency gain, a low pass filter ($F(s) = 1/Ts+1$) is used as seen in Figure 5.3 where T is the filter time constant.

5.5.2 Low-level Control Design

The low-level control scheme (L_i) is considered in two subparts which are the altitude (C_{Pi}) and the attitude (C_{Ai}) as seen in Figure 5.2. The low-level control design is responsible for tracking and stabilizing of ith quadrotor UAV in the altitude by PID and the attitude by ALQC / AMC. These sub-control modules generate the effective control inputs of u_{zi} and $\hat{u}^*_{\varphi i}$, and then by mixing the control inputs via (2.5), the motor control input v_{ri} is produced. Both operating frameworks are stated as follows.

Altitude Control Design (PID)

Altitude controller C_{Pi} is designed to succeed longitudinal tracking of ith quadrotor UAV. By the altitude model (5.6), a PID control law is used for V_i as

$$u_{zi} = K_{Pzi}e_{zi} + K_{Izi}\int_0^t e_{zi}dt + K_{Dzi}\dot{e}_{zi}. \tag{5.16}$$

where $e_{zi} = (p_{zdi} - p_{zi})$.

Attitude Control Design

Adaptive attitude control schemes are designed based on the indirect approach. First, an LS based PI algorithm is separately developed to estimate the unknown inertias as shown in 5.4. Then, a mixing-based adaptive controller is designed to improve individual tracking and robustness as well as the formation performance of ith quadrotor UAV. An ALQC scheme is also designed to compare the formation performances. These designs are analyzed with more details in the sections 5.6 and 5.7.

5.6 On-line Parameter Identification

To overcome the inertial uncertainties in the attitude (5.10), an on-line LS based PI algorithm is utilized with ALQC and AMC schemes as shown in Figure 5.4. Following [74], we first form a linear parametric model, then design the LS algorithm. Consider (5.10) for ith quadrotor UAV in the form of transfer function as

$$s^2\varphi_i = \frac{\sigma_\varphi Kb}{J_{\varphi i}(s+b)}u_{\varphi i}. \tag{5.17}$$

Parametric Model: The parametric model is defined for (5.17) avoiding need for signal differentiation and the associated noise sensitivity issue by use of the stable filter $\frac{1}{(s+\lambda)^2}$, $\lambda > 0$, as

$$z_{\varphi i} = \theta_i^*\Phi_{\varphi i}, \tag{5.18}$$
$$z_{\varphi i} = \frac{s^2}{(s+\lambda)^2}\varphi_i, \theta_i^* = \frac{1}{J_{\varphi i}}, \Phi_{\varphi i} = \frac{\sigma_\varphi Kb}{(s+\lambda)^2(s+b)}u_{\varphi i},$$

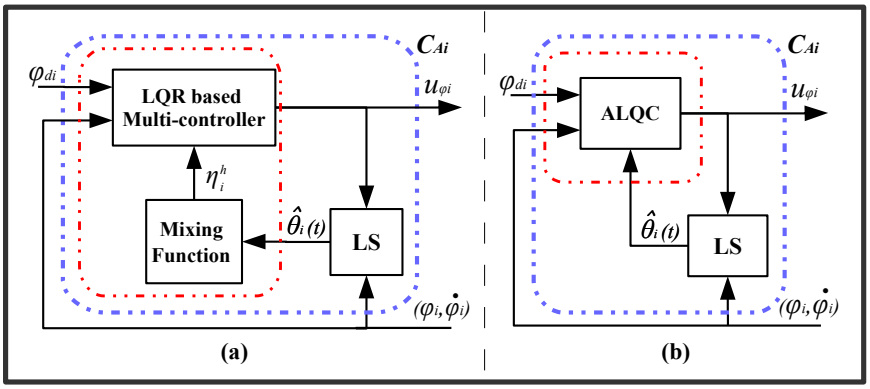

Figure 5.4: Adaptive control schemes: (a) AMC and (b) ALQC.

where Euler angles φ_i and control signals $u_{\varphi i}$ are measurable, and K, b, and σ_φ are constant parameters, respectively.

Recursive LS: To generate the estimate $\hat{\theta}_i$ of the uncertain inertia parameter θ_i^*, we apply the recursive LS algorithm [74] with forgetting factor to (5.18) as

$$\begin{aligned}
\dot{\hat{\theta}}_i(t) &= Pr(\mathbf{P}\epsilon\Phi_{\varphi i}) = \begin{cases} \mathbf{P}(t)\epsilon(t)\Phi_{\varphi i}(t), & \text{if } \underline{\theta}_i < \hat{\theta}_i < \overline{\theta}_i \\ 0, & \text{otherwise} \end{cases}, \\
\dot{\mathbf{P}}(t) &= \begin{cases} \beta\mathbf{P}(t) - \frac{\Phi_{\varphi i}^2(t)}{m_n^2(t)}\mathbf{P}^2(t), & \text{if } \underline{\theta}_i < \hat{\theta}_i < \overline{\theta}_i \\ 0, & \text{otherwise} \end{cases}, \\
\epsilon(t) &= \frac{z_{\varphi i}(t) - \hat{z}_{\varphi i}(t)}{m_n^2(t)}, \qquad m_n^2(t) = 1 + \Phi_{\varphi i}^2(t),
\end{aligned} \tag{5.19}$$

where $\mathbf{P}(t) \in \mathbb{R}$ is the positive covariance term with $\mathbf{P}(0) > 0$, $m_n(t)$ is the normalizing signal, β is the forgetting factor and $\epsilon(t)$ is the estimation error. Assumed that the upper and lower bounds of θ_i^* are known, i.e. $\overline{\theta}_i \geq \theta_i^*(t) \geq \underline{\theta}_i > 0$. $Pr(.)$ is the projection operator which maintains $\hat{\theta}_i(t) \in [\underline{\theta}_i, \overline{\theta}_i]$, for all $t \geq 0$.

Lemma 5.6.1 (Stability and Convergence)**.** *Consider the LS based PI algorithm, applied to the attitude dynamics* (5.17)*. It is guaranteed that all the signals in* (5.19)*, including* $\mathbf{P}$ *and* $\mathbf{P}^{-1}$*, are bounded and* $\hat{\theta}_i(t) \in [\underline{\theta}_i, \overline{\theta}_i]$*. Further, if* $\Phi_{\varphi ni} = \frac{\Phi_{\varphi i}}{m}$ *persistently exciting, i.e. if* $\frac{1}{T}\int_t^{t+T} \Phi_{\varphi ni}^2 d\tau \geq \alpha_0$ *for all* $t \geq 0$ *and some* $T, \alpha_0 > 0$*, then* (5.19) *ensures that* $\theta_i(t) \to \theta_i^*$ *as* $t \to \infty$*. The convergence of* $\theta_i(t) \to \theta_i^*$ *is exponential for* $\beta > 0$*.*

Proof. The result is a direct corollary of the more general Theorem 3.7.4 and 3.10.1 in [74]. □

5.7 Adaptive Attitude Control Laws

Two particular adaptive control laws, which are ALQC and AMC schemes, are studied based on the designed PI algorithm (5.19) and the infinite-time LQR [10] for the attitude model (5.10). Both control laws base on the LQR design as a nominal controller. Hence, the nominal LQR procedure is firstly presented as follows:

Let consider the quadrotor UAV dynamics from (5.10) as

$$\dot{x} = Ax + Bu_{\varphi}, \tag{5.20}$$

where $A \in \mathbb{R}^{4x4}$ is a matrix, and $B \in \mathbb{R}^4$ is a matrix. Then, design a nominal LQR for minimizing performance measurement of (5.20) with the cost function

$$J = \int (x^T Q x + R u_{\varphi}^2) dt, \tag{5.21}$$

where $Q \in \mathbb{R}^{4x4}$ is a positive definite matrix and $R \in \mathbb{R}$ is a positive scalar. We calculate the optimal gain $K_c \in \mathbb{R}^{1x4}$ as

$$K_c = R^{-1} B^T P, \tag{5.22}$$

where $P = P^T > 0 \in \mathbb{R}^{4x4}$ is an auxiliary matrix calculated by solving the Riccati equation as

$$A^T P + PA - PBR^{-1}B^T P + Q = 0. \tag{5.23}$$

After obtaining K_c, the state-feedback control law is

$$u_{\varphi} = -K_c x. \tag{5.24}$$

So that the closed-loop nominal LQR control law becomes

$$\dot{x} = (A - BK_c)x. \tag{5.25}$$

Lemma 5.7.1 (Nominal LQR Stability)**.** *Consider the nominal LQR design procedure* (5.21)-(5.24) *for the dynamics* (5.20)*. Then, the closed-loop system* (5.25) *is asymptotically stable.*

Proof. Under Assumption 3.2.1 from (pp.44-45) of [10], Lemma from (pp.46) of [10] guarantees that P is positive definite since (A, D), where D is any matrix such that $DD' = Q$, is completely observable and (A, B) is stabilizable for the parameters: $b, K, \sigma_\varphi, J_\varphi > 0$. So that the closed-loop nominal LQR control law (5.25) is asymptotically stable. □

5.7.1 Adaptive Linear Quadratic Control (ALQC)

In this section, adaptive linear quadratic control (ALQC) is designed for ith quadrotor UAV as seen in Figure 5.4 based on the nominal LQR design with the PI algorithm. Since the input matrix B_i includes inertial uncertainties, the LS based PI algorithm (5.19) is derived to estimate $\hat{\theta}_i$ of θ_i^* for all $t \geq 0$. By combining the estimate $\hat{\theta}_i$ with the LQR design (5.21)-(5.24), the time-varying state-feedback control law is obtained as

$$\hat{u}_{\varphi i}^* = -\hat{K}_{ci} x_i. \tag{5.26}$$

where $\hat{K}_{ci}$ is the on-line optimal control gain matrix.

Lemma 5.7.2 (ALQC Stability)**.** *Consider the attitude dynamics* (5.20) *for ith quadrotor UAV and design ALQC by following the nominal LQR steps* (5.21)-(5.24) *with the estimation* $\hat{\theta}_i(t)$ (5.19) *of* $\theta_i^*(t)$*. The adaptive optimal control law* (5.26) *is asymptotically stable.*

Proof. The control law (5.26) is asymptotically stable by Lemma 5.6.1 and Lemma 5.7.1 with guaranteed $\overline{\theta}_i \geq \hat{\theta}_i(t) \geq \underline{\theta}_i > 0$, for all $t \geq 0$. □

5.7.2 Proposed Adaptive Mixing Control (AMC)

This section presents an adaptive mixing control (AMC) approach applied the attitude of ith quadrotor UAV. The proposed AMC scheme uses a blending strategy between candidate controllers calculated based on the nominal LQR while it deals with overcoming inertial uncertainties as well as disturbance and sensor noises. The detail of the AMC approach is discussed in earlier studies [16, 33, 92]. In this section, the AMC procedure [92] is firstly introduced for a linear SISO plant which contains unknown parameters, disturbance and

sensor noise as,

$$
\begin{aligned}
y &= G(s,\theta^*)u + d, && (5.27)\\
G(s,\theta^*) &= G_N(s,\theta^*)(1+\triangle_m(s)), && (5.28)\\
G_N(s,\theta^*) &= \frac{N(s,\theta^*)}{D(s,\theta^*)}, && (5.29)\\
y_m &= y + \nu, && (5.30)
\end{aligned}
$$

where y_m is measured system output of y, θ^* is unknown plant parameter, $G_N(s,\theta^*)$ is the transfer function of the nominal plant with unknown parameters, $\triangle_m(s)$ is the multiplicative model uncertainty, d is the disturbance and ν is sensor noise on the system. The control objective is to regulate the output y to zero. In the AMC design, to accomplish the objective, there are four conditions that have to be satisfied [16, 92] as follows:

1. Interval of the unknown parameter θ^* is known,
2. $G_N(s,\theta^*)$ is strictly proper,
3. $\triangle_m(s)$ is proper and analytic in $\text{Re}(s) \geq \frac{-\delta_0}{2}$,
4. $D(s,\theta^*)$ is a monic polynomial with known degree.

Then, we consider the state-space realization of (5.28) for further state-space based control design

$$
\begin{aligned}
\dot{x}_m &= A_m x_m + B_m u_m, && (5.31)\\
y_m &= C_m x_m + d + \nu, && (5.32)
\end{aligned}
$$

where (A_m, B_m) is stabilizable and (C_m, A_m) is detectable to satisfy the control objective. Thus, under conditions 1-4, the proposed AMC scheme is developed considering (5.20) in the form of (5.31) for ith quadrotor UAV model. The AMC scheme consists of three main steps as illustrated in Figure 5.4: Adaptive law (LS scheme), Candidate controllers (developed off-line sets and used in multi-controller), and Mixing scheme as follows.

Adaptive law: Considering the adaptive mixing control literature, the gradient algorithm has been used in [16, 92] with parameter projection. Another method, the LS based adaptive law has been studied in [33]. Since the LS algorithm is less affected by the noise and inaccuracies in the observed data [74], the LS algorithm with parameter projection is used in the proposed AMC design. The LS based PI scheme has already designed in

section 5.6. Therefore, it performs separately and serves the estimation $\hat{\theta}_i$ to candidate controllers and mixing strategy.

Candidate controllers: Composing candidates and transition regions between each other, we define n subsets based on a priori knowledge on bounds of the uncertain parameter θ_i^*

$$\Omega_i = (\underline{\theta}_i, \overline{\theta}_i] = \{\theta_i^* \in \Omega_i | \ \underline{\theta}_i < \theta_i^* \leq \overline{\theta}_i\}, \tag{5.33}$$

where assumed that $\underline{\theta}_i$ and $\overline{\theta}_i$ are known. Then, Ω_i is separated into common n subsets and let us define the subset range Ω_i^h for candidate controllers as

$$\Omega_i^h = [\underline{\theta}_i^h, \overline{\theta}_i^h] \in \{\Omega_i^1, \Omega_i^2, ..., \Omega_i^n\}, \quad h = 1, 2, ..., n \tag{5.34}$$

where Ω_i^h, $\underline{\theta}_i^h$ and $\overline{\theta}_i^h$ are the pre-defined range, the lower and upper bounds for each subset, respectively. Ω_i^h is chosen that the intersection of each transition subset pair is non-empty $\Omega_i^h \cap \Omega_i^{h+1} \neq \emptyset$. Hence, transition subsets satisfy the condition $\underline{\theta}_i^{(h+1)} < \overline{\theta}_i^{(h)}$ where $h = [1, 2, \ldots, n-1]$.

For each subset Ω_i^h, a candidate controller is designed off-line as

$$u_i^h = C_i^h, \quad h = 1, 2, ..., n \tag{5.35}$$

where C_i^h is the candidate controller which meets the control objectives for Ω_i^h. Therefore, the state-feedback controller law is obtained based on the nominal LQR steps (5.20)-(5.24) as

$$C_i^h : u_i^h = -K_{ci}^h x_i, \tag{5.36}$$

where K_{ci}^h is the state feedback gain vector.

Hence, the set of candidate controllers are considered as

$$\Lambda \triangleq \{C_i^h\}_{h \in \{1,2,...,n\}}. \tag{5.37}$$

Lemma 5.7.3 (Candidate Stability)**.** *Consider the set Ω_i of the known bounds of θ_i^* which consists of the union of n subsets as*

$$\Omega_i = \bigcup_{h=1}^{n} \Omega_i^h \subset (\underline{\theta}_i, \overline{\theta}_i]. \tag{5.38}$$

Choose a fixed control parameter as $\theta_i^{ho} = \left(\frac{\underline{\theta}_i^h + \overline{\theta}_i^h}{2}\right)$ for each candidate subset where $h \in \{1, 2, ..., n\}$ as

$$\theta_i^{ho} \in \Omega_i^h = \{\theta_i^{ho} \in \mathbb{R} | \ \underline{\theta}_i^h < \theta_i^{ho} < \overline{\theta}_i^h\}. \tag{5.39}$$

Design each closed-loop control law (5.36), which is asymptotically stable for the fixed control parameter θ_i^{ho}, in (5.37).

Proof. The stability of each control law (5.36) in (5.37) is directly satisfied based on the Lemma 5.7.1 and the fixed $\theta_i^{ho} > 0$. □

Mixing scheme: We now select and employ bump functions to provide a smooth switching between the candidate controllers. Bump functions are represented as $\eta_i^h \in \{\eta_i^1, \eta_i^2, \eta_i^3, ..., \eta_i^n\}$. A mixing function is selected for each candidate range as

$$\varrho_i^h(\hat{\theta}_i) \quad = \quad \left(\frac{\hat{\theta}_i - a_i^h}{b_i^h} \right), \tag{5.40}$$

where a_i^h and b_i^h are bump function parameters, and (5.40) defines a bump function as

$$\eta_i^h(\hat{\theta}_i) \quad = \quad \begin{cases} e^{\frac{-1}{1-(\varrho_i^h)^2}} & , \text{if } \left|\varrho_i^h\right| < 1 \\ 0 & , otherwise. \end{cases} \tag{5.41}$$

Then, mixing performance gains are calculated as

$$\kappa_i^h(\hat{\theta}_i) = \frac{\eta_i^h(\hat{\theta}_i)}{\sum_{h=1}^n \eta_i^h(\hat{\theta}_i)}, \tag{5.42}$$

where $\kappa_i^h(\hat{\theta}_i) = 0$ if $\hat{\theta}_i \notin \Omega_i^h$.

Therefore, by the set of candidate controllers (5.37) and the mixing performance gains (5.42), the adaptive mixing control scheme is obtained as the following formula

$$\hat{u}_{\varphi i}^* = \sum_{h=1}^{n} \kappa_i^h(\hat{\theta}_i) u_i^h. \tag{5.43}$$

Lemma 5.7.4 (AMC Stability)**.** *Consider the AMC design (5.40)-(5.43) working with the PI (5.19). Select bump function parameters a_i^h and b_i^h for each properly selected candidate subset Ω_i^h. So that the mixing performance gains are only activated for intersection of two neighbor candidate subsets as*

$$\hat{\theta}_i \in \Omega_i^h \cap \Omega_i^{h+1} = [\underline{\theta}_i^h, \overline{\theta}_i^h] \cap [\underline{\theta}_i^{h+1}, \overline{\theta}_i^{h+1}] = [\underline{\theta}_i^{h+1}, \overline{\theta}_i^h]. \tag{5.44}$$

Then, the mixing control scheme becomes

$$\hat{u}_{\varphi i}(\hat{\theta}_i) = -\left[\kappa_i^h(\hat{\theta}_i)K_{ci}^h + \kappa_i^{h+1}(\hat{\theta}_i)K_{ci}^{h+1}\right] x_i \tag{5.45}$$

where it is designed that $\kappa_i^h + \kappa_i^{h+1} = 1$. *Thus, guarantee that the scheme* (5.45) *is Hurwitz stable when* $\hat{\theta}_i \in \Omega_i^h \cap \Omega_i^{h+1}$.

Proof. Consider the model (5.20) in form of the general controller canonical form where A and B matrices can be written as

$$A = \begin{bmatrix} 0 & 1 & 0 & \dots & 0 \\ 0 & 0 & 1 & \ddots & \vdots \\ \vdots & \vdots & \ddots & \ddots & 0 \\ 0 & 0 & \dots & 0 & 1 \\ -a_m & -a_{m-1} & \dots & -a_2 & -a_1 \end{bmatrix}, B = \begin{bmatrix} 0 \\ \vdots \\ \vdots \\ 0 \\ b_0 \end{bmatrix}. \tag{5.46}$$

Then, characteristic equation of the closed-loop controller of (5.46) for ith quadrotor UAV with the estimation $\hat{\theta}_i$ can be found as

$$c_i(s) = (sI - A_i + \hat{B}_i K_{ci}) \tag{5.47}$$

$$c_i(s) = (s^m + a_{i1}s^{m-1} + \cdots + a_{im}) + \hat{b}_{i0}(K_{ci}^m s^{m-1} + \cdots + K_{ci}^1) \tag{5.48}$$

By (5.45) and (5.48), we have the mixing characteristic equation $C(s)$ when $\hat{\theta}_i \in \Omega_i^h \cap \Omega_i^{h+1}$ as

$$C(c_i^h, c_i^{h+1}) = \left(\kappa_i^h c_i^h(s) + \kappa_i^{h+1} c_i^{h+1}(s)\right) \tag{5.49}$$

By Lemma 5.6.1 guaranteeing $\hat{b}_0 > 0\ \forall t$ and following Theorem 2.3 of [28], $C(c_i^h, c_i^{h+1})$ is Hurwitz stable since $c_i^h(s)$ and $c_i^{h+1}(s)$ are Hurwitz stable and if and only if

$$eig(W) = eig(H^{-1}(c_i^h)H(c_i^{h+1})) \in (0, \infty], \tag{5.50}$$

where Hurwitz matrix $H(.)$ associated with the polynomial $h(s) \in C(c_i^h, c_i^{h+1})$. The detail proofs are given in [28]. □

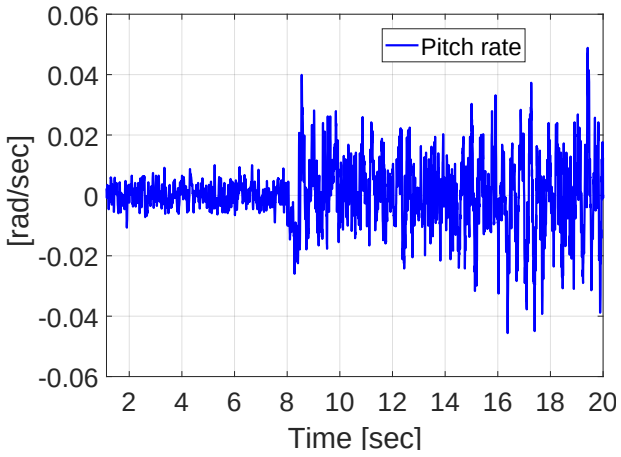

Figure 5.5: Qball-X4's pitch rate measurement for 20 [sec].

5.8 Real-time Testbed and Simulations

5.8.1 Real-time Testbed System

In the simulations, we consider that the multi quadrotor UAV testbed system is composed of Qball-X4 quadrotors developed by Quanser Inc. [172]. The Qball-X4 quadrotor system has been introduced in section 3.8.1

5.8.2 Adding the noise effect into the simulation

For more realistic simulation, we add Gaussian noises characterized by measuring Qball-X4 testbed's sensors. The Qball-X4 is off-line switched on idle running for 20 [sec] to measure pitch rate from IMU as shown in Figure 5.5. By the measured data, the variance and mean value are calculated as

$$\rho = \frac{1}{r}\sum_{i=1}^{r}(w_\phi), \quad \text{and} \quad Var(w_\phi) = \frac{1}{r}\sum_{i=1}^{r}(w_\phi - \rho)^2 \tag{5.51}$$

where $Var(w_\phi)$ is the variance value, and ρ is the average of the noisy data. Then, the characterized noises are added to the attitude dynamics.

Table 5.1: The off-line calculated candidate controller gains

Sets	Gains (K_{ci}^h)			
Ω_i^h	k_1	k_2	k_3	k_4
Ω_i^1	0.018257418	0.066549024	0.029999841	0.641136268
Ω_i^2	0.018257418	0.063712188	0.019879852	0.805576366
Ω_i^3	0.018257418	0.062640956	0.016173044	0.923532064
Ω_i^4	0.018257418	0.062034229	0.014101452	1.019855195
Ω_i^5	0.018257418	0.061629867	0.012732009	1.102934544
Ω_i^6	0.018257418	0.061335083	0.011739312	1.176831973
Ω_i^7	0.018257418	0.061107543	0.010976320	1.243882949
Ω_i^8	0.018257418	0.060924803	0.010365603	1.305577123
Ω_i^9	0.018257418	0.060773698	0.009861993	1.362933702
Ω_i^{10}	0.018257418	0.060645928	0.009437131	1.416686371
Ω_i^{11}	0.018257418	0.060535963	0.009072189	1.467384069

5.8.3 Control Design Parameters

All control parameters are set for real-time based simulations and the Qball-X4's parameters are taken as presented in Section 3.8.1. Sensor noises are characterized as $Var(w_\phi) = 0.0003$ and $\rho = 0.000721$ by (5.51). Reference angle PD control parameters are $K_{Pli} = 0.7$ and $K_{Dli} = 0.4$ and altitude PID control parameters are $K_{Pzi} = 0.006$, $K_{Izi} = 0.008$ and $K_{Dzi} = 0.002$. In the LS, forgetting factor, initial covariance and initial unknown parameter value are chosen $\beta = 0.1$, $\mathbf{P}(0) = 10^5$ and $\theta_i(0) = 5$, respectively. In the nominal LQR, the ideal cost is determined by weightings as $Q = \text{diag}(150\ 0\ 20000\ 25)$ and $R = 30000$. In the AMC, the number of candidates is selected as $n = 11$. The minimum and maximum bounds of θ_i^* are considered $\underline{\theta}_i = 5 < \theta_i^* < \overline{\theta}_i = 77$. Then, the interval of subsets is taken $\Omega_i = [5, 77]$. n subset candidates are assigned as $\Omega_i^1 = [5, 10]; \Omega_i^2 = [7, 17]; \Omega_i^3 = [14, 24]; \Omega_i^4 = [21, 31]; \Omega_i^5 = [28, 38]; \Omega_i^6 = [35, 45]; \Omega_i^7 = [42, 52]; \Omega_i^8 = [49, 59]; \Omega_i^9 = [56, 66]; \Omega_i^{10} = [63, 73]; \Omega_i^{11} = [70, 77]$. Bump functions parameters selected for each subset as $a_i^h \in \{5, 12, 19, 26, 33, 40, 47, 54, 61, 68, 75\}$ and $b_i^h = 5$. The off-line calculated candidate gains are given in table 5.1.

5.8.4 Simulation Results

Simulation results present the formation performances of the multi quadrotor UAV system with N=5 vehicles in *leader-follower* structure. The initial positions of quadrotor UAVs are $p_1(0) = (9, 1, 0.2)^T$; $p_2(0) = (8, -1, 0.2)^T$; $p_3(0) = (8, 1, 0.2)^T$; $p_4(0) = (7, 0, 0.2)^T$; $p_5(0) = (7, -1, 0.2)^T$. Spiral motion way-points are generated by $p_r^k(t) = (10\cos(0.04t), 10\sin(0.04t), 0.025t)^T$ where $t = T_s k$ and the sampling time $T_s = 0.05$. Spiral motion scenarios are performed to maintain desired formation distance $d_{ij}^* = 5\ [m]$ and $5\sqrt{3}\ [m]$ based on the desired relative positions: $R_{(1,2)}^* = (-\frac{5}{2}, -\frac{5}{2}\sqrt{3}, 0)^T$, $R_{(1,3)}^* = (-5, 0, 0)^T$, $R_{(2,3)}^* = (-\frac{5}{2}, \frac{5}{2}\sqrt{3}, 0)^T$, $R_{(1,4)}^* = (-\frac{15}{2}, -\frac{5}{2}\sqrt{3}, 0)^T$, $R_{(2,4)}^* = (-5, 0, 0)^T$, $R_{(3,4)}^* = (-\frac{5}{2}, -\frac{5}{2}\sqrt{3}, 0)^T$, $R_{(2,5)}^* = (-\frac{15}{2}, \frac{5}{2}\sqrt{3}, 0)^T$, $R_{(3,5)}^* = (-5, 0, 0)^T$, and $R_{(4,5)}^* = (-\frac{5}{2}, \frac{5}{2}\sqrt{3}, 0)^T$.

The formation performances of both control schemes are satisfied in terms of formation requirements as seen in Figures 5.6 and 5.7 as well as satisfying individual tracking performances of all quadrotor UAVs. Figure 5.13 presents $\hat{\theta}_{\phi 1}$ of the *leader* for both scenarios. The PI algorithm works well and both $\theta_{\phi 1}^*$ approach to ideal value after 50 [*sec*], but they do not converge to ideal value because of the noise. Although we can able to adjust the convergence time period for the estimation which is chosen a long time for this case study, we have designed the PI algorithm by selecting the parameters with small initial values of θ_i^*, forgetting factor β, covariance θ_0 to show the effectiveness of the proposed AMC design during the poor transient convergence period. Therefore, both control strategies work poorly at the convergence time period than their steady-state performances because of the poor transient estimation performance and initial positions of the quadrotor UAVs. After the estimation is converged around the ideal value after 50 [*sec*], the formation schemes work satisfactorily with small errors for maintaining the desired rigid distances as seen in Figure 5.8 and 5.9.

During the poor estimation performances at the beginning of simulations between 0 [*sec*] - 50 [*sec*], the ALQC design has bigger transient formation distance errors with overshoot, undershoot and chattering as seen clearly in Figures 5.8 and 5.10. This behavior is also based on the ALQC scheme's control gains change sharply at each instant time. On the other hand, the proposed AMC scheme compensates these negative effects as seen in 5.9 and 5.11 and it eliminates chattering effects and large transient errors on the control design because of providing smooth blending for calculation of control gains at each instant time. During the AMC test, Figure 5.12 presents how to generate the smooth blending by using the bump function with the on-line estimation.

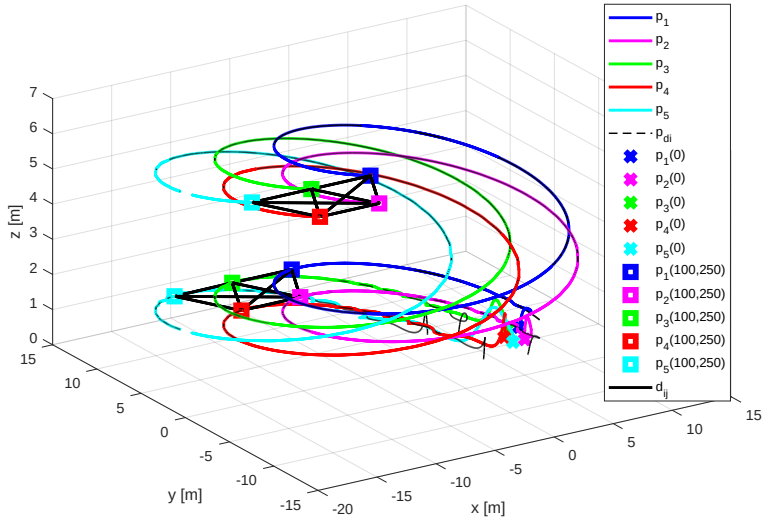

Figure 5.6: Spiral formation motion in 3D for ALQC.

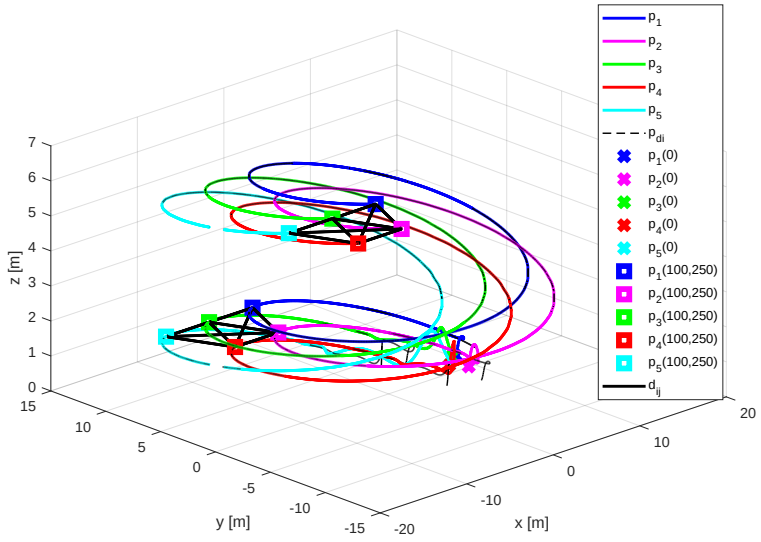

Figure 5.7: Spiral formation motion in 3D for AMC.

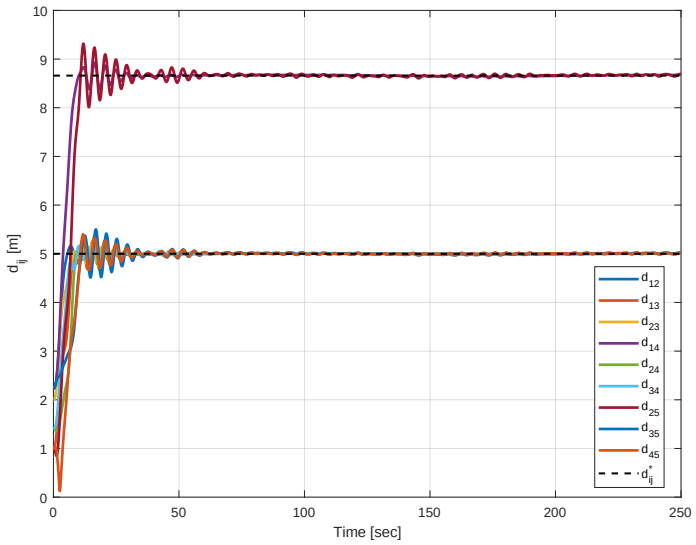

Figure 5.8: Formation distances among quadrotor UAVs for ALQC.

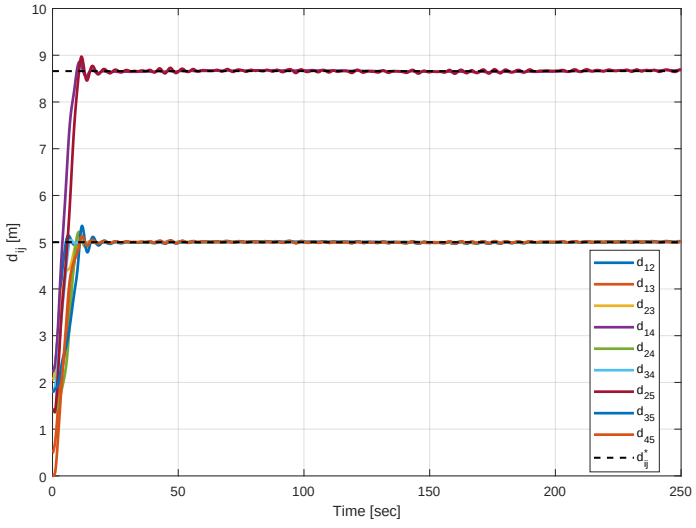

Figure 5.9: Formation distances among quadrotor UAVs for AMC.

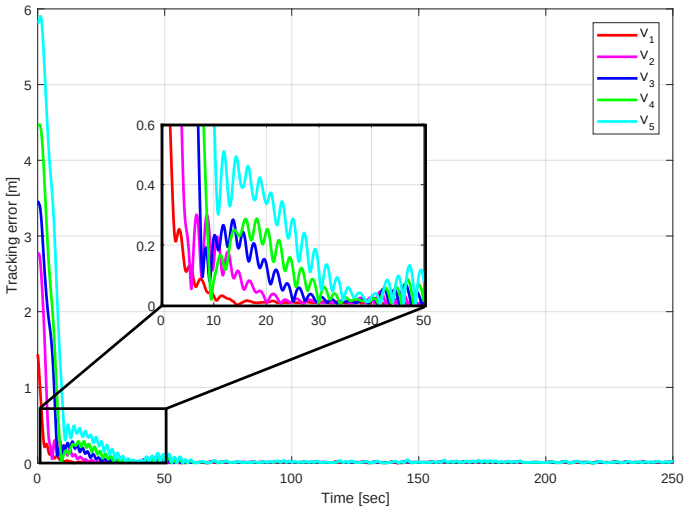

Figure 5.10: Mean Square tracking errors for ALQC.

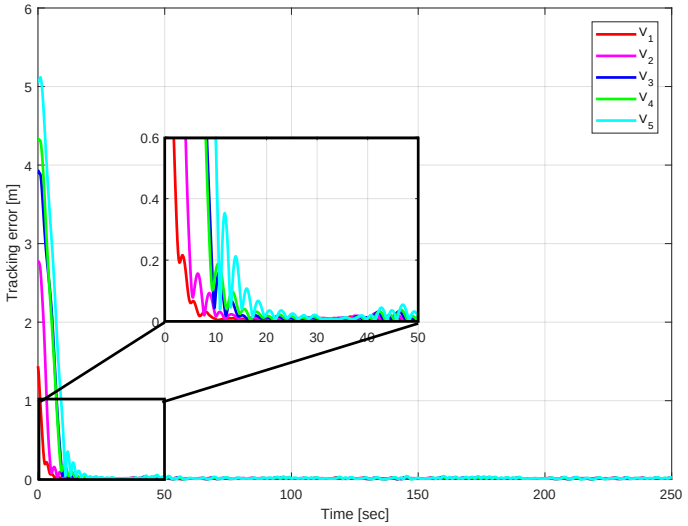

Figure 5.11: Mean Square tracking errors for AMC.

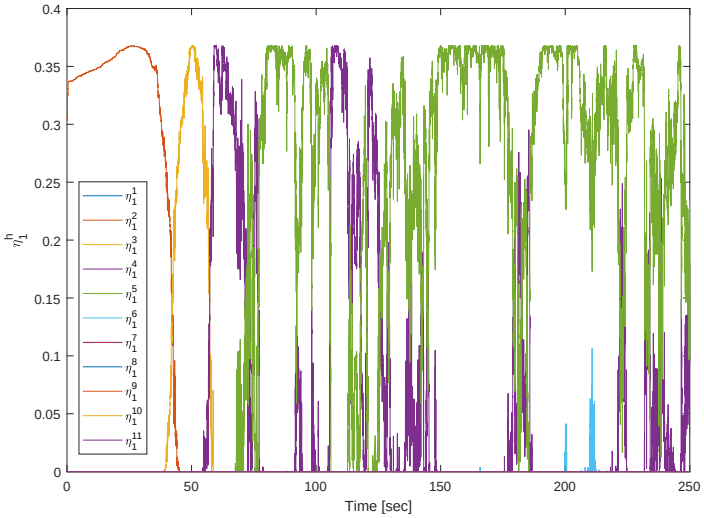

Figure 5.12: Bump functions of candidate subsets for the estimation $\hat{\theta}_{\phi 1}$ of the leader quadrotor UAV.

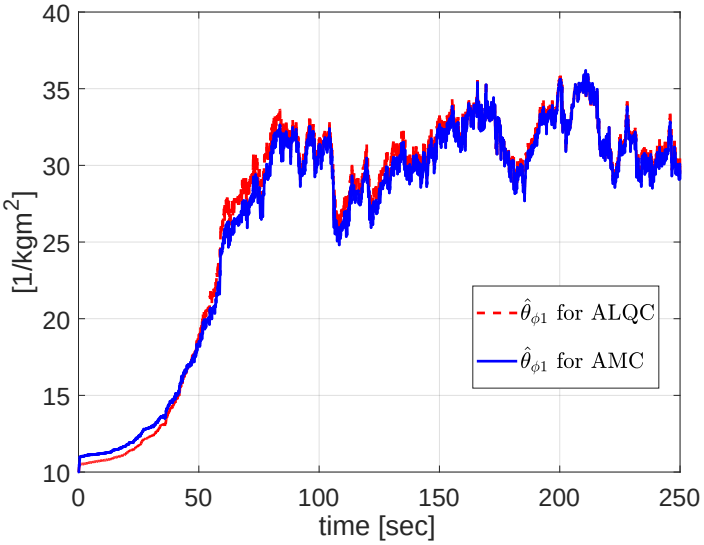

Figure 5.13: $\hat{\theta}_{\phi 1}$ estimation of $\theta^*_{\phi 1}$ for the leader quadrotor UAV.

5.9 Summary and Remarks

In this chapter, a two-level, distributed formation scheme has been designed to keep persistently the formation shape of the multi quadrotor UAV system for the realistic quadrotor UAV dynamics. At the individual control, we have developed the AMC and compared with ALQC. In order to suppress the negative effects of inertial uncertainties in the attitude model, an online PI model is developed for both control schemes. The proposed AMC scheme have used to increase formation maintenance and robustness by using the switching method under uncertainties, disturbances, and noises. The ALQC has also been designed to compare both controllers and to show the effectiveness of the proposed AMC by the real-time based simulations. Performances of both adaptive formation control algorithms have been evaluated on realistic quadrotor UAV model by simulation tests. Both simulations are based the realistic model of the quadrotor UAV (developed from first principle dynamics as well as using data collected from real-time experiments), and we witness the high performance of the proposed AMC scheme. Successful formation results show the efficiency of the proposed AMC scheme.

Chapter 6

Optimal Tracking and Formation Control of Fixed-wing UAVs

In Chapters 3 and 5, we have proposed a linear quadratic tracking (LQT) control law for optimal attitude tracking of quadrotor UAVs and a distributed control law for formation maintenance of multi-quadrotor UAV systems. In this chapter, we extend these designs to lateral motion control of (Piccolo-controlled) small fixed-wing UAVs. We design LQT control schemes for trajectory tracking of the small fixed-wing UAVs and extend these designs to distributed formation control of a multiple fixed-wing UAV system. The surveillance tasks are simulated, and the main results are presented for the two cases: tracking and formation.

6.1 Lateral Motion Model of Small Fixed-wing UAV

The simplified nonlinear motion model (2.26) of fixed-wing UAVs is presented in Chapter 2. In this section, we simplify and partition (2.26) to obtain separate linear lateral model which is considered in the two sub-models as following:

a) Linear position model:

$$\begin{aligned} \dot{x}_l(t) &= A_l x_l(t) + B_l v_{cl}(t), \quad l \in \{x, y\}, \\ p_l(t) &= C_l x_l(t), \end{aligned} \tag{6.1}$$

where $A_l = \begin{bmatrix} 0 & 1 \\ 0 & -\frac{1}{\alpha_v} \end{bmatrix}$, $B_l = \begin{bmatrix} 0 \\ \frac{1}{\alpha_v} \end{bmatrix}$, $C_l = \begin{bmatrix} 1 \\ 0 \end{bmatrix}^T$, and $x_l = \begin{bmatrix} p_l \\ v_l \end{bmatrix}$. x_l, v_{cl}, p_l, v_l and α_v represent states, control input, position, velocity, and inertial related dynamic parameter for the lateral model, respectively.

b) Linear heading model:

$$\begin{aligned} \dot{x}_\psi(t) &= A_\psi x_\psi(t) + B_\psi w_c(t), \\ \psi(t) &= C_\psi x_\psi(t), \end{aligned} \tag{6.2}$$

where $A_\psi = \begin{bmatrix} 0 & 1 \\ 0 & -\frac{1}{\alpha_\psi} \end{bmatrix}$, $B_\psi = \begin{bmatrix} 0 \\ \frac{1}{\alpha_\psi} \end{bmatrix}$, $C_\psi = \begin{bmatrix} 1 \\ 0 \end{bmatrix}^T$, and $x_\psi = \begin{bmatrix} \psi \\ w \end{bmatrix}$. x_ψ, w_c, ψ, w and α_ψ represent states, control input, heading, angular velocity and inertial related dynamic parameter for the heading model, respectively.

Remark 6.1.1. *The dynamic systems have input constraints such that* $0 < v_{min} < v_c < v_{max}$ *and* $-w_{min} < w_c < w_{max}$ *since the real-time fixed-wing UAV works in limited velocity and angular velocity.*

6.2 Problem Statement for Fixed-level Motion

Consider a fixed-wing UAV and a system S of $N \geq 3$ fixed-wing UAVs moving in $\mathbb{R}^2$ with the lateral motion model (6.1) and (6.2). For an equilateral formation case of the UAV system S in 2D as discussed in section 5.3, let $F_S = (S, G_S, D_S)$ be a 2D minimally persistent formation in *leader-follower* structure. Before the problem definition, the following assumptions are made.

Assumption 6.2.1. *The states of the fixed-wing UAVs are measurable.*

Assumption 6.2.2. *The fixed-wing UAVs are held at the constant altitude for planar motion tasks. The desired path is known for tracking task of a single UAV and formation task of leader UAV* V_1.

Assumption 6.2.3. *Desired relative positions of first* V_2 *and ordinary* V_i *followers are known as* $R^*_{(1,2)}$ *and* $R^*_{(j,i)}$, $j \in \{i-1, i-2\}$ *to establish* d^*_{ij} *and formation geometry.*

Assumption 6.2.4. *The fixed-wing UAVs are equipped with the autopilot avionic devices whose dynamics can be modeled as the simplified forms presented in Section 6.1.*

Design a distributed formation control scheme and LQT control schemes as follows:

1. At the formation level, design an on-line distributed supervisor (P_S) and a reference heading generator (P_H) under Assumptions 6.2.1-6.2.3 to generate $p_{di}(t) = [p_{xdi}(t), p_{ydi}(t)]^T$ and $\psi_{di}(t)$ of V_i.

2. Design the lateral position control unit to generate the command signal v_{ci} for feeding the autopilot under Assumption 6.2.4. Design an infinite-horizon LQT controller to generate an optimal control signal $v_{ci}(t) = v_{ci}^*(t) = \|v_{cli}^*(t)\|$ so that $p_{li}(t)$ tracks its desired trajectory $p_{ldi}(t)$, minimizing the cost function for predefined quadratic performance optimal tracking and energy consumption

$$J_{vi} = \frac{1}{2}\int_0^\infty (Qe_{li}^2(t) + Rv_{cli}^2(t))dt, \tag{6.3}$$

   where Q and R are positive constant weighting terms and

$$e_{li}(t) = p_{ldi}(t) - p_{li}(t), \tag{6.4}$$

   is the lateral position tracking *error*.

3. Design the heading control unit to generate the command signal w_{ci} for feeding the autopilot under Assumption 6.2.4. Design an infinite-horizon LQT controller to generate the optimal attitude control signal $w_{ci}(t) = w_{ci}^*(t)$ so that $\psi_i(t)$ tracks its desired trajectory $\psi_{di}(t)$, minimizing the cost function for predefined quadratic performance optimal tracking and energy consumption

$$J_{wi} = \frac{1}{2}\int_0^\infty (Qe_{wi}^2(t) + Rw_{ci}^2(t))dt, \tag{6.5}$$

   where Q and R are positive constant weighting terms and

$$e_{wi}(t) = \psi_{di}(t) - \psi_i(t) \tag{6.6}$$

   is the heading tracking *error*.

Remark 6.2.1. *Note that we follow the leader UAV design $i = 1$ of Problems 1-3 for trajectory tracking control of a single fixed-wing UAV.*

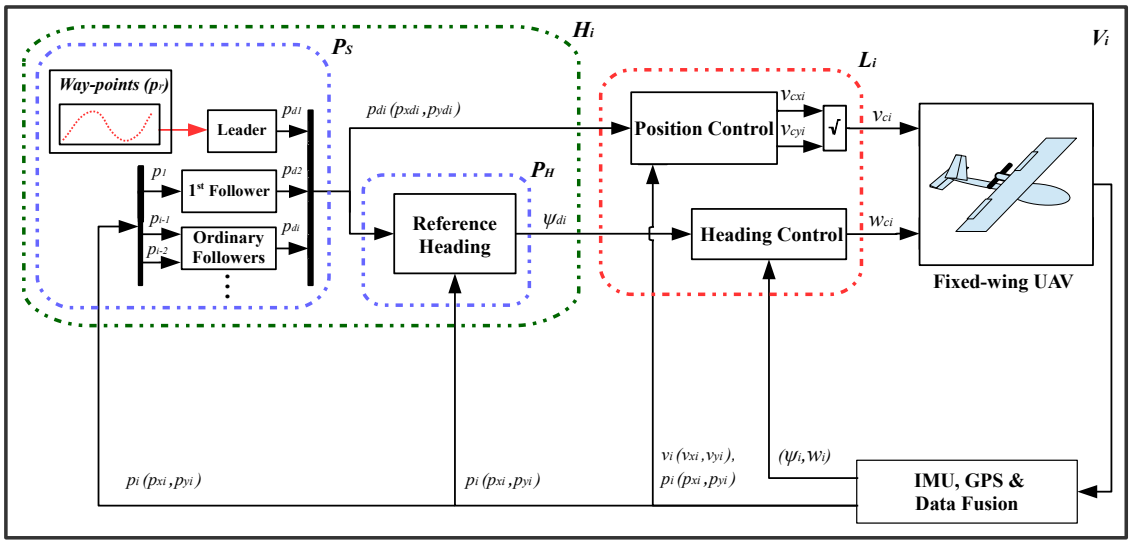

Figure 6.1: Fixed-wing UAV formation control block diagram.

6.3 High-level Control: Desired Trajectory and Heading Derivation

We now derive a distributed, hierarchical, asymmetric high-level controller structure to solve the control problems. The high-level module H_i of each agent V_i's controller within the proposed distributed control scheme consists of two submodules which generate the desired position and heading via the formation supervisor (P_S) and reference heading generator (P_H) as shown in Figure 6.1.

On-line Distributed Formation Supervisor

Desired trajectory $p_{di}(t) = [p_{xdi}(t), p_{ydi}(t)]^T$ of V_i is generated on-line by this submodule, depending on whether V_i is the *leader* ($i = 1$), *first* follower ($i = 2$), or *ordinary* follower ($i \geq 3$), as follows:

Leader: V_1 is responsible to track the pre-defined trajectory $p_{d1}(t)$ at each time instant t.

First Follower: V_2 only follows *leader*. Its desired trajectory $p_{d2}(t)$ is generated as

$$p_{d2}(t) = \left[p_1(t) + R^*_{(1,2)}\right]. \tag{6.7}$$

Ordinary Followers: $V_i,\ i = 3, .., N$ follows previous two neighbors. The desired trajectory $p_{di}(t)$ of V_i is obtained as

$$p_{di}(t) = \frac{1}{2}\sum_j \left[p_j(t) + R^*_{(j,i)}\right]. \tag{6.8}$$

Note that the above formation rules are designed by following Section 5.5.1.

Reference Heading Generation

For ith fixed-wing UAV, we write the following control rule which always directs the heading angle to the desired position as

$$\psi_{di}(t) = \tan^{-1}\left(\frac{p_{ydi}(t) - p_{yi}(t)}{p_{xdi}(t) - p_{xi}(t)}\right). \tag{6.9}$$

6.4 Low-level Control: Optimal Linear Quadratic Tracking (LQT) Control Design

In this section, the LQT control scheme for lateral tracking of ith fixed-wing UAV is developed following generic LQT control design as established in Section 3.6.2. The approach is to apply the control laws (3.28), (3.30), (3.31) to the system models (6.1) and (6.2). Implementation of the control law (3.30) requires $\bar{P}$ from (3.28) and $\bar{g}(t)$ from (3.31). Note that a generic control analysis is presented for both the models (6.1) and (6.2) since their system matrices A, B, C are same. Therefore, the RE, the approximate vector signal $\bar{g}(t)$ and the optimal control signal are obtained, respectively as

$$-\bar{P}A - A^T\bar{P} + \bar{P}BR^{-1}B^T\bar{P} - C^TQC = 0, \tag{6.10}$$

$$\bar{g}(t) = [A^T - \bar{P}BR^{-1}B^T]^{-1}[-C^TQz(t)], \tag{6.11}$$

$$u^*(t) = -R^{-1}B^T\bar{P}x(t) + R^{-1}B^T\bar{g}(t), \tag{6.12}$$

where $A = \begin{bmatrix} 0 & 1 \\ 0 & -\alpha \end{bmatrix}$, $B = \begin{bmatrix} 0 \\ \alpha \end{bmatrix}$, $C = \begin{bmatrix} 1 \\ 0 \end{bmatrix}^T$.

Solving (6.10) for $\bar{P} = \begin{bmatrix} \bar{P}_1 & \bar{P}_2 \\ \bar{P}_2 & \bar{P}_3 \end{bmatrix} \in \Re^{2\times 2}$, we obtain

$$0 = -(\alpha^2 \bar{P}_2^2/R) + Q, \tag{6.13a}$$
$$0 = -\bar{P}_1 + \alpha \bar{P}_2 + ((\alpha^2 \bar{P}_2 \bar{P}_3)/R), \tag{6.13b}$$
$$0 = 2\bar{P}_2 - 2\alpha \bar{P}_3 - ((\alpha^2 \bar{P}_3^2)/R), \tag{6.13c}$$

Solving (6.11) for $\bar{g}(t) = [\bar{g}_1(t)\ \bar{g}_2(t)]^T \in \Re^2$, we obtain

$$\bar{g}_1(t) = [(\alpha + (\bar{P}_3\alpha^2)/R)][(RQ)/(\bar{P}_2\alpha^2)]z(t), \tag{6.14a}$$
$$\bar{g}_2(t) = [(RQ)/(\bar{P}_2\alpha^2)]z(t). \tag{6.14b}$$

6.5 Calculation of LQT Control Parameters

For both position and heading control models, the inertial related dynamics parameter, the error and the control weighting parameters are chosen same as $\alpha = \alpha_l = \alpha_\psi = 100$, $Q = 200$ and $R = 1$. Hence, the LQT control design as explained in detail in Section 6.4 is followed for a generic calculation of both models as follows.

The entry $\bar{P}_2$ of $\bar{P}(t)$ is calculated by (6.13a) as

$$\bar{P}_2 = \sqrt{(QR)/\alpha} = 1.4142. \tag{6.15}$$

Then, by using (6.15) in (6.13c), the quadratic polynomial $10000\bar{P}_3 + 200\bar{P}_3 - 2.8284 = 0$ is obtained as a function of $\bar{P}_3$, and solving the quadratic polynomial, the entry $\bar{P}_3$ is found as

$$\bar{P}_3 = 0.0096. \tag{6.16}$$

The remaining entry $\bar{P}_1$ of $\bar{P}$ is calculated by using (6.15) and (6.16) in (6.13b) as

$$\bar{P}_1 = 276.71. \tag{6.17}$$

Table 6.1: Small fixed-wing UAV specifications used in simulations

Parameter	Definition	Value
w_{min} for all UAVs	Minimum angular velocity	-1.2 [rad/sec]
w_{max} for all UAVs	Maximum angular velocity	1.2 [rad/sec]
v_{min} for all UAVs	Minimum velocity	5 [m/sec]
v_{max} for leader UAV	Maximum velocity	7 [m/sec]
v_{max} for first follower UAV	Maximum velocity	7.5 [m/sec]
v_{max} for ordinary follower UAV	Maximum velocity	8 [m/sec]

Therefore, for both models, $\bar{P}$ and the vector signal $\bar{g}(t)$ are obtained as follows:

$$\bar{P} = \begin{bmatrix} 276.71 & 1.4142 \\ 1.4142 & 0.0096 \end{bmatrix} \text{ and } \bar{g}(t) = \begin{bmatrix} 276.71\ z(t) \\ 1.4142\ z(t) \end{bmatrix}, \tag{6.18}$$

where $\bar{g}(t)$ represents $\bar{g}_l(t)$ for $z(t) = p_{ld}(t)$ of the position control and $\bar{g}_\psi(t)$ for $z(t) = \psi_d(t)$ of the heading control.

Remark 6.5.1. *After all, using* (6.18) *in* (6.12)*, optimal position* $v^*_{cl}(t)$ *and heading* $w^*_c(t)$ *control inputs for ith fixed-wing UAV are obtained as following:*

$$v^*_{cli}(t) = -R^{-1}B^T\bar{P}x_{li}(t) + R^{-1}B^T\bar{g}_{li}(t), \tag{6.19}$$
$$w^*_{ci}(t) = -R^{-1}B^T\bar{P}x_{\psi i}(t) + R^{-1}B^T\bar{g}_{\psi i}(t), \tag{6.20}$$

6.6 Simulations and Results

The small fixed-wing UAV specifications used in simulations are presented in Table 6.1. After setting all control parameters from Section 6.5 with the sampling rate 200 $[Hz]$ by using MATLAB/ *Simulink*®, we have simulated the proposed schemes for tracking control of the single fixed-wing UAV and formation maintenance control of the multiple fixed-wing UAV system. For both cases, surveillance missions by following the spiral reference trajectory generated by $p_{d1}(t) = (3t\cos(\frac{t}{200}\cos(2\pi)), 3t\cos(\frac{t}{200}\cos(2\pi)))^T$ are simulated as follows.

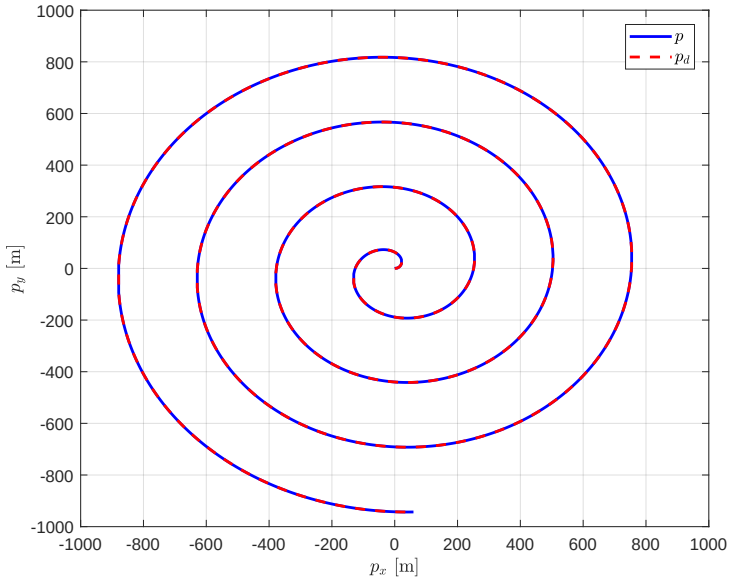

Figure 6.2: Spiral surveillance motion of a fixed-wing UAV.

6.6.1 Simulation results of a single fixed-wing UAV

A numerical simulation is employed for a fixed-wing UAV with the initial position $p(0) = (-0.5, 0.1)^T$ and a spiral trajectory. All corresponding results are presented in Figures 6.2-6.6. The performances of the proposed control scheme satisfy the tracking requirements as seen in Figures 6.2-6.4.

6.6.2 Simulation results of a multiple fixed-wing UAV system

A numerical simulation is performed for a multi fixed-wing UAV system with N=3 vehicles in *leader-follower* structure. The initial positions of UAVs are $p_1(0) = (-0.5, 0.1)^T$; $p_2(0) = (-10, -60)^T$; $p_3(0) = (50, -30)^T$. Spiral motion scenarios are employed to maintain desired formation distance $d^*_{ij} = 100\ [m]$ based on the desired relative positions: $R^*_{(1,2)} = (-50, -50\sqrt{3})^T$, $R^*_{(1,3)} = (50, -50\sqrt{3})^T$, $R^*_{(2,3)} = (100, 0)^T$.

All corresponding results are presented in Figures 6.7-6.11. The formation performances of the proposed distributed control scheme satisfy the formation requirements as seen in Figures 6.7 and 6.8 as well as the individual tracking performances of all UAVs at the low-level.

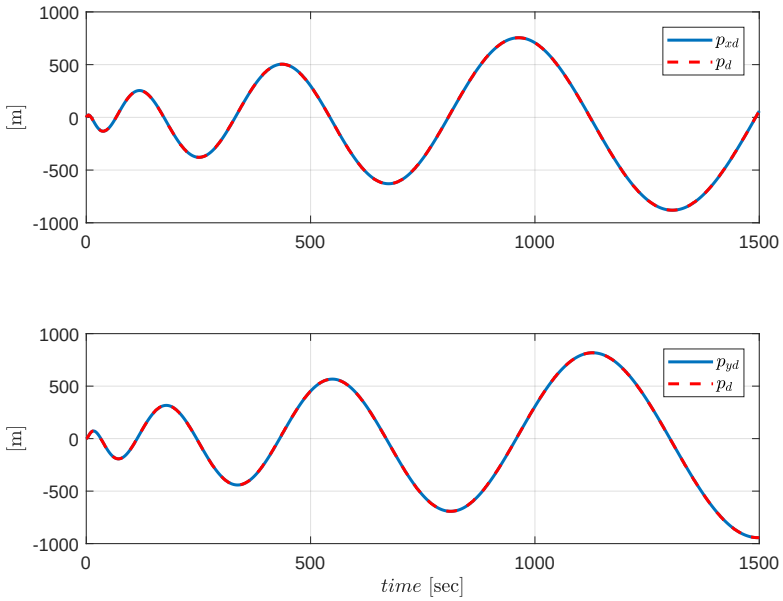

Figure 6.3: Lateral trajectory tracking performances.

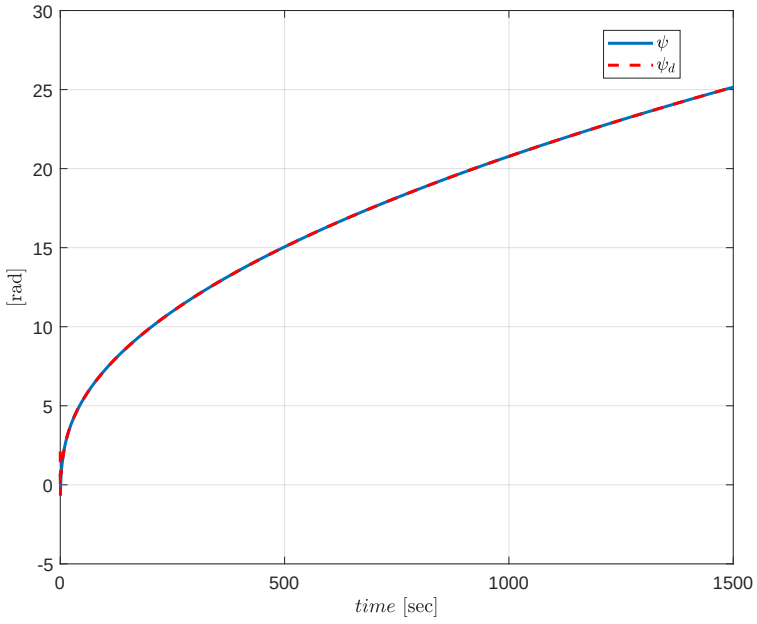

Figure 6.4: Heading tracking performance.

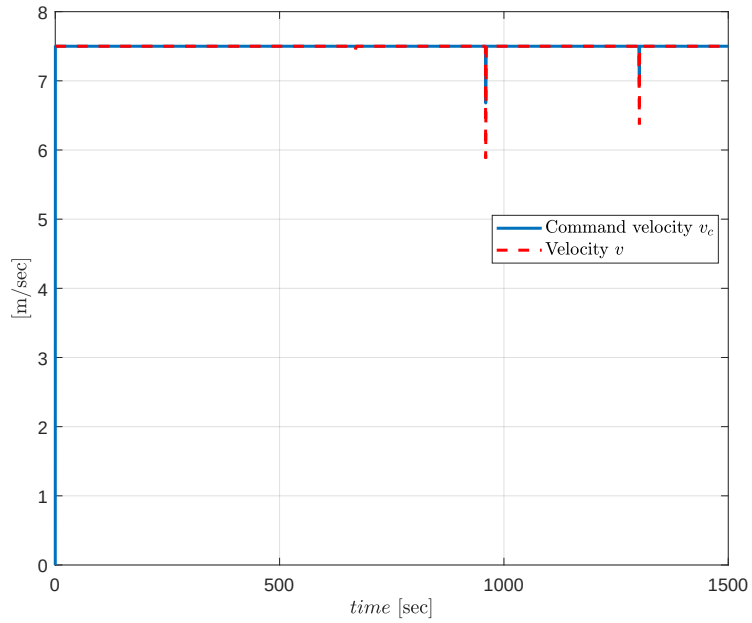

Figure 6.5: Commanded and actual velocities.

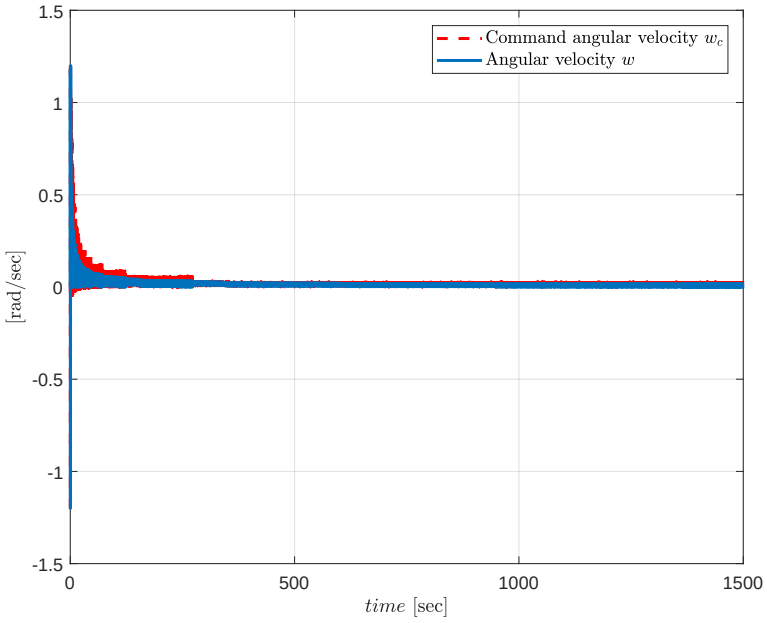

Figure 6.6: Commanded and actual angular velocities.

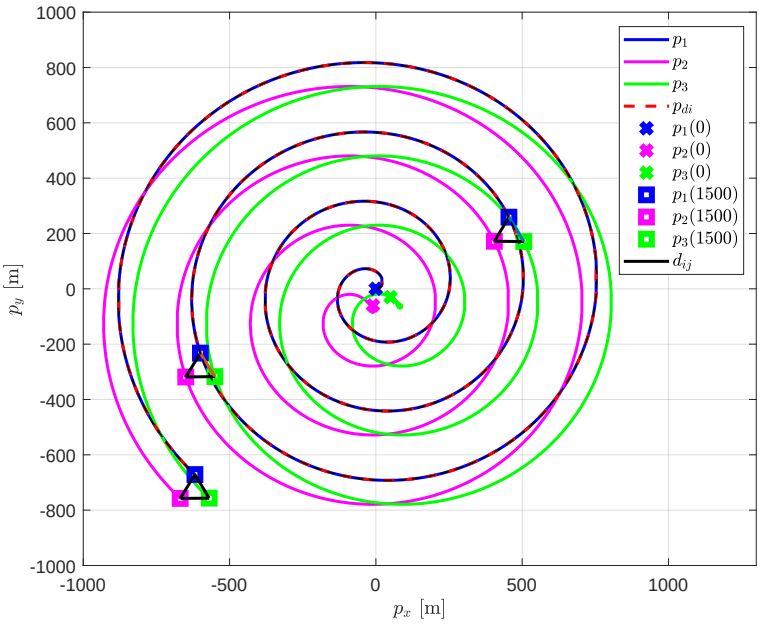

Figure 6.7: Spiral surveillance motion of a multiple fixed-wing UAV system in formation.

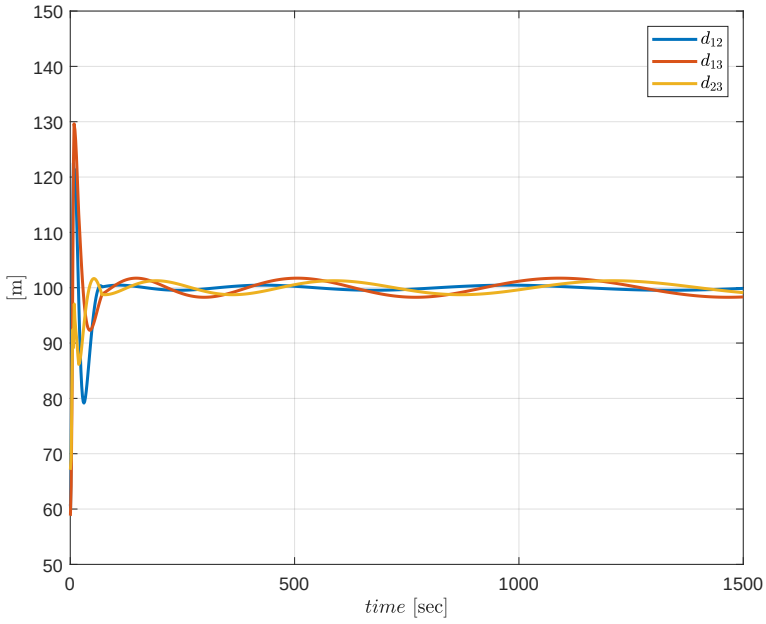

Figure 6.8: Formation maintenance performances for d_{ij}.

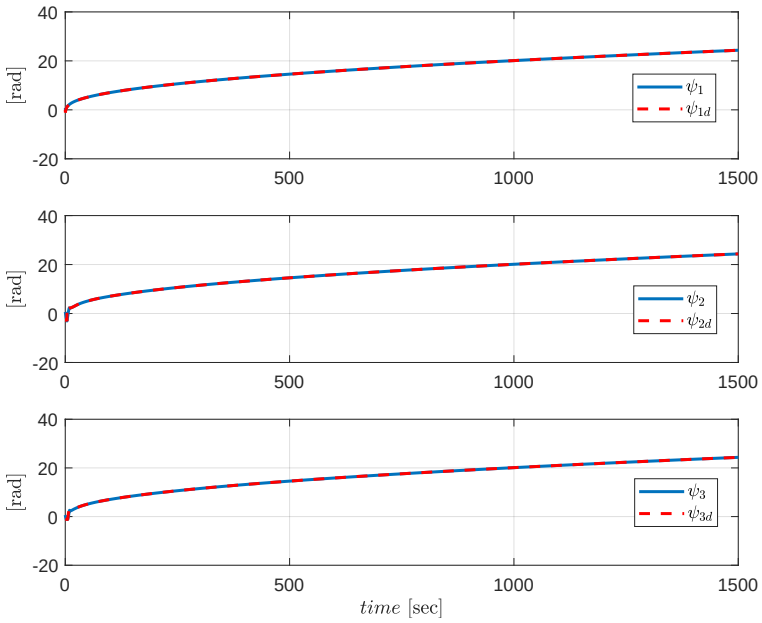

Figure 6.9: Heading tracking performances for V_i.

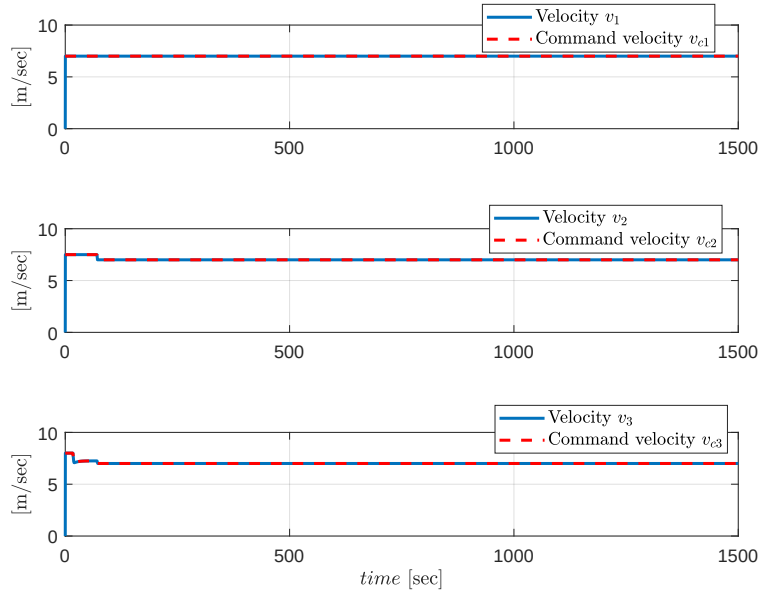

Figure 6.10: Commanded and actual velocities for V_i.

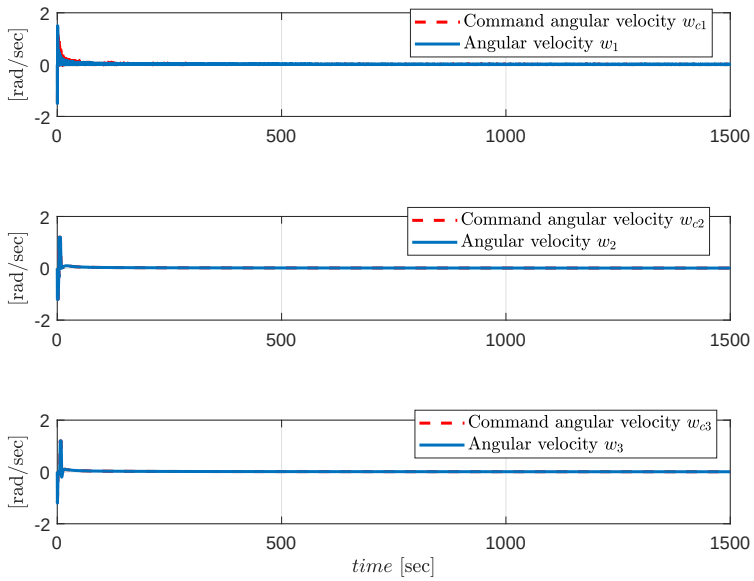

Figure 6.11: Commanded and actual angular velocities for V_i.

6.7 Summary and Remarks

The linear quadratic tracking (LQT) schemes have been developed to control and stabilize the lateral motion of a small fixed-wing UAV system. Then, the two-level, hierarchical, distributed formation controller has been designed for a multiple fixed-wing UAV system with three vehicles. All analytical analyses and designs are verified by surveillance mission simulations for both tracking and formation maintenance control cases. It is witnessed that the LQT schemes in the low (individual) level work successfully in terms of the optimal tracking performances. It is also observed that at the high (formation) level, the distributed laws are practical and maintain successfully desired formation shape by associating with the low (individual) level controllers.

Chapter 7

Concluding Remarks

This thesis has studied robust, optimal and nonlinear control design for trajectory tracking of single-UAV systems and formation maintenance of multi-UAV systems. These control problems have been addressed for both quadrotor and small fixed-wing UAVs.

For trajectory tracking of single-UAV systems, Chapter 3 has presented a novel infinite-horizon ALQT control design for the attitude of the quadrotor UAV in an optimal sense. ALQT is selected for this purpose because it is real-time implementable and robust to effect of modeling uncertainties. In the experiments, the attitude measurement noises, which come from IMU sensors, are compensated using a Kalman filter to obtain a more reliable attitude estimation and compared with a complementary filter. In Chapter 4, a backstepping based robust adaptive controller with guaranteed tracking errors has been studied and tested in case of under-actuated dynamics, nonlinearities and model uncertainties. The proposed design is capable of transferring the constrained tracking error to an unconstrained form for adjusting transient and steady-state behaviors within prescribed bounds. It also compensates effects of model nonlinearities and uncertainties. *We have concluded that the tracking objectives in Chapters 3 and 4 are achieved and experimentally validated utilizing the proposed controllers even in the existence of under-actuation, nonlinearities, uncertainties and sensor noises in the quadrotor UAV motion dynamics.*

For formation maintenance of multi-UAV systems, a two-level control structure is introduced for constructing high (formation) and low (individual) level controllers, separately. This separation helps efficient and systematic control synthesis addressing robustness to effects of uncertainties and disturbances as well as optimality at both levels, independently. In Chapter 5, using the proposed two-level control, at the high-level, a distributed hierarchical formation control scheme has been designed in *leader-follower* structure. Formation

maintenance is ensured by utilizing tools of rigid graph theory for performing cohesive motion in 3D. At the low-level, the proposed adaptive mixing based controller is designed to compensate the effect of real dynamics issues for enhancing tracking performance and robustness by providing smoother control action. *We have concluded that the multi quadrotor UAV system achieves the formation control objectives with the proposed controller even in the existence of parametric uncertainties in the quadrotor UAV motion dynamics. Especially, the proposed control scheme compensates the negative effects of the indirect adaptive approach which come from poor transient estimation time of the parameter identification algorithm.* Furthermore, in Chapter 6, the proposed single-UAV linear quadratic tracking control and multi-UAV two-level control designs have been extended and studied to fixed-wing UAV systems. *Hence, the proposed two-level control approach is modular and practical in the sense that it can be employed easily to various types of multiple UAV systems which have different motion characteristics.*

Some of the potential future works and shortcomings that can be studied as a continuation of this thesis are as follows:

(i) In Chapter 3, a potential future direction is to extend optimal linear quadratic attitude tracking control design for altitude and yaw dynamics to perform fully autonomous motion tasks. It is also observed that the heading (yaw) estimation is affected by magnetic disturbances in experiments. Yaw estimation can be improved by following the solution methods in the literature such as those in [50].

(ii) The proposed position control scheme with guaranteed tracking performance designed in Chapter 4 can be extended to formation tasks for guaranteeing formation maintenance performances. One of the shortcomings of the proposed control design is as it lacks analysis for external disturbances such as wind gust. This can be addressed with disturbance rejection approaches, and the robustness of the proposed controller can be improved against real-world disturbances during flight missions.

(iii) For Chapter 5, it would be a good extension to analyze the formation maintenance and robustness of the multi quadrotor UAV system for actuator failures, and study of other cooperative tasks such as cooperative surveillance and joint tasks with ground vehicles. Another future direction is to implement the proposed formation control scheme on a real multiple quadrotor UAV system for an experimental validation. As a future solution for shortcoming of Chapter 5, the nominal LQR control design can be studied combining with a disturbance rejection method to eliminate internal disturbance effects of ignored modeling terms and real-world disturbances such as wind gust.

Bibliography

[1] A. Abdessameud and F. Janabi-Sharifi, "Image-based tracking control of VTOL unmanned aerial vehicles," *Automatica,* vol. 53, pp. 111–119, 2015.

[2] R. Alba-Flores and E. Barbieri, "Real-time infinite horizon linear-quadratic tracking controller for vibration quenching in flexible beams," in *Proc. IEEE International Conference on Systems, Man, and Cybernetics,* pp. 38-43, Taipei, Taiwan, October 2006.

[3] K. Alexis, G. Nikolakopoulos and A. Tzes, "Design and experimental verification of a constrained finite time optimal control scheme for the attitude control of a quadrotor helicopter subject to wind gusts," in *Proc. IEEE International Conference on Robotics and Automation,* pp. 1636-1641, Anchorage, Alaska, USA, May 2010.

[4] K. Alexis, G. Nikolakopoulos and A. Tzes, "Experimental model predictive attitude tracking control of a quadrotor helicopter subject to wind-gusts," in *Proc. Mediterranean Control Conference,* pp. 1461-1466, Marrakech, Morocco, June 2010.

[5] K. Alexis, G. Nikolakopoulos and A. Tzes, "Switching model predictive attitude control for a quadrotor helicopter subject to atmospheric disturbances," *Control Engineering Practice,* vol. 19 , no. 10, pp. 1195-1207, 2011.

[6] K. Alexis, G. Nikolakopoulos and A. Tzes, "Model predictive quadrotor control: attitude, altitude and position experimental studies," *IET Control Theory and Applications,* vol. 6, no. 12, pp. 1812-1827, 2012.

[7] K. Alexis, G. Nikolakopoulos, R. Siegwart and A. Tzes, "Robust model predictive flight control of unmanned rotorcrafts," *Journal of Intelligent and Robotic Systems,* vol. 81 , no. 3-4, pp. 443-469, 2016.

[8] E. Altug, J.P. Ostrowski and R. Mahony, "Control of a quadrotor helicopter using visual feedback," in *Proc. IEEE International Conference on Robotics and Automation,* pp. 73-77, Washington, DC, May 2002.

[9] Y. Ameho, F. Niel, F. Defay, J.M. Biannic and C. Berard, "Adaptive control for quadrotors," in *Proc. IEEE International Conference on Robotics and Automation,* pp. 5376-5381, Karlsruhe, Germany, May 2013.

[10] B.D.O. Anderson and J.B. Moore, *Optimal control: linear quadratic methods.* Courier Corporation, 2007.

[11] B.D.O. Anderson, B. Fidan, C. Yu and D. Walle, "UAV formation control: theory and application," *in Recent advances in learning and control,* Ser. Lecture Notes in Control and Information Sciences, New York: Springer, 2008, vol. 371, pp. 15-33.

[12] B.D.O. Anderson, C. Yu, B. Fidan and J.M. Hendrickx, "Rigid graph control architectures for autonomous formations," *IEEE Control Systems Magazine,* vol. 28, no. 6, pp. 48-63, 2008.

[13] M. E. Antonio-Toledo, E. N. Sanchez, A. Y. Alanis, J. A. Florez and M. A. Perez-Cisneros, "Real-time integral backstepping with sliding mode control for a quadrotor UAV," in *Proc. IFAC-PapersOnLine,* vol. 51, no. 13, pp. 549–554, January 2018.

[14] A.J. Baerveldt and R. Klang, "A low-cost and low-weight attitude estimation system for an autonomous helicopter," in *Proc. IEEE International Conference on Intelligent Engineering Systems,* pp. 391-395, Budapest, Hungary, September 1997.

[15] T. Balch and R.C. Arkin, "Behavior-based formation control for multirobot teams," *IEEE Trans. on Robotics and Automation,* vol. 14, no. 6, pp. 926-936, 1998.

[16] S. Baldi, P. Ioannou and E. Mosca, "Multiple model adaptive mixing control: the discrete-time case," *IEEE Trans. on Automatic Control,* vol. 57, no. 4, pp. 1040-1045, 2012.

[17] E. Barbieri and R. Alba-Flores, "On the infinite-horizon LQ tracker," *Systems and Control Letters,* vol. 40, no. 2, pp. 77-82, 2000.

[18] J.D. Barton, "Fundamentals of small unmanned aircraft flight," *Johns Hopkins APL technical digest,* vol. 31, no. 2, pp. 132-149, 2012.

[19] M.A.M. Basri, A.R. Husain and K.A. Danapalasingam, "Intelligent adaptive backstepping control for MIMO uncertain non-linear quadrotor helicopter systems," *Transactions of the Institute of Measurement and Control,* vol. 37, no. 3, pp. 345-361, 2015.

[20] I. Bayezit and B. Fidan, "Distributed cohesive motion control of flight vehicle formations," *IEEE Trans. Industrial Electronics,* vol. 60, no. 12, pp. 5763-5772, December 2013.

[21] R.W. Beard, D. Kingston, M. Quigley, D.'Snyder, R. Christiansen, W. Johnson, T. McLain and M.A. Goodrich, "Autonomous vehicle technologies for small fixed-wing UAVs," *Journal*

of Aerospace Computing, Information and Communication, vol. 2, no. 1, pp. 92-108, January 2005.

[22] R.W. Beard, T.W. McLain, D.B. Nelson, D. Kingston and D. Johanson, "Decentralized cooperative aerial surveillance using fixed-wing miniature UAVs," *Proceedings of the IEEE*, vol. 94, no. 7, pp. 1306-1324, 2006.

[23] R.W. Beard and T.W. McLain, *Small unmanned aircraft theory and practice.* Princeton University Press, New Jersey, 3rd ed., 2012.

[24] C. P. Bechlioulis and G. A. Rovithakis, "Adaptive control with guaranteed transient and steady state tracking error bounds for strict feedback systems," *Automatica,* vol. 45, no. 2, pp. 532-538, 2009.

[25] A. Benallegue, A. Mokhtari and L. Fridman, "Highorder sliding-mode observer for a quadrotor UAV," *Int. Journal of Robust and Nonlinear Control,* vol. 18, no. 4-5, pp. 427-440, 2008.

[26] L. Benziane, A. El Hadri, A. Seba, A. Benallegue and Y. Chitour, "Attitude estimation and control using linearlike complementary filters: theory and experiment," *IEEE Transactions on Control Systems Technology,* vol. 24, no. 6, pp. 2133-2140, 2016.

[27] L. Besnard, Y.B. Shtessel and B. Landrum, "Quadrotor vehicle control via sliding mode controller driven by sliding mode disturbance observer," *Journal of the Franklin Institute,* vol. 349, no. 2, pp. 658-684, March 2012.

[28] S. Białas, "A necessary and sufficient condition for the stability of convex combinations of stable polynomials or matrices," *Control and Cybernetics*, vol. 33, no. 4, pp. 589-597, 2004.

[29] H. Bonyan Khamseh and F. Janabi-Sharifi, "UKF-based LQR control of a manipulating unmanned aerial vehicle," *Unmanned Systems*, vol. 5, no. 3, pp. 131, 2017.

[30] S. Bouabdallah, A. Noth and R. Siegwart, "PID vs LQ control techniques applied to an indoor micro quadrotor," in *Proc. IEEE/RSJ Intelligent Robots and Systems,* pp. 2451-2456, Sendai, Japan, September-October 2004.

[31] S. Bouabdallah and R. Siegwart, "Backstepping and sliding-mode techniques applied to an indoor micro quadrotor," in *Proc. IEEE International Conference on Robotics and Automation,* pp. 2260-2264, Barcelona, Spain, April 2005.

[32] K. Büyükkabasakal, B. Fidan, A. Savran and N. Köksal, "Real-time implementation of mixing adaptive control on quadrotor UAVs," in *Proc. European Control Conference,* pp. 3597-3602, Linz, Austria, July 2015.

[33] K. Büyükkabasakal, B. Fidan and A. Savran, "Mixing adaptive fault tolerant control of quadrotor UAV," *Asian Journal of Control,* vol. 19, no. 4, pp. 1441-1454, July 2017.

[34] D. Cabecinhas, R. Cunha and C. Silvestre, "A globally stabilizing path following controller for rotorcraft with wind disturbance rejection," *IEEE Trans. Control Systems Technology,* vol. 23, no. 2, pp. 708-714, 2013.

[35] P. Castillo, A. Dzul and R. Lozano, "Real-time stabilization and tracking of a four-rotor mini rotorcraft," *IEEE Trans. Control Systems Technology,* vol. 12, no. 4, pp. 510-516, 2004.

[36] P. Castillo, R. Lozano and A. Dzul, "Stabilization of a mini rotorcraft with four rotors," *IEEE control systems magazine,* vol. 25, no. 6, pp. 45-55, 2005.

[37] M. Chen and M. Huzmezan, "A combined MBPC/2DOF H-infinite controller for a quadrotor UAV," in *Proc. AIAA Atmospheric Flight Mechanics Conference and Exhibit,* pp. 5520, Austin, Texas, August 2003.

[38] S.H. Chiew, W. Zhao and T.H. Go, "Coordination with robust control lyapunov function approach," *Journal of Intelligent and Robotic Systems,* vol. 78, no. 3-4, pp. 499-515, 2015.

[39] Y. Choi and H. Ahn, "Nonlinear control of quadrotor for point tracking: actual implementation and experimental tests," *IEEE/ASME Trans. on Mechatronics,* vol. 20, no. 3, pp. 1179-1192, 2015.

[40] J.L. Crassidis and F.L. Markley, "Unscented filtering for spacecraft attitude estimation," *Journal of Guidance, Control, and Dynamics,* vol. 26, no. 4, pp. 536-542, 2003.

[41] A. Das, F. Lewis and K. Subbarao, "Backstepping approach for controlling a quadrotor using Lagrange form dynamics," *Journal of Intelligent and Robotic Systems,* vol. 56, no. 1-2, pp. 127-151, 2009.

[42] A.K. Das, R. Fierro, V. Kumar, J.P. Ostrowski, J. Spletzer and C.J. Taylor, "A vision-based formation control framework," *IEEE Trans. on Robotics and Automation,* vol. 18, no. 15, pp. 813-825, October 2002.

[43] H.G. De Marina, F.J. Pereda, J.M. Giron-Sierra, and F. Espinosa, "UAV attitude estimation using unscented Kalman filter and TRIAD," *IEEE Transactions on Industrial Electronics,* vol. 59, no. 11, pp. 4465-4474, 2012.

[44] J.P. Desai, J.P. Ostrowski and V. Kumar, "Modeling and control of formations of nonholonomic mobile robots," *IEEE Trans. Robotics and Automation,* vol. 17, no. 6, pp. 905-908, December 2001.

[45] Z.T. Dydek, A.M. Annaswamy and E. Lavretsky, "Adaptive control of quadrotor UAVs in the presence of actuator uncertainties," in *Proc. AIAA Infotech@ Aerospace,* pp. 1-9, April 2010.

[46] Z.T. Dydek, A.M. Annaswamy and E. Lavretsky, "Adaptive control of quadrotor UAVs: a design trade study with flight evaluations," *IEEE Trans. on Control Systems Technology,* vol. 21, no. 4, pp. 1400-1406, 2013.

[47] A. Ebrahimi, F. Janabi-Sharifi and A. Ghanbari, "UavisBug: mini UAV vision-based 3D motion planning and obstacle avoidance in an unknown indoor environment," *Canadian Aeronautics and Space Journal,* vol. 60, no. 1, pp. 9–21, 2014.

[48] B. Etkin and L.D. Reid, *Dynamics of flight: stability and control.* John Wiley and Sons, New York, NY, 3rd ed., 1996.

[49] S. Evren, F. Yavuz and M. Unel, "High Precision stabilization of pan-tilt systems using reliable angular acceleration feedback from a master-slave Kalman filter," *Journal of Intelligent and Robotic Systems,* vol. 88, no. 1, pp. 97-127, 2017.

[50] B. Fan, Q. Li and T. Liu, "How magnetic disturbance influences the attitude and heading in magnetic and inertial sensor-based orientation estimation," *Sensors,* vol. 18, no. 1, pp. 76, 2018.

[51] S. Fekri, M. Athans and A. Pascoal, "Issues, progress and new results in robust adaptive control," *International Journal of Adaptive Control and Signal Processing,* vol. 20, pp. 519-579, 2006.

[52] H. Ferdinando, H. Khoswanto and D. Purwanto, "Embedded Kalman filter for inertial measurement unit (IMU) on the ATMega8535," in *Proc. IEEE International Symposium on Innovations in Intelligent Systems and Applications,* pp. 1-5, Trabzon, Turkey, July 2012.

[53] B. Fidan, B.D.O. Anderson, C. Yu and J. Hendrickx, "Persistent autonomous formations and cohesive motion control," in *in Modeling and Control of Complex Systems,* P.A. Ioannou and A. Pitsillides, Eds. Boca Raton, FL: CRC Press, 2007, ch. 8, pp. 247–275.

[54] E. Foxlin, "Inertial head tracker sensor fusion by a complementary separate bias Kalman filter," in *Proc. IEEE Virtual Reality Annual Inter-national Symposium,* pp. 185-194, Santa Clara, CA, March 1996.

[55] F. Gavilan, R. Vazquez and S. Esteban, "Trajectory tracking for fixed-wing UAV using model predictive control and adaptive backstepping," in *Proc. IFAC-PapersOnLine,* vol. 48-9, pp. 132-137, 2015.

[56] V. Gazi and B. Fidan, "Coordination and control of multi-agent dynamic systems: Models and approaches," in *International Workshop on Swarm Robotics.* Springer, 2006, pp. 71-102.

[57] F. Giulietti, L. Pollini and M. Innocent, "Autonomous formation flight," *IEEE Control Systems Magazine,* vol. 20, no. 6, pp. 34-44, December 2000.

[58] X. Gong, Z. Hou, C. Zhao, Y. Bai and Y. Tian, "Adaptive backstepping sliding mode trajectory tracking control for a quad-rotor," *Int. Journal of Automation and Computing,* vol. 9, no. 5, pp. 555-560, 2012.

[59] J.A. Guerrero, P. Castillo, S. Salazar and R. Lozano, "Mini rotorcraft flight formation control using bounded inputs," *Journal of Intelligent and Robotic Systems,* vol. 64, no. 1-4, pp. 175-186, 2012.

[60] J.A. Guerrero, P.C. Garcia and Y. Challal, "Quadrotors formation control," *Journal of Intelligent and Robotic Systems,* vol. 70, no. 1-4, pp. 221-231, 2013.

[61] S. Güler, N. Köksal and B. Fidan, "Adaptive control of a three-agent surveillance swarm with constant speed constraint," in *Proc. 9th Asian Control Conference,* pp. 1-6, Istanbul, Turkey, June 2013.

[62] S. Güler, N. Köksal, B. Fidan and V. Gazi, "Indirect adaptive formation control with nonlinear dynamics and parametric uncertainty," in *Proc. 9th Asian Control Conference,* pp. 1-6, Istanbul, Turkey, June 2013.

[63] C.S. Ha, Z. Zuo, F.B. Choi and D. Lee, "Passivity-based adaptive backstepping control of quadrotor-type UAVs," *Robotics and Autonomous Systems,* vol. 62, no. 9, pp. 1305-1315, 2014.

[64] M. Hedayatpour, M. Mehrandezh and F. Janabi-Sharifi, "A unified approach to configuration based dynamic analysis of quadcopters for optimal stability," in *Proc. IEEE/RSJ Int. Conference on Intelligent Robots and Systems (IROS),* pp. 5116-5121, Vancouver, BC, Canada, September 2017.

[65] B.S.M. Henriques, "Estimation and control of a quadrotor attitude," Master of Science, Instituto Superior Técnico, Lisbon University, Portugal, 2011.

[66] J.R. Hervas, M. Reyhanoglu, H. Tang and E. Kayacan, "Nonlinear control of fixed-wing UAVs in presence of stochastic winds," *Commun Nonlinear Sci Numer Simulat,* vol. 33, pp. 57-69, 2016.

[67] F. Hoffmann, N. Goddemeier and T. Bertram, "Attitude estimation and control of a quadrocopter," in *Proc. IEEE/RSJ International Conference on Intelligent Robots and Systems,* pp. 1072-1077, Taipei, Taiwan, October 2010.

[68] W. Honig and N. Ayanian, "Flying multiple UAVs using ROS," *Robot Operating System (ROS), Studies in Computational Intelligence 707,* A. Koubaa (ed.), Springer, 2017, vol. 707, pp. 83–118.

[69] W. Hönig, J.A. Preiss, T.K.S. Kumar, G.S. Sukhatme and N. Ayanian, "Trajectory planning for quadrotor swarms," *IEEE Trans. on Robotics,* vol. 34, no. 4, pp. 856-869, 2018.

[70] J. Hu and G. Feng, "Distributed tracking control of leader-follower multi-agent systems under noisy measurement," *Automatica*, vol. 46, no. 8, pp. 1382-1387, 2010.

[71] C. Hua, J. Chen and X. Guan, "Adaptive prescribed performance control of QUAVs with unknown time-varying payload and wind gust disturbance," *Journal of the Franklin Institute,* vol. 355, no. 14, pp. 6323-6338, 2018.

[72] C. Hua, J. Chen and Y. Li, "Leader-follower finite-time formation control of multiple quadrotors with prescribed performance," *International Journal of Systems Science,* vol. 48, no. 12, pp. 2499-2508, 2017.

[73] M. Huang, B. Xian, C. Diao, K. Yang and Y. Feng, "Adaptive tracking control of underactuated quadrotor unmanned aerial vehicles via backstepping," in *Proc. American Control Conference,* pp. 2076-2081, Baltimore, MD, USA, June-July 2010.

[74] P.A. Ioannou and B. Fidan, *Adaptive control tutorial.* SIAM Society for Industrial & Applied Mathematics, 2006.

[75] P.A. Ioannou and J. Sun, *Robust adaptive control.* Dover Publications, 2012.

[76] S. Islam, P.X. Liu and A. El Saddik, "Nonlinear adaptive control for quadrotor flying vehicle," *Nonlinear Dynamics,* vol. 78, no. 1, pp. 117-133, 2014.

[77] S. Islam, P.X. Liu and A. El Saddik, "Robust control of four-rotor unmanned aerial vehicle With disturbance uncertainty," *IEEE Trans. on Industrial Electronics,* vol. 62, no. 3, pp. 1563-1571, 2015.

[78] C. Izaguirre-Espinosa, A.J. Munoz-Vazquez, A. Sanchez-Orta, V. Parra-Vega and P. Castillo, "Attitude control of quadrotors based on fractional sliding modes: theory and experiments," *IET Control Theory Applications,* vol. 10, no. 7, pp. 825-832, 2016.

[79] Y. Ji, Y. Yu, W. Zhang and C. Sun, "Attitude control of a quadrotor unmanned aerial vehicle based on linear extended state observer," in *Proc. Chinese Control and Decision Conference,* pp. 1350-1355, Qingdao, China, July 2015.

[80] E.N. Johnson and S.K. Kannan, "Adaptive trajectory control for autonomous helicopters," *Journal of Guidance, Control, and Dynamics,* vol. 28, no. 3, pp. 524–538, 2005.

[81] Y. Kang and J.K. Hedrick, "Linear tracking for a fixed-wing UAV using nonlinear model predictive control," *IEEE Trans. on Control System Technology,* vol. 17, no. 5, pp. 1202-1210, 2009.

[82] S.M. Kang and H.S. Ahn, "Design and realization of distributed adaptive formation control law for multi-agent systems with moving leader," *IEEE Trans. on Industrial Electronics*, vol. 63, no. 2, pp. 1268-1279, 2016.

[83] S.M. Kang, M.C. Park and H.S. Ahn, "Distance-based cycle-free persistent formation: global convergence and experimental test with a group of quadcopters," *IEEE Trans. on Industrial Electronics*, vol. 64, no. 1, pp. 380-289, 2017.

[84] F. Kendoul, "Survey of advances in guidance, navigation, and control of unmanned rotorcraft systems," *Journal of Field Robotics,* vol. 29, no. 2, pp. 315-378, 2012.

[85] F. Kendoul, Z. Yu and K. Nonami, "Guidance and nonlinear control system for autonomous flight of minirotorcraft unmanned aerial vehicles," *Journal of Field Robotics,* vol. 27, no. 3, pp. 311-334, 2010.

[86] H.K. Khalil, *Nonlinear systems.* Prentice-Hall, Upper Saddle River, NJ, second ed., 1996.

[87] A. Kim and M. Golnaraghi, "A quaternion-based orientation estimation algorithm using an inertial measurement unit," in *Proc. Position Location and Navigation Symposium,* pp. 268-272, Monterey, CA, USA, April 2004.

[88] N. Köksal, "Implementation of decentralized formation control on multi-quadrotor systems," M.Sc. Thesis, University of Waterloo, 2014.

[89] N. Köksal, B. Fidan and K. Büyükkabasakal, "Real-time Implementation of Decentralized Adaptive Formation Control on Multi-Quadrotor Systems," in *Proc. Europen Control Conference,* pp. 3162-3167, Linz, Austria, July 2015.

[90] N. Köksal, H. An and B. Fidan, "Two-Level Nonlinear Tracking Control of a Quadrotor Unmanned Aerial Vehicle," in *Proc. IFAC-PapersOnLine,* vol. 49, no. 17, pp. 254-259, 2016.

[91] N. Köksal, M. Jalalmaab and B. Fidan, "Adaptive Linear Quadratic Attitude Tracking Control of a Quadrotor UAV Based on IMU Sensor Data Fusion," *Sensors,* vol. 19, no. 1, pp. 46, 2019.

[92] M. Kuipers and P. Ioannou, "Multiple model adaptive control with mixing," *IEEE Trans. on Automatic Control,* vol. 55, no. 8, pp. 570-578, 2010.

[93] A. Kushleyev, D. Mellinger, C. Powers and V. Kumar, "Towards a swarm of agile micro quadrotors," *Autonomous Robots*, vol. 35, no. 4, pp. 287-300, 2013.

[94] D. Lee, H.J. Kim and S. Sastry, "Feedback linearization vs. adaptive sliding mode control for a quadrotor helicopter," *Int. Journal of Control, Automation, and Systems,* vol. 7, no. 3, pp. 419-428, 2009.

[95] T. Lee, "Robust adaptive attitude tracking on SO(3) with an application to a quadrotor UAV," *IEEE Transactions on Control Systems Technology,* vol. 21, no. 5, pp. 1924-1930, 2013.

[96] T. Lee, M. Leok and N.H. McClamroch, "Geometric tracking control of a quadrotor UAV on SE(3)," in *Proc. IEEE Conference on Decision and Control,* pp. 5420-5425, Atlanta, GA, USA, December 2010.

[97] T. Lee, M. Leok and N.H. McClamroch, "Nonlinear Robust Tracking Control of a Quadrotor UAV on SE(3)," *Asian Jounal of Control,* vol. 15, no. 2, pp. 391–408, 2013.

[98] S. Lesecq, S. Gentil and N. Daraoui, "Quadrotor attitude estimation with data losses," in *Proc. European Control Conference,* pp. 3851-3856, Budapest, Hungary, August 2009.

[99] Z. Li, H.H.T. Liu, B. Zhu, H. Gao and O. Kaynak, "Nonlinear robust attitude tracking control of a table-mount experimental helicopter using output feedback," *IEEE Trans. on Industrial Electronics,* vol. 62, no. 9, pp. 5665-5676, 2015.

[100] W. Li and J. Wang, "Effective adaptive Kalman filter for MEMS-IMU/magnetometers integrated attitude and heading reference systems," *The Journal of Navigation,* vol. 66, no. 1, pp. 99-113, 2013.

[101] H. Lim, J. Park, D. Lee and H.J. Kim, "Build your own quadrotor: open-source projects on unmanned aerial vehicles," *IEEE Robotics and Automation Magazine,* vol. 19, no. 3, pp. 33-45, 2012.

[102] H. Liu, Y. Bai, G. Lu and Y. Zhong, "Robust attitude control of uncertain quadrotors," *IET Control Theory and Applications,* vol. 7, no. 11, pp. 1583-1589, 2013.

[103] H. Liu, D. Li, Z. Zuo and Y. Zhong, "Robust three-loop trajectory tracking control for quadrotors with multiple uncertainties," *IEEE Trans. on Industrial Electronics,* vol. 63, no. 4, pp. 2263-2274, 2016.

[104] H. Liu, D. Li, J. Xi and Y. Zhong, "Robust attitude controller design for miniature quadrotors," *Int. Journal of Robust and Nonlinear Control,* vol. 26, no. 4, pp. 681-696, 2016.

[105] H. Liu, J. Xi and Y. Zhong, "Robust attitude stabilization for nonlinear quadrotor systems with uncertainties and delays," *IEEE Transactions on Industrial Electronics,* vol. 64, no. 7, pp. 5585-5594, 2017.

[106] C. Liu, W.H. Chen, "Disturbance rejection flight control for small fixed-wing unmanned aerial vehicles," *Journal of Guidance, Control, and Dynamics,* vol. 39, no. 12, pp. 2804-2813, 2016.

[107] T. Madani and A. Benallegue, "Backstepping control for a quadrotor helicopter," in *Proc. IEEE/RSJ International Conference on Intelligent Robots and Systems,* pp. 3255-3260, Beijing, China, October 2006.

[108] T. Madani and A. Benallegue, "Control of a qadrotor mini-helicopter via full state backstepping technique," in *Proc. IEEE Conference on Decision and Control,* pp. 1515-1520, San Diego, CA, USA, December 2006.

[109] Ø. Magnussen, M. Ottestad and G. Hovland, "Experimental validation of a quaternion-based attitude estimation with direct input to a quadcopter control system," in *Proc. IEEE International Conference on Unmanned Aircraft Systems,* pp. 480-485, Atlanta, GA, USA, May 2013.

[110] R. Mahony, T. Hamel and J.M. Pflimlin, "Complementary filter design on the special orthogonal group SO(3)," in *Proc. IEEE Conference on Decision and Control Conference and European Control Conference,* pp. 1477-1484, Seville, Spain, December 2005.

[111] J.L. Marins, X. Yun, E.R. Bachmann, R.B. McGhee and M.J. Zyda, "An extended Kalman filter for quaternion-based orientation estimation using MARG sensors," in *Proc. IEEE/RSJ International Conference on Intelligent Robots and Systems,* Vol.4, pp. 2003-2011, Maui, HI, USA, October-November 2001.

[112] D. Mellinger, M. Shomin, N. Michael and V. Kumar, "Cooperative grasping and transport using multiple quadrotors," *In Distributed Autonomous Robotic Systems of Series Springer Tracts in Advanced Robotics*, vol. 83, pp. 545–558, Berlin: Springer, 2013.

[113] H. Modares and F.L. Lewis, "Linear quadratic tracking control of partially-unknown continuous-time systems using reinforcement learning," *IEEE Transactions on Automatic Control,* vol. 59, no. 11, pp. 3051-3056, 2014.

[114] M. Mohammadi and A.M. Shahri, "Adaptive nonlinear stabilization control for a quadrotor UAV: theory, simulation and experimentation," *Journal of Intelligent and Robotic Systems,* vol. 72, no. 1, pp. 105-122, 2013.

[115] Y. Morel and A. Leonessa, "Direct adaptive tracking control of quadrotor aerial vehicles," in *Proc. Conference on Recent Advances in Robotics,* pp. 1-6, Miami, Florida, May 2006.

[116] D.S. Naidu, *Optimal control systems.* CRC press, 2002.

[117] K.S. Narendra and J. Balakrishnan, "Adaptive control using multiple models," *IEEE Trans. on Automatic Control,* vol. 42, no. 2, pp. 171-187, February 1997.

[118] NaturalPoint, Inc, *http://www.naturalpoint.com/optitrack/products/v100-r2/,* Accessed: February 18, 2014.

[119] C. Nicol, C.J.B. Macnab and A. Ramirez-Serrano, "Robust adaptive control of a quadrotor helicopter," *Mechatronics,* vol. 21, no. 6, pp. 927-938, 2011.

[120] K.K. Oh, M.C. Park and H.S. Ahn, "A survey of multi-agent formation control," *Automatica,* vol. 53, pp. 424-440, 2015.

[121] R. Olfati-Saber and R.M. Murray, "Graph rigidity and distributed formation stabilization of multi-vehicle systems," in *Proc. IEEE Conference on Decision and Control,* pp. 2965-2971, Las Vegas, Nevada, December 2002.

[122] N.S. Özbek, M. Önkol and M.Ö. Efe, "Feedback control strategies for quadrotor-type aerial robots: a survey," *Transactions of the Institute of Measurement and Control,* vol. 38, no. 5, pp. 529–554, 2016.

[123] U. Pilz, A.P. Popov and H. Werner, "Robust controller design for formation flight of quadrotor helicopters," in *Proc. IEEE Conference on Decision and Control/Chinese Control Conference,* pp. 8322-8327, Shanghai, China, December 2009.

[124] M. Qian, B. Jiang, H. H. Liu and N. Lu, "Dynamic surface fault tolerant tracking control design for UAV with transient performance," in *Proc. IFAC-PapersOnLine,* pp. 208–213, 2015.

[125] G.V. Raffo, M.G. Ortega and F.R. Rubio, "Backstepping/nonlinear H-infinite control for path tracking of a quadrotor unmanned aerial vehicle," in *Proc. American Control Conference,* pp. 3356-3361, Seattle, WA, USA, June 2008.

[126] G.V. Raffo, M.G. Ortega and F.R. Rubio, "An integral predictive/nonlinear H_∞ control structure for a quadrotor helicopter," *Automatica,* vol. 46, no. 1, pp. 29-39, January 2010.

[127] H. Ramirez-Rodriguez, V. Parra-Vega, A. Sanchez-Orta and O. Garcia-Salazar, "Robust backstepping control based on integral sliding modes for tracking of quadrotors," *ISA Transactions,* vol. 73, no. 1, pp. 51-66, 2014.

[128] A. Ratnoo, P.B. Sujit and M. Kothari, "Adaptive optimal path following for high wind flights," in *Proc. 18th IFAC World Congress,* pp. 12985-12990, Milano, Italy, August 2011.

[129] G.G. Redhyka, D. Setiawan and D. Soetraprawata, "Embedded sensor fusion and moving-average filter for Inertial Measurement Unit (IMU) on the micro controller-based stabilized platform," in *Proc. IEEE International Conference on Automation, Cognitive Science, Optics, Micro Electro-Mechanical System, and Information Technology,* pp. 72-77, Bandung, Indonesia, October 2015.

[130] H. Rehbinder and X. Hu, "Nonlinear state estimation for rigid-body motion with low-pass sensors," *Systems and Control Letters,* vol. 40, no. 3, 183-190, 2000.

[131] W. Ren and E. Atkins, "Nonlinear trajectory tracking for fixed wing UAVs via backstepping and parameter adaptation," in *Proc. the AIAA Guidance, Navigation, and Control Conference and Exhibit,* pp. 3606-3616, San Francisco, CA, USA, August 2005.

[132] W. Ren, J.S. Sun, R.W. Beard and T. McLain, "Experimental validation of an autonomous control system on a mobile robot platform," *IET Control Theory and Applications,* vol. 1, no. 6, pp. 1621-1629, 2007.

[133] W. Ren and R.W. Beard, "Trajectory tracking for unmanned air vehicles with velocity and heading rate constraints," *IEEE Trans. on Control System Technology,* vol. 12, no. 5, pp. 706-716, September 2004.

[134] A. Richards, J. Bellingham, M. Tillerson and J. How, "Coordination and control of multiple UAVs," in *Proc. AIAA Guidance, Navigation, and Control Conference and Exhibit,* pp. 1-11, Monterey, CA, USA, August 2002.

[135] F. Rinaldi, A. Gargioli and F. Quagliotti, "PID and LQ regulation of a multirotor attitude mathematical modelling, simulations," *Journal of Intelligent and Robotic Systems,* vol. 73, no. 1-4, pp. 33-50, 2014.

[136] R. Ritz and R. D'Andrea, "Carrying a flexible payload with multiple flying vehicles," in *Proc. IEEE/RSJ Int. Conference on Intelligent Robots and Systems,* pp. 3465-3471, Tokyo, Japan, November 2013.

[137] V. Roldão, R. Cunha, D. Cabecinhas, C. Silvestre and P. Oliveira, "A leader-following trajectory generator with application to quadrotor formation flight," *Robotics and Autonomous Systems,* vol. 62, no. 10, pp. 1597-1609, 2014.

[138] K. Rudin, M. Hua, G. Ducard and S. Bouabdallah, "A robust attitude controller and its application to quadrotor helicopters," in *Proc. 18th IFAC World Congress,* pp. 10379-10384, Milano, Italy, August-September 2011.

[139] T. Ryan and H.J. Kim, "LMI-based gain synthesis for simple robust quadrotor control," *IEEE Trans. on Automation Science and Engineering,* vol. 10, no. 4, pp. 1173-1178, 2013.

[140] J.J. Xiong and G.B. Zhang, "Global fast dynamic terminal sliding mode control for a quadrotor UAV," *ISA Transactions,* vol. 66, pp. 233-240, 2017.

[141] J.J. Xiong and E.H. Zheng, "Position and attitude tracking control for a quadrotor UAV," *ISA Transactions,* vol. 53, pp. 725-731, 2014.

[142] R. Xu and Ü. Özgüner, "Sliding mode control of a quadrotor helicopter," in *Proc. IEEE Conference on Decision and Control,* pp. 4957-4962, San Diego, CA, USA, December 2006.

[143] R. Xu and Ü. Özgüner, "Sliding mode control of a class of underactuated systems," *Automatica,* vol. 44, no. 1, pp. 233-241, 2008.

[144] H.G. Tanner, G.J. Pappas and V. Kumar, "Leader-to-formation stability," *IEEE Trans. on Robotics and Automation,* vol. 20, no. 3, pp. 443-455, June 2004.

[145] A. Tayebi and S. McGilvray, "Attitude stabilization of a VTOL quadrotor aircraft," *IEEE Trans. on Control Systems Technology,* vol. 14, no. 3, pp. 562-571, May 2006.

[146] A. Tayebi, "Unit quaternion-based output feedback for the attitude tracking problem," *IEEE Trans. on Automatic Control,* vol. 53, no. 6, pp. 1516-1520, July 2008.

[147] H. Wang and M. Chen, "Trajectory tracking control for an indoor quadrotor UAV based on the disturbance observer," *Transactions of the Institute of Measurement and Control,* vol. 38, no. 6, pp. 675-692, 2016.

[148] L. Wang and J. Su, "Robust disturbance rejection control for attitude tracking of an aircraft," *IEEE Trans. Control Systems Technology,* vol. 23, no. 6, pp. 2361-2368, 2015.

[149] W. Wang and C. Wen "Adaptive actuator failure compensation control of uncertain nonlinear systems with guaranteed transient performance," *Automatica,* vol. 46, no. 12, pp. 2082-2091, 2010.

[150] Y. Wang, Q. Wu and Y. Wang, "Distributed consensus protocols for coordinated control of multiple quadrotors under a directed topology," *IET Control Theory and Applications,* vol. 7, no. 24, pp. 1780-1792, 2013.

[151] S. Wang and Y. Yang, "Quadrotor aircraft attitude estimation and control based on Kalman filter," in *Proc. Chinese Control Conference,* pp. 5634-5639, Hefei, China, July 2012.

[152] M. Wang, Y. Yang, R.R. Hatch and Y. Zhang, "Adaptive filter for a miniature MEMS based attitude and heading reference System," in *Proc. IEEE Position Location and Navigation Symposium,* pp. 193-200, Monterey, CA, USA, 2004.

[153] I. Sa and P. Corke, "System identification, estimation and control for a cost effective open-source quadcopter," in *Proc. IEEE International Conference Robotics and Automation,* pp. 2202-2209, Saint Paul, MN, USA, May 2012.

[154] A.M. Sabatini, "Quaternion-based extended Kalman filter for determining orientation by inertial and magnetic sensing," *IEEE Transactions on Biomedical Engineering,* vol. 53, no. 7, pp. 1346-1356, 2006.

[155] A.M. Sabatini, "Kalman-filter-based orientation determination using inertial/magnetic sensors: observability analysis and performance evaluation," *Sensors,* vol. 11, no. 10, pp. 9182-9206, 2011.

[156] A.C. Satici, H. Poonawala and M.W. Spong, "Robust optimal control of quadrotor UAVs," *IEEE Access,* vol. 1, pp. 79-93, 2013.

[157] Z. Song and K. Sun, "Adaptive compensation control for attitude adjustment of quad-rotor unmanned aerial vehicle," *ISA Transactions,* vol. 69, pp. 242-255, 2017.

[158] E. Stingu and F. Lewis, "Design and implementation of a structured flight controller for a 6DoF quadrotor using quaternions," in *Proc. IEEE 17th Mediterranean Conference on Control and Automation,* pp. 1233-1238, Thessaloniki, Greece, June 2009.

[159] M. St-Pierre and D. Gingras, "Comparison between the unscented Kalman filter and the extended Kalman filter for the position estimation module of an integrated navigation information system," in *Proc. IEEE Intelligent Vehicles Symposium,* pp. 831-835, Parma, Italy, June 2004.

[160] P.B. Sujit, S. Saripalli and J.B. Sousa, " Unmanned aerial vehicle path following: a survey and analysis of algorithms for fixed-wing unmanned aerial vehicles," *IEEE Control Systems,* vol. 34, no. 1, pp. 42-59, 2014.

[161] E.C. Suicmez and A.T. Kutay, "Optimal path tracking control of a quadrotor UAV," in *Proc. International Conference on Unmanned Aircraft Systems,* pp. 115-125, Orlando, FL, USA, May 2014.

[162] A. Yesildirek and B. Imran, "Nonlinear control of quadrotor using multi Lyapunov functions," in *Proc. American Control Conference,* pp. 3844-3849, Portland, OR, USA, June 2014.

[163] C. Yu, J.M. Hendrickx, B. Fidan, B.D.O. Anderson and V.D. Blondel, "Three and higher dimensional autonomous formations: rigidity, persistence and structural persistence," *Automatica,* vol. 43, no. 3, pp. 387-402, 2007.

[164] B. Yüksek, A. Vuruskan, U. Özdemir, M.A. Yükselen and G. İnalhan, "Transition flight modeling of a fixed-wing VTOL UAV," *Journal of Intelligent and Robotic Systems,* vol. 44, no. 1-4, pp. 82-105, December 2016.

[165] D. Zelazo, A. Franchi, H.H. Bulthoff and P.R. Giordano, "Decentralized rigidity maintenance control with range-only measurements for multi-robot systems," *Int. J. of Robotics Research,* vol. 34, no. 1, pp. 105-128, 2015.

[166] W. Zeng, B. Xian, C. Diao, Q. Yin, H. Li and Y. Yang, "Nonlinear adaptive regulation control of a quadrotor unmanned aerial vehicle," in *Proc. IEEE International Conference on Control Applications,* pp. 133-138, Denver, CO, USA, September 2011.

[167] B. Zhao, B. Xian, Y. Zhang and X. Zhang, "Nonlinear robust adaptive tracking control of a quadrotor UAV via immersion and invariance methodology," *IEEE Trans. on Industrial Electronics,* vol. 62, no. 5, pp. 2891-2902, 2015.

[168] B. Zhou, H. Satyavada and S. Baldi, "Adaptive path following for unmanned aerial vehicles in time-varying unknown wind environments," in *Proc. American Control Conference,* pp. 1127-1132, Seattle, WA, USA, May 2017.

[169] Z.G. Zhou, Y.A. Zhang, X.N. Shi and D. Zhou, "Robust attitude tracking for rigid spacecraft with prescribed transient performance," *International Journal of Control,* vol. 90, no. 11, pp. 2471-2479, 2017.

[170] Z. Zuo and C. Wang, "Adaptive trajectory tracking control of output constrained multirotors systems," *IET Control Theory and Applications,* vol. 8, no. 13, pp. 1163-1174, 2014.

[171] Analog Devices, "Tri-axis inertial sensor with magnetometer, ADIS16405," Norwood, MA, USA, 2009: http://www.analog.com/media/en/technical-documentation/data-sheets/ADIS16400_16405.pdf, Accessed: July 26, 2018.

[172] Quanser Inc., "Qball-X4:User Manual", Document number:830, 2013.